

Master Thesis

University of Ioannina
Department of Physics
Section of Astrogeophysics

*Hall Magnetohydrodynamics equilibrium states
for fusion plasmas via Hamiltonian variational
principles*



Angelos Giannis

Supervisor: Professor George Throumoulopoulos

Ioannina, 2023



Ιωάννινα, 19/06/2023

Προς
τη Γραμματεία του Τμήματος
Φυσικής
του Πανεπιστημίου Ιωαννίνων

ΠΡΑΚΤΙΚΟ ΕΞΕΤΑΣΗΣ ΜΕΤΑΠΤΥΧΙΑΚΗΣ ΔΙΠΛΩΜΑΤΙΚΗΣ ΕΡΓΑΣΙΑΣ

Σήμερα 19 Ιουνίου και ώρα 12, ενώπιον της ορισθείσας τριμελούς εξεταστικής επιτροπής αποτελούμενη από τους καθηγητές κ.κ.:

1. Γεώργιο Θρουμουλόπουλο (Επιβλέπων)
2. Αλέξανδρο Νίντο (Αξιολογητής 1)
3. Βασίλειο Αρχοντή (Αξιολογητής 2)

πραγματοποιήθηκε η εξέταση της Διπλωματικής Εργασίας του κ. Άγγελου Γιαννή φοιτητή του Τμήματος Φυσικής, με Α.Μ. 400807, με θέμα: «Καταστάσεις ισορροπίας πλάσματος σύντηξης στα πλαίσια της Μαγνητοϋδροδυναμικής Hall μέσω Χαμιλτονιανών παραλλακτικών αρχών» (Ελληνικά) «Hall Magnetohydrodynamics equilibrium states for fusion plasmas via Hamiltonian variational principles» (Αγγλικά)

Κατά την αξιολόγηση η τριμελής Επιτροπή βαθμολόγησε ως ακολούθως:

	Αντικείμενα αξιολόγησης	Επιβλέπων	Αξιολογητής 1	Αξιολογητής 2	Μέσος όρος
1	Ανάπτυξη θέματος [40%]	10	10	10	10
2	Έντυπη παρουσίαση (κείμενο εργασίας) (20%)	10	10	10	10
3	Δημόσια παρουσίαση εργασίας (20%)	10	10	10	10
4	Επιστημονική κατάρτιση υποψηφίου (20%)	10	10	10	10
Συνολικός Βαθμός:					10

Τα ανωτέρω αντικείμενα αξιολόγησης εγκρίθηκαν στην υπ' αριθ. 527/27.01.2020 Συνέλευση του οικείου Τμήματος.

ME2

Η συλλογή και η επεξεργασία των δεδομένων προσωπικού χαρακτήρα που υποβάλλονται πραγματοποιείται σύμφωνα με τα οριζόμενα στις διατάξεις του Ν.4624/19 και του Κανονισμού (ΕΕ)2016/2019. Το Πανεπιστήμιο Ιωαννίνων συλλέγει και επεξεργάζεται τα δεδομένα προσωπικού χαρακτήρα αποκλειστικά στο πλαίσιο της υλοποίησης του σκοπού της παρούσας διαδικασίας. Για το χρονικό διάστημα που τα προσωπικά δεδομένα θα παραμείνουν στη διάθεση του Πανεπιστημίου Ιωαννίνων το υποκείμενο έχει τη δυνατότητα να ασκήσει τα δικαιώματά του σύμφωνα με τους όρους του Γενικού Κανονισμού Προστασίας Δεδομένων Προσωπικού Χαρακτήρα 2016/679 (Ε.Ε.) και τα οριζόμενα στα άρθρα 34 και 35 Ν. 4624/2019. Υπεύθυνη Προσωπικών Δεδομένων του Ιδρύματος είναι η κα. Σταυρούλα Σταθαρά (email: dro@uoi.gr).



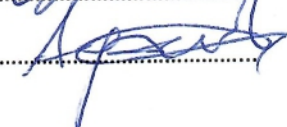
Βεβαιώνουμε ότι η Διπλωματική Εργασία έχει παρουσιαστεί επιτυχώς.

Η Τριμελής Επιτροπή (Υπογραφές):

1.

2.

3.

Γ. Βραυλιουδάκης




Γνώμη τριμελούς εξεταστικής επιτροπής (προαιρετικό):

Τα μέλη της επιτροπής μετά την εξέταση δήλωσαν ομόφωνα ότι έμειναν ικανοποιημένοι από την παρουσίαση και επιστημονική κατάρτιση του υποψηφίου και έκριναν ομόφωνα ότι η εργασία είναι επιστημονικά ορθή και υψηλού επιπέδου.

*In memoriam of my beloved grandfather, Lazaros Papadopoulos, and the grandfather I never met,
Evangelos Giannis*



This Master's Thesis was conducted within the framework of the University of Ioannina's participation in the National Program of Controlled Thermonuclear Fusion in the Hellenic Republic.

In fact, we are the result of a series of unlikely chain events. The materials that make up our bodies were created inside giant stars through nuclear fusion, and due to stellar evolution they were eventually found in this small corner of our galaxy; the corner where our solar system and the planet we inhabit were born.

Pavlos Kastanas

Table of contents

Acknowledgements	ix
Abstract	xi
1 Prelude to plasma physics and controlled thermonuclear fusion	1
1.1 Plasma, the fourth state of matter	1
1.2 Plasma criteria	3
1.2.1 Quasineutrality - Debye shielding	3
1.2.2 Collective behaviour	4
1.2.3 Dominance of electrostatic interactions	4
1.3 Controlled thermonuclear fusion	5
1.3.1 Fundamental concepts and ulterior goal	5
1.3.2 Toroidal confinement systems	7
1.3.2.1 Tokamaks	8
1.3.2.2 Stellarators	10
1.3.2.3 Field-reversed configurations (FRCs) and Spheromaks	10
1.3.3 Theorems for the magnetic confinement of plasma	12
1.4 Plasma modelling	13
1.4.1 From kinetic to fluidistic description	14
1.4.2 The Magnetohydrodynamics (MHD) model	15
1.4.2.1 Basic assumptions and formulation	15
1.4.2.2 Spitzer's law - Ideal Magnetohydrodynamics	16
1.4.2.3 Alfvén's theorem - Comparing ideal with non-ideal models	17
1.4.3 The Hall Magnetohydrodynamics (Hall MHD) model	18
1.4.3.1 Two-fluid generalisation of the ideal MHD model	18
1.4.3.2 Alfvén normalisation scheme	19
1.4.3.3 Reduction to Hall MHD	20
1.5 Motivation and aim	21
1.6 Thesis outline	22
2 Equilibria construction via the Energy-Casimir variational principle	25
2.1 Hamiltonian formulation for ideal fluid models	25
2.1.1 Canonical Hamiltonian description	25
2.1.2 Non-canonical Hamiltonian description	27
2.1.3 The Energy-Casimir variational principle	28
2.2 Axisymmetric Hall MHD equilibria	29
2.3 Ansatz for the free functions - Equilibria cases	33
3 A family of analytic solutions to the Grad-Shafranov-Bernoulli system	35
3.1 Double Beltrami equilibria	35
3.1.1 Direct derivation of the double Beltrami system via the Energy-Casimir variational principle	35
3.1.2 Double Beltrami system in terms of the flux functions	37
3.1.3 Solution to the double Beltrami equations	38
3.1.3.1 Homogeneous system	38

3.1.3.2	Non-homogeneous system	42
3.2	Equilibria in terms of the Whittaker functions	43
3.2.1	Homogeneous system	43
3.2.2	Non-homogeneous system	44
3.3	Solovév equilibria	45
3.3.1	Static MHD Solovév solution	46
3.3.2	Hall MHD Solovév solution	48
3.4	Generic equilibria	49
4	Applications of the solutions to axisymmetric fusion devices	53
4.1	Tokamak-relevant equilibria	53
4.1.1	Geometry of the D-shaped Tokamak boundary	53
4.1.2	Boundary conditions	55
4.1.3	Double Beltrami equilibrium	56
4.1.3.1	Equilibrium construction	56
4.1.3.2	Equilibrium quantities	59
4.1.4	Whittaker equilibrium	64
4.1.4.1	Equilibrium construction	64
4.1.4.2	Equilibrium quantities	67
4.2	FRC Solovév equilibrium	71
4.2.1	Equilibrium construction	71
4.2.2	Equilibrium quantities	72
5	Conclusions and future prospects	77
5.1	Summary and main conclusions	77
5.2	Future prospects	79
	Appendices	81
A	An alternative way to solve the Double Beltrami system	81
B	Generalisation of the Double Beltrami Grad-Shafranov equation for helical symmetry	83
C	Digression on the Whittaker functions	85
	Bibliographical references	89
	List of figures	97

Acknowledgements

It is with great gratitude that I acknowledge the invaluable guidance and support of my esteemed supervisor, Mr. George Throumoulopoulos. For without his astute feedback, generous allocation of time, and steadfast commitment to the betterment of my pursuits, these lines would simply not be written. I sincerely thank him for the collaboration we had, both on a scientific level and on a personal level. Furthermore, I would like to express my appreciation to the two other members of my thesis examination committee, Mr. Vasileios Archontis and Mr. Alexander Nindos for their constructive and valuable comments.

I am also deeply grateful to Dimitrios Kaltsas, who has also been a catalyst for completing the current thesis due to his unstinting support, his precious scientific comments and the help he provided me in developing the code. His enthusiasm for Plasma Physics topics was very supportive for me, as he imparted his love for the subject and thus pushed me to probe my way of thinking, to the point of writing this thesis.

I would also like to thank the other members of the Plasma Physics group of the Physics Department, Mr. George Poulipoulis and Mr. Achilleas Evangelias, as in our weekly meetings we exhausted issues related to the current scientific literature and formulated our concerns in a climate of fruitful dialogue.

Finally, I am profoundly grateful to my family and friends, whose unwavering love and support have been my constant source of inspiration throughout this journey. This achievement has been made possible owing to their faith in my abilities.

Abstract

Equilibrium equations for magnetically confined, axisymmetric plasmas are derived by means of Hamiltonian variational principles. This approach stems from the non-canonical Hamiltonian structure of Hall Magnetohydrodynamics (Hall MHD), the simplest, quasineutral two-fluid model that incorporates contributions due to ion Hall drifts. The axisymmetric Casimir invariants - functionals that Poisson-commute with any arbitrary functional of the dynamical variables - are used, along with the Hamiltonian functional to apply the Energy-Casimir variational principle for axisymmetric two-fluid plasmas with incompressible ion flows. The aforementioned variational principle results in a system of equations of the Grad-Shafranov Bernoulli (GS-Bernoulli) type with four free functions that are dictated by the Hall MHD model. A family of analytic solutions to the GS-Bernoulli system is then recovered, based on specific ansatzes for the free functions. These solutions are subsequently applied to Tokamak-relevant and FRC-relevant configurations using proper shaping methods. The Hall MHD model predicts a departure of the ion velocity surfaces from the magnetic surfaces on which the electron-fluid surfaces lie. This causes a separation of the two fluids (viz. the electron and the ion ones), which subsequently results in sub-Alfvénic ion flows and the development of poloidal electric fields. The pressure profile is peaked on the magnetic axis and exhibits a fine stratification inside a poloidal cross-section, which is desirable for the effective confinement of plasma. The relevance of these solutions to laboratory and astrophysical plasmas is finally discussed, with particular focus on systems that involve length scales on the order of the ion skin depth.

1

Prelude to plasma physics and controlled thermonuclear fusion

I have never thought that you could obtain the extremely clumpy, heterogeneous universe we have today, strongly affected by plasma processes, from the smooth, homogeneous one of the Big Bang, dominated by gravitation.

Hannes Alfvén

1.1 Plasma, the fourth state of matter

Since ancient times, man was already familiar with the solid and liquid state which he called respectively the first and second states of matter. It took numerous centuries before the third state, the gaseous one, was identified, while the fourth state of matter was discovered much more recently. So it came to pass that in 1928, an American scientist named Irving Langmuir used the term "plasma" to describe "regions containing balanced charges of ions and electrons", a state he encountered whilst studying the behaviour of gases in electric discharge experiments [1]. When we heat a solid body, it melts and becomes a liquid. If we heat the liquid, then it turns into a gas, and on further heating the gas becomes ionised. This happens because when temperatures are high enough, the building blocks that comprise the gas (i.e. atoms or molecules) undergo violent collisions due to their intense thermal motion, causing the electrons to be stripped away from the ions. This process is called ionisation, and results in a collection of electrons and positive ions, as well as neutral particles. The physics of this gas is now governed by the electromagnetic interactions between electrons and ions. It is therefore commonly accepted that by the term "plasma", we mean gases that have undergone ionisation, i.e. have been separated into the individual elements of their atoms (electrons and nuclei). However, not every ionised gas can necessarily be classified as plasma. In particular, certain specific criteria must be met, which will be discussed below.

In order to acknowledge the abundance of plasma in our universe, one needs only gaze in the night sky; everything that we can see is the part of normal matter that is in the plasma state, emitting radiation. This includes our Sun and all the other stars, as well as the interplanetary, interstellar and intergalactic medium [2]. But why does plasma not appear under normal conditions on Earth? The reasons for this are mainly two. First, plasma can only exist in vacuum conditions, otherwise the air would eventually cool the plasma and ion-electron recombination¹ in atoms or molecules would take place. This explains why about 99% of the baryonic matter in the universe is in plasma state [3]. The second reason can be easily un-

¹Recombination is the opposite process of ionisation.

derstood, if one considers the well-known Saha equation, which gives us the percentage of ionisation in a gas that is in thermodynamic equilibrium [2]:

$$\frac{n_i}{n_n} \approx 2.4 \times 10^{21} \frac{T^{3/2}}{n_i} e^{-\frac{U_i}{k_B T}}, \quad (1.1)$$

where n_i , n_n are the number densities of ions and neutral atoms respectively, T is the temperature in K , k_B is the Boltzmann constant and U_i is the ionisation energy of the gas, i.e. the energy required to strip away an electron from the gas atom. Here we note that n_i in the denominator indicates the dependence of the recombination rate on the ions (as the density of ions increases, the ionised-neutral ratio decreases due to recombination) [2]. Considering atmospheric air at room temperature (let us suppose that it consists only of nitrogen atoms in thermodynamic equilibrium), we assume $n_n \approx 10^{25} m^{-3}$, $T \approx 300 K$ and $U_i = 14.5 eV$. Substituting these values into (1.1), we obtain:

$$\frac{n_i}{n_n} \approx 10^{-122}, \quad (1.2)$$

which is infinitesimally small. From the above example it can be deduced that in normal conditions prevailing on Earth, it is not possible for matter to exist in plasma state. However, as the temperature increases, the exponential in (1.1) dominates and so the ratio n_i/n_n increases rapidly. At sufficiently high temperatures ($T \gtrsim 10^5 K$), we have practically complete ionisation, such as occurs in the centre of stars or even in stellar coronae [4], [5]. In practice, however, the transition point between the gas and plasma phase is not specific; it has been established that a 0.1% degree of ionisation is enough for a gas to attain clear plasma properties, while a degree of 1% means approximately perfect conductivity (fully-ionised plasma) [6]. Hence, owing to the abundance of charged particles, it is evident that a plasma is characterised by a high degree of electrical conductivity, a concept that will be better understood in the section to follow.

Although plasmas are not a customary phenomenon in our planet, there are some instances where gases obtain plasma properties. More specifically, lightning strikes, aurora borealis, electric sparks or even neon lights and plasma display screens are a few examples of plasma in our planet. Since plasmas can be found in our universe in a range of number densities and temperatures, we illustrate some notable cases in Figure 1.1.

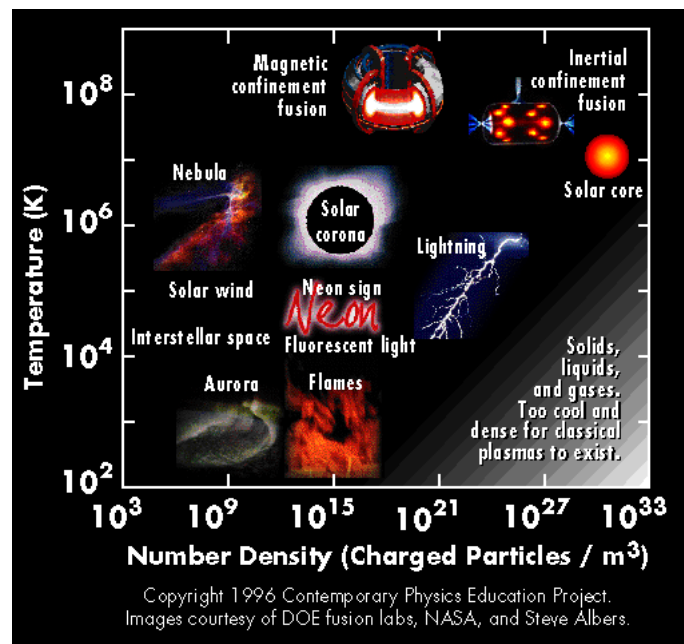


Figure 1.1: The various manifestations of plasma in our universe.

1.2 Plasma criteria

As mentioned above, not every single ionised gas can be characterized as plasma. Below we discuss the 3 criteria that ought to be met for this purpose.

1.2.1 Quasineutrality - Debye shielding

In contrast to strong nuclear interactions between nuclei that are extremely short ranged, electromagnetic interactions that are dominant in a plasma affect charged particles at a significantly longer range. Therefore, we intuitively expect that what happens in a neighborhood of the plasma will affect, more or less, the other charges as well. We can quantify this by placing an electrode of positive charge Q inside a plasma, as shown in Fig. 1.2.

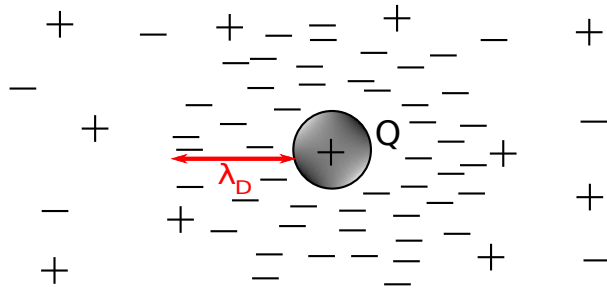


Figure 1.2: Debye shielding in plasma.

The role of electrostatic forces, as we see, is decisive. Placing the positive electrode results in a concentration of negative charge around it in order to neutralize the local charge density created. The negative charges therefore “shield” the rest of the plasma from the externally applied electric field. This phenomenon is a very fundamental property of plasma and is called **Debye shielding**. If the plasma was “cold”, i.e. if there were no thermal motions ($T \rightarrow 0$), then we would have complete shielding and around the electrode there would be exactly equal and opposite charge ($-Q$) at zero distance. In this case, the electric field inside the plasma space would be equal to zero: $E = \mathbf{0}$. In a more realistic case, however, where we have thermal motions and $T > 0$, the charges at the edges of the region around the electrode can escape due to thermal motions and create an electric field $E \neq \mathbf{0}$ in the plasma space [2]. It is not difficult to calculate the thickness of the region. Using the one-dimensional Poisson’s equation in the International System of Units (SI) ² for the scalar potential ϕ :

$$\nabla^2 \phi = \frac{d^2 \phi}{dx^2} = -\frac{1}{\epsilon_0} e [n_i(\phi) - n_e(\phi)], \quad (1.3)$$

with $n_i(\phi)$ and $n_e(\phi)$ being the ion and electron number densities respectively ³; ϵ_0 is the vacuum permittivity, and e is the elementary charge, we can show that the potential satisfies a relation of the form

$$\phi(x) = \phi_0 e^{-\frac{|x|}{\lambda_D}}, \quad (1.4)$$

where ϕ_0 is a constant. In equation (1.4) we defined a very fundamental quantity, the so-called **Debye length**

$$\lambda_D = \left(\frac{\epsilon_0 k_B T_e}{n e^2} \right)^{\frac{1}{2}}. \quad (1.5)$$

²Which we will use for this thesis.

³In sufficiently large distances where $\phi \rightarrow 0$, we have $n_i = n_e = n$.

Relation (1.4) reveals that the potential decreases exponentially with the distance from the electrode, a reasonable behaviour since each layer of plasma now has more electrons. We also note that the shielding length λ_D is a function of the electron temperature only, which we expect intuitively as the electrons are more mobile than ions and rush to shield the externally applied field. As T_e increases, λ_D also increases, so the shielding becomes less efficient. It is worth noting that, despite the long range of electrostatic forces in the vacuum, inside the plasma the particles interact weakly with each other at distances longer than the Debye length. The Debye length can therefore be used as a measure of the range of Coulomb interactions within the plasma [2].

From the preceding arguments it is clear that, if some charge concentration is created in the plasma, then the deviation from neutrality is shielded by the Debye sphere of dimensions λ_D . Outside this sphere, it holds that $\phi = \text{const.}$ and from relation (1.3) we get $n_i - n_e \simeq 0$, leaving the rest of the plasma unaffected. Thus, if the condition

$$\lambda_D \ll L \quad (1.6)$$

holds, with L being a reference length scale of our system, then the plasma can be considered **macroscopically neutral**, for phenomena of the same length scale as L . In this case, we say that the plasma is **quasi-neutral** and then

$$n_e \simeq n_i = n. \quad (1.7)$$

However, it should be stressed that the plasma is not completely neutral as there are electromagnetic forces that are the main cause of all the important processes that take place in it [2], [7], [8].

1.2.2 Collective behaviour

Debye shielding is the first example of collective behaviour we have seen in a plasma. However, for the shielding to be acceptable in terms of statistical physics, there must be a large number of charged particles N_D within the Debye sphere. Since

$$N_D = \frac{4}{3}\pi\lambda_D^3 n, \quad (1.8)$$

the above assumption means that

$$N_D \gg 1, \quad (1.9)$$

which implies that

$$\lambda_D \gg n^{-1/3} = r_m, \quad (1.10)$$

where r_m is the mean distance between two interacting particles.

1.2.3 Dominance of electrostatic interactions

In addition to the above two criteria, there is a third requirement that a gas must meet in order to be classified as plasma, which relates to scattering between its constituent particles. Using the definition of the Debye length λ_D and the thermal velocity $v_{th} = \sqrt{(2k_B T)/m_e}$, we define ⁴ the frequency of the electrostatic oscillations that take place in the plasma

$$\omega_p = \sqrt{\frac{ne^2}{\epsilon_0 m_e}}, \quad (1.11)$$

⁴At this point we used the so-called heavy-ion approximation, i.e. we assumed that ions have infinite mass - hence infinite inertia - relative to electrons. This means that only electrons participate in any change in the kinetic state of the plasma, while ions do not respond. This approximation is satisfactory, since in a protonic plasma the ions have 1836 times the mass of the electrons.

where m_e is the electron mass. Considering the average collision time between charges and neutral atoms τ , it is evident that the condition

$$\omega_p \tau \gg 1 \tag{1.12}$$

should hold in order for electrostatic interactions to be dominant.

The three aforementioned criteria for classifying a gas as a plasma can be summarised as follows

$\lambda_D \ll L$ (Debye shielding - quasineutrality),	(1.13)
$N_D \gg 1$ (Collective behaviour),	(1.14)
$\omega_p \tau \gg 1$ (Dominance of electrostatic interactions).	(1.15)

Finally, it is worth stating that from another point of view conditions (1.13) and (1.15) express that plasma is shielded effectively from DC and AC electric fields respectively [7].

1.3 Controlled thermonuclear fusion

Having presented the basic principles governing plasmas, one may reasonably ask the usefulness of studying the fourth state of matter. Apart from the prominent role of the plasma in the universe (where, as we mentioned previously, it makes up about 99% of baryonic matter), there is a multitude of reasons why its capricious behaviour is worth looking into. The most important of these is the achievement of thermonuclear fusion on laboratory grounds.

It is a widely accepted fact that global energy demands - especially for electricity - are increasing due to perpetual advances in technology [9], the development of civilisation [10] and climate change [11]. What's more, the depletion of fossil fuels is now a reality. In particular, it is estimated that by the end of this century most - if not all - of the world's fossil fuel reserves will be exhausted [12]. Apart from fossil fuels, we also have in our disposal renewable energy sources, such as wind, hydroelectricity, etc., which are not sufficient to meet the energy needs of large urban centres because of the problems they have in their storage [13]. Therefore, it seems clear that humanity will have to turn to other forms of energy which are more efficient, more environmentally friendly and - if feasible - almost inexhaustible. A first step was taken in the second half of the 20th century, with the discovery of nuclear fission. Fission reactors are still used extensively today, mainly by countries such as the United States of America, China, France, etc. and make a significant contribution to meet our energy needs. However, fission residues are radioactive with long half-lives, polluting the environment and making them difficult and costly to store. In addition, fission as a process is a chain reaction, which makes it particularly dangerous, as we have seen in the past from nuclear accidents (Fukushima, Chernobyl, etc.). Although efforts are constantly being made to upgrade the current fission reactors, the stocks of nuclear fuel (e.g. ²³⁵U, which is one of the most widely used fissile materials) are running out [14]. Nuclear fusion is a promising alternative; that is why a large part of the scientific community and beyond is investing in it.

1.3.1 Fundamental concepts and ulterior goal

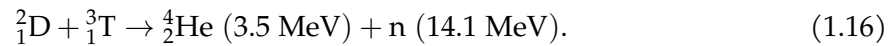
Controlled thermonuclear fusion is a complex problem which remains to date an "open" research topic. To achieve it, most fields of physics have been mobilised and the development of technology in new areas has been significantly advanced. It is a very ambitious scientific endeavour as it is intended to solve the world's energy problem. The reason why life thrives on Earth is indeed nuclear fusion, for it is the way in which energy is produced inside the stars, including our Sun. As a process, it is the reverse of fission, in that two lighter nuclei come together, yielding a heavier nucleus, energy and other subatomic particles. The energy production is attributed to the mass excess of the reactants over the products, which translates

into energy by virtue of the renowned Einstein's mass-energy equivalence relation. As fusion reactions are exothermic, this energy is released into the environment.

Several ways of achieving thermonuclear fusion have been proposed from the second half of the 20th century to the present day. The most important of these are Magnetic Confinement Fusion (MCF) and Inertial Confinement Fusion (ICF). In the first case, the fuel is introduced into closed chambers and is heated to very high temperatures, capable of initiating fusion reactions. In such conditions, the fuel acquires plasma properties and it is confined by means of strong magnetic fields, because the motions of charges in a magnetic field are limited. This is due to the anisotropy exhibited by the Lorentz force (1.27) parallel and perpendicular to the magnetic field. In the second case, a small deuterium-tritium target is bombarded with strong laser beams or energetic particles, which causes its adiabatic compression, hence its heating. Although recent advances have been made in the field of ICF [15], the present work examines nuclear fusion from the scope of magnetic confinement, as this method has given us the most promising results to date.

The reason why we choose magnetic fields is because of the confinement properties they possess. To begin with, the charged particles that make up the plasma drift around each magnetic line of force. In this way, the magnetic field "constricts" the plasma and the charges attach themselves to its field lines. What's more, the magnetic field can be treated as a kind of non-material container, as we want the plasma not to come into contact with the reactor walls to avoid any transmutations. The second reason is attributed to Alfvén's theorem which will be examined in Section 1.4.2.3. Since the plasma as a fluid moves along with the magnetic field lines (the magnetic field is "frozen" in the plasma), the construction of the geometry of the magnetic field largely guarantees us the geometry of the plasma. Finally, the thermal conductivity of the plasma exhibits anisotropy parallel and perpendicular to the magnetic field lines. Thus, heat is very easily released along a field line, but is prevented from being transported perpendicular to them, thus facilitating the confinement of the plasma. This property is also seen in plasma loops that appear in the solar corona, where each field line "has its own atmosphere" [4], [5], [8].

It is speculated that the first fusion reactors will be based on the fusion of deuterium and tritium:



This reaction is preferred over the so-called proton-proton chain [5], which takes place in the core of our Sun, because firstly it has a lower ignition temperature and secondly it has a large cross section for intermediate energies - larger even than the D-³He and D-D fusion reactions [7] as we can see in Fig. 1.3.

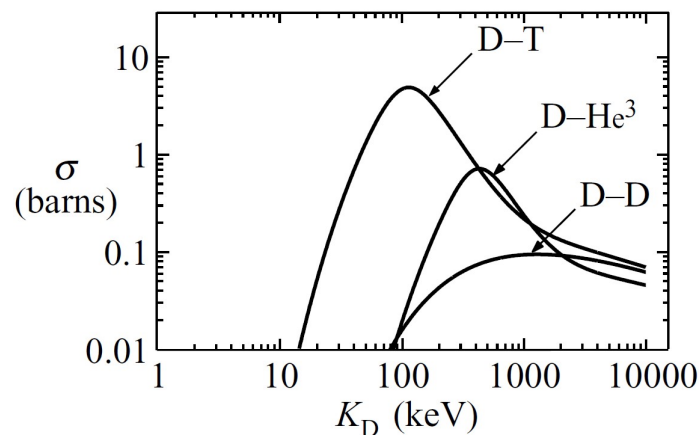


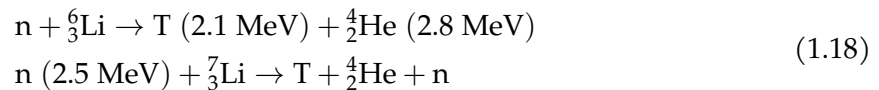
Figure 1.3: Experimentally measured cross sections for the D-T, D-³He, and D-D fusion reactions as a function of deuterium energy $K_D = m_D v_D^2 / 2$ [16].

In addition, deuterium is abundant in seawater, at 0.015% of hydrogen, so we have an almost inexhaustible source of energy. To quantify this, it is enough to consider that one litre of seawater can give us about 1010 J of energy through fusion, which is 300 times more than the energy yielded by burning one litre of petrol (conventional fuel) [8]. In addition, as we can see, no radioactive elements are produced, so we do not further pollute the environment. Tritium, although radioactive, has a very short half-life and is not considered a long-lived radioactive product like many of the fission residues. Another advantage of fusion over fission is that fusion is not a chain reaction, so it is a *controlled* process [2]. In order to have fusion reactions like in (1.16), we need to heat the fuel (deuterium and tritium) to very high temperatures⁵ of the order of 10^7 K. This is because the Coulomb potential is repulsive and, since we want to bring together two positively charged nuclei, it is evident that we need sufficiently high thermal velocities to bring the nuclei close together so as to exert the strong nuclear force, fusing them into heavier elements. In this case we are talking about thermonuclear fusion reactions. At these temperatures, matter is in a state of plasma, which is almost completely ionised. It is also preferable to have relatively high number densities, because in this way the possibility of thermonuclear reactions is increased. Unfortunately, there are more issues to be addressed; in order for fusion to be self-sustaining, the energy gains from fusion reactions must be greater than the energy used to heat the plasma and make up for the energy losses. This proposal is summarised in the so-called Lawson criterion [17], according to which

$$n\tau_E T \geq 10^{-21} \text{ m}^{-3} \text{ sec keV}, \quad (1.17)$$

where τ_E is a parameter called the energy confinement time. The higher the value of this parameter, the lower the rate of energy dissipation. Indicatively, for magnetic confinement a typical value is $\tau_E \approx 1$ sec. This criterion is therefore an important necessary (but not sufficient!) condition for fusion [7].

Finally, there is another issue with D-T fusion, which concerns the very high energy of neutrons, as we can see from (1.16). Neutrons have a small mass compared to helium nuclei (alpha particles) and so due to conservation of momentum they gain more energy after the reaction. The problem is that neutrons are electrically neutral, so they cannot be confined by the magnetic field and - during the confinement of plasma - they will escape at high velocities towards the walls. One solution that has been proposed is to coat the reactor walls with a ${}^6_3\text{Li}$ "mantle" so that neutrons are bound by the following reactions, releasing heat:



In this manner, we are shielded from energetic neutrons, we gain heat and at the same time we secure tritium, which is our fuel along with deuterium [8].

1.3.2 Toroidal confinement systems

For several decades, the question of choosing the right system for the confinement of plasma has been a constant concern for scientists. The first systems proposed were the θ and z pinches, cylindrical systems in which all reference quantities (current density, magnetic field, pressure, etc.) depend on a single spatial variable, the radial coordinate r - viz. they are one-dimensional. In particular, they were the most symmetric systems proposed for magnetic confinement, but unfortunately they were unsuccessful in achieving this goal because of the particle and energy losses that they exhibited in both their ends [18]. At this point it is reasonable to wonder what would happen if we joined the two ends of the pinches and got a closed system. In this case, the straight axis of the cylinder becomes circular (**magnetic axis**) and we are talking about *closed toroidal magnetic confinement systems*. For these toroidal geometries, and for the needs of this thesis, we will use the usual cylindrical coordinate system (R, ϕ, Z) ,

⁵These temperatures exceed those found in the core of the Sun.

where R is the major radius of the torus, ϕ is the angle across the toroidal direction (toroidal angle) and Z is the vertical coordinate.

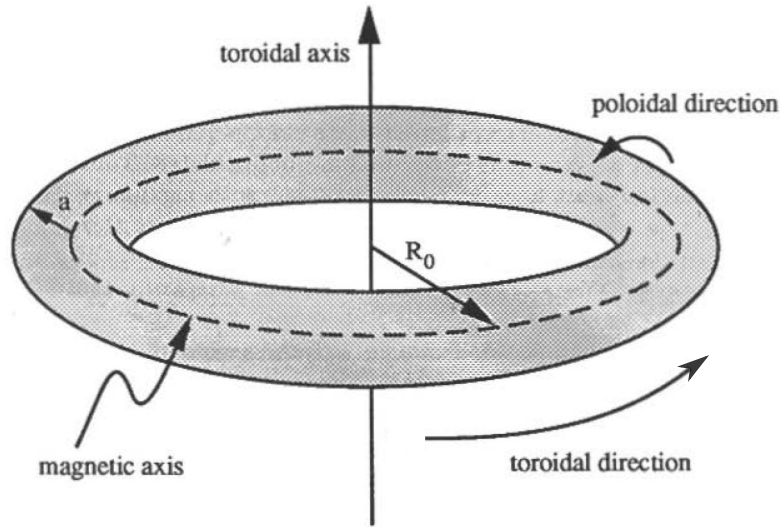


Figure 1.4: The general geometry of a toroidal magnetic confinement system [19].

The geometry of a general toroidal system is depicted in Fig. 1.4. We have also defined the **toroidal** and **poloidal** directions. The former corresponds to the direction we follow as the toroidal angle ϕ varies (i.e. the direction of the magnetic axis), while the latter lies on any plane defined by a torus cross-section for a given toroidal angle. If we consider the small and large radii of the torus a and R_0 respectively, a useful geometric parameter is the *aspect ratio of the torus*, b [2]:

$$b = \frac{R_0}{a}. \quad (1.19)$$

In the case where $b \gg 1$, the torus reduces to a z -pinch and becomes a linear confinement system.

In the subsections that follow we examine some of the most important magnetic confinement systems with which we expect to achieve controlled thermonuclear fusion.

1.3.2.1 Tokamaks

In the 1960s, the Soviet Union proposed the **Tokamak**, a closed system for achieving magnetic confinement. As we can see in Figure 1.5, this system is of toroidal geometry, and the magnetic field is helical, having two components: the toroidal B_ϕ and the poloidal B_p , with the toroidal field usually being much stronger than the poloidal one: $B_p \approx 0.1B_\phi$. The helicity of the magnetic field is a necessary condition for the confinement, as we shall see below. In essence, the Tokamak is nothing else but a transformer, generating the strong toroidal field B_ϕ mainly by means of external coils and the poloidal field B_p inductively from the plasma itself. In particular, a primary circuit is used to produce a time-varying toroidal current inductively, which in turn gives us the poloidal field. The toroidal current, in addition to generating the poloidal magnetic field, also heats the plasma ohmically [8].

A basic property of Tokamaks is **axial symmetry** (or **axisymmetry**), viz. the fact that every scalar quantity A depends solely on the variables R and Z and hence

$$A = A(R, Z) \Leftrightarrow \frac{\partial A}{\partial \phi} = 0. \quad (1.20)$$

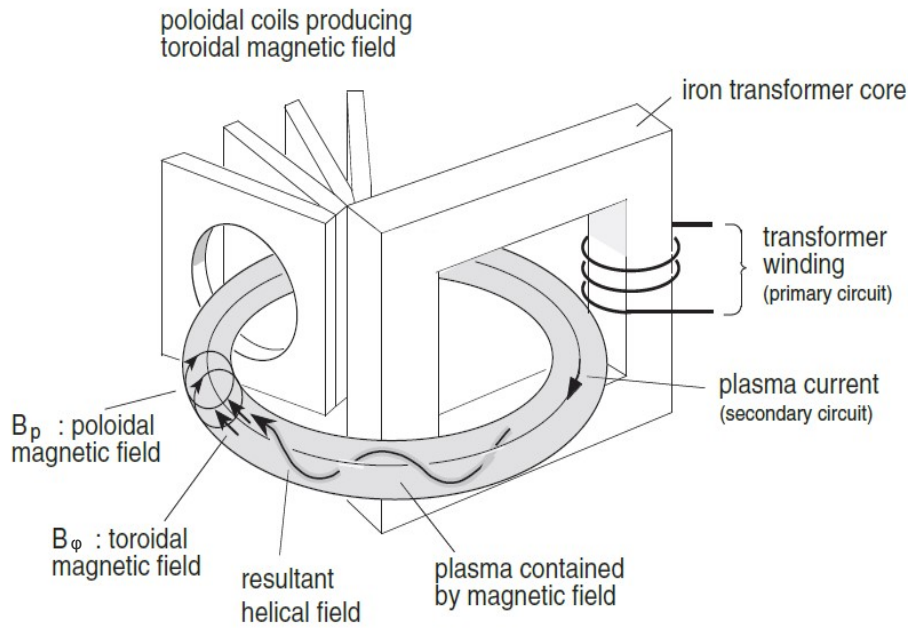


Figure 1.5: Schematic representation of the magnetic confinement in a Tokamak [8].

This basic property makes the Tokamak a two-dimensional system, as every single quantity does not depend on the toroidal angle ϕ and therefore facilitates the study of physics in it and makes its construction easier. Besides this, the plasma in Tokamaks is organised into well-defined, nested toroidal magnetic surfaces. In essence, every magnetic surface is in fact a pressure isosurface, to which the current density and magnetic field vectors lie tangentially. This is illustrated in Figure 1.6. Owing to this behaviour, we can define a *flux function* Ψ , which is the (normalised) poloidal magnetic flux,

$$\Psi = \frac{1}{2\pi} \int_S B_p dS, \quad (1.21)$$

where S is any surface on the R, ϕ plane. Each magnetic surface is characterised by a specific poloidal flux, in the sense that it has its own “ Ψ -label”, and thus we can use Ψ as a radial coordinate [18], [20].

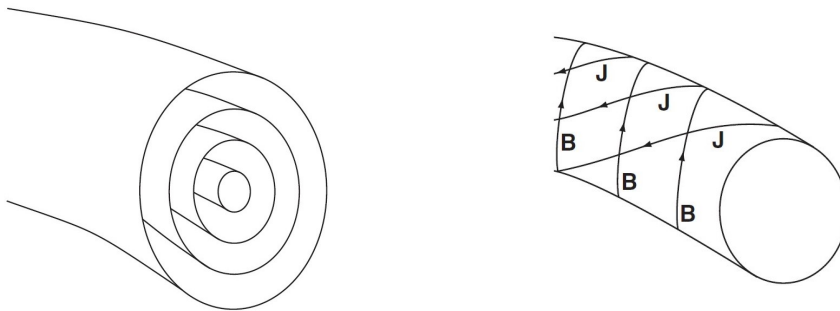


Figure 1.6: Schematic representation of the pressure isosurfaces, as well as the current density and magnetic field vectors in a Tokamak device [18].

The disadvantages of Tokamak include its pulsed operation due to transformers - which strains the system in the long run [21], its vulnerability to current-driven instabilities [22] and the fact that in Tokamaks the heating and confinement of plasma are carried out simultaneously. Moreover, in view of the behaviour of the plasma specific resistivity that is discussed

in Section 1.4.2.2, it is clear that the ohmic heating of plasma is intractable in thermonuclear temperatures.

1.3.2.2 Stellarators

In addition to the Tokamak, another closed magnetic confinement device, the **Stellarator**, had been proposed earlier. This system is also of toroidal geometry (Fig. 1.7), but in this case the magnetic field helicity is achieved exclusively by means of external helical coils.

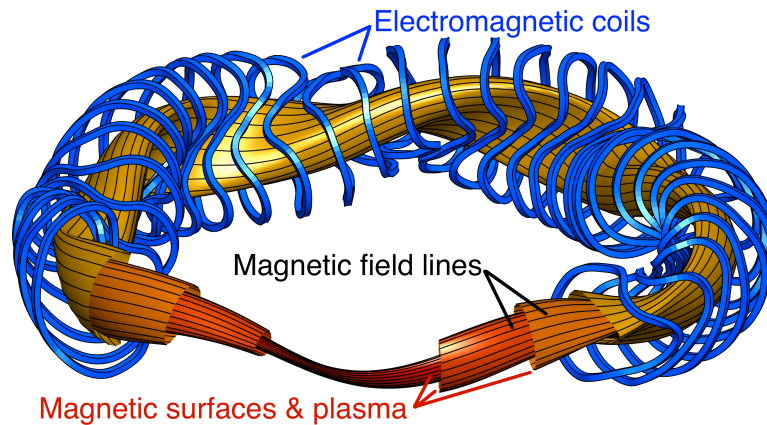


Figure 1.7: Schematic representation of the magnetic confinement in the W7-X Stellarator in Greifswald, Germany. From "Stellarators, Confining plasma with carefully shaped magnetic fields" (https://terpconnect.umd.edu/~mattland/projects/1_stellarators/)

Unlike Tokamaks, Stellarators are characterised by a lack of symmetry and therefore all reference quantities depend on all three coordinates (R, ϕ, Z) . This makes it difficult both to construct the Stellarator and to study the physics of the plasma in it. In addition, due to the lack of symmetry, the topology of the magnetic surfaces is not well defined. Another drawback is that due to the absence of the induced toroidal current, we are not given the possibility of heating the plasma ohmically. Finally, another downside has been identified in [23], namely that there are generally unconfined particle orbits regardless of the magnetic field strength. The Stellarator, however, in contrast to the Tokamak has many advantages, e.g. its operation is continuous and not pulsed, so we do not have to constantly induce a current in the plasma. Apart from that, the Stellarator is free of current-driven instabilities and the plasma is characterised by relatively high densities [24].

In general, the Tokamak - despite its drawbacks - seems to be so far the most successful and promising system in achieving the task of magnetic confinement, due to the symmetry it exhibits around its major axis. It also has enough magnetically conductive coatings to cover most instabilities. However, research does not rest on the study of the Tokamak alone. Precisely because the Stellarator exhibits greater complexity, various ideas and methods have been enlisted to study the physics and solve the problems that arise in it.

In the next subsection we proceed to study another class of toroidal systems that will be used for the needs of the current thesis.

1.3.2.3 Field-reversed configurations (FRCs) and Spheromaks

The above two fusion devices comprise the two main toroidal confinement systems that are employed for the achievement of controlled thermonuclear fusion. Nevertheless, there also exists another class of axisymmetric toroidal systems that do not require coils passing through the central penetration of the torus. These are known in the literature as *compact toroids*, and include the **Field-Reversed Configuration (FRC)** and the **Spheromak**.

The geometry of a field-reversed configuration is shown in Figure 1.8. In order to create such a fusion device, one starts from the well known *magnetic mirror* configuration, viz. a magnetic field which exhibits a variation of its magnitude along the direction of the field lines (in other words, $\nabla B \parallel B$). Let us suppose that inside the mirror there exists plasma of cylindrical arrangement, and that we induce a toroidal current in some way, with such direction that it produces a poloidal magnetic field that opposes the other, external one. In that manner, the configuration *reverses* the magnetic field, and hence its name.

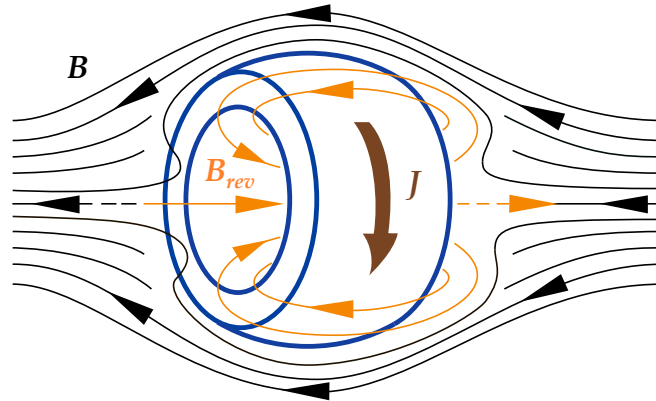


Figure 1.8: Schematic representation of a field-reversed configuration: a toroidal electric current (brown arrow) is induced inside a cylindrical plasma (blue region), creating a poloidal magnetic field (orange), reversed with respect to the direction of the externally applied magnetic field (black). From Wikipedia: https://en.wikipedia.org/wiki/Field-reversed_configuration#/media/File:Field-Reversed_Configuration.svg

It is evident from Figure 1.8 that FRCs have no toroidal magnetic field; the plasma is confined solely by a poloidal magnetic field. This in turn means that the said configurations have a technological structure much simpler than the conventional toroidal systems. In addition, FRCs are by their very nature inherently pulsed devices, in contrast to Tokamaks which need external transformers in order to create the toroidal current [7].

The class of compact toroids also includes the so-called Spheromak, which is nothing else than a field-reversed configuration *with* an internal toroidal magnetic field. This field may have the same or the opposite direction with the toroidal plasma flow. The difference between a Spheromak and a FRC is illustrated in Fig. 1.9.

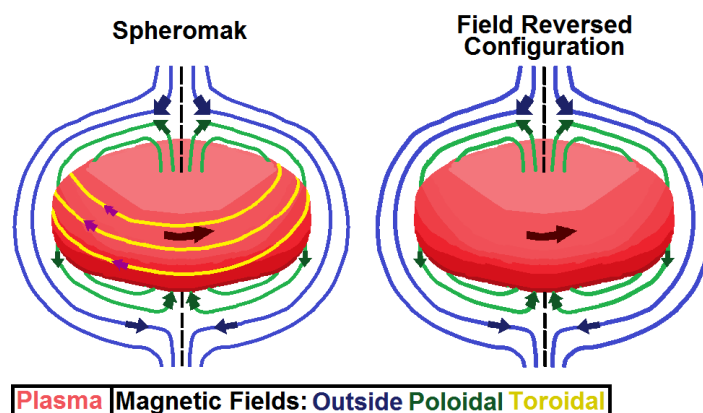


Figure 1.9: A comparison between Spheromaks and field reversed configurations. From Wikipedia: https://en.wikipedia.org/wiki/Spheromak#/media/File:A_comparison_of_an_FRC_and_A_Spheromak.png

Finally, it should be stressed that although both of the said toroids are compact, the plasma is still organised in toroidal geometry and as a matter of fact, configurations with closed and nested magnetic surfaces can be constructed.

Apart from the toroidal systems mentioned above, numerous other devices have been proposed for the magnetic confinement of plasma, the analysis of which, however, is beyond the scope of this thesis.

1.3.3 Theorems for the magnetic confinement of plasma

It turns out that for the successful confinement of plasma, one must be aware of certain theorems that should hold at all times. In this section we briefly discuss those theorems, as well as their proofs.

The necessity of magnetic field helicity mentioned earlier is summarised in the following theorem:

Theorem 1. *There exists no static ⁶ equilibrium state that can be achieved with a purely toroidal or purely poloidal magnetic field.*

Proof. Let us suppose that the magnetic field is purely toroidal. Due to the transverse variation of the magnetic field, the charges separate, thus creating a vertical electric field. Therefore, the plasma moves towards the walls due to the subsequent $E \times B$ drift [2], as shown in Fig. 1.10. With a purely poloidal field, confinement is not achieved due to kink instability [8].

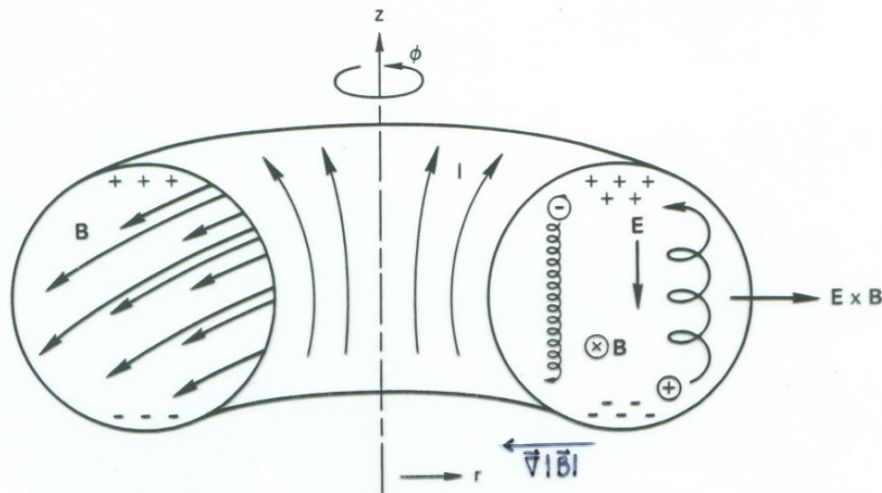


Figure 1.10: Necessity for the helicity of the magnetic field for a purely toroidal field.

Another useful theorem, also known as the Shafranov's Virial theorem [25], is the following:

Theorem 2. *There exists no equilibrium state where the plasma is self-confined, i.e. part of the magnetic field must be generated by external coil currents.*

The proof of this theorem is presented in [18]. Finally, one might wonder why we use magnetic fields and not electric fields to confine the plasma. The answer is given by the following theorem:

Earnshaw's Theorem. *A charged particle cannot be kept in stable equilibrium only by electrostatic forces.*

⁶The term *static* refers to the assumption of zero flow.

Proof. Consider an arrangement of point charges as in Figure 1.11, where the charges are placed at the vertices of a cube.

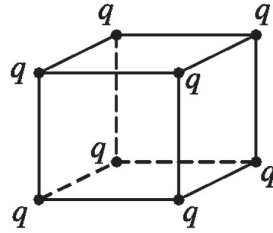


Figure 1.11: Point charges in cubic arrangement [26].

At first glance, it seems that a homonymous charge in the centre of the cube would be held there, equally repelled by the other charges. In order to have a stable equilibrium, we would need the scalar potential ϕ to present a local minimum at this point (the centre of the cube). However, due to the fact that the Laplace equation does not tolerate local maxima or minima [26], this point that appears to be a point of stable equilibrium is actually a *saddle point*.

1.4 Plasma modelling

Since a plasma is a collection of charged particles of different species that exhibit collective behavior while being influenced mainly by the electromagnetic forces - whether externally applied or generated by the plasma per se - the need for a framework that describes the interaction between such sources and the electromagnetic fields arises. As far as the electromagnetic fields are concerned, they are given to us via the so-called field equations, which read - if we employ SI units - in the Minkowski space $\mathbb{R}^{1,3}$:

$$\partial_\mu F^{\mu\nu} = \mu_0 J^\nu, \quad \text{and} \quad \partial_\mu G^{\mu\nu} = 0, \quad (1.22)$$

where $J^\nu = (\frac{s}{\epsilon_0}, J_1, J_2, J_3)$ is the four-current, with s being the charge density and J_i the three spacial current density components, $F^{\mu\nu}$ is the field tensor and $G^{\mu\nu} = \epsilon^{\mu\nu\rho\sigma} F_{\rho\sigma}$ is the Poincaré dual tensor, $\partial_\mu = (\epsilon_0 \partial_t, \nabla)$ is the four-derivative, and μ_0 is the vacuum permeability [27]. In ordinary vector form, equations (1.22) reduce to

$$\nabla \cdot \mathbf{E} = \frac{s}{\epsilon_0} \quad (\text{Gauss's Law}), \quad (1.23)$$

$$\nabla \cdot \mathbf{B} = 0 \quad (\text{Absence of magnetic monopoles}), \quad (1.24)$$

$$\nabla \times \mathbf{E} = -\frac{\partial \mathbf{B}}{\partial t} \quad (\text{Faraday's law}), \quad (1.25)$$

$$\nabla \times \mathbf{B} = \mu_0 \mathbf{J} + \mu_0 \epsilon_0 \frac{\partial \mathbf{E}}{\partial t} \quad (\text{Ampère-Maxwell law}). \quad (1.26)$$

Eqs. (1.23)-(1.26) tell us how the charge density $s(\mathbf{r}, t)$ and current density $\mathbf{J}(\mathbf{r}, t)$ produce the fields \mathbf{E} and \mathbf{B} . But in order to perceive *how the fields affect the charges*, we need the Lorentz force, which in SI units reads

$$\mathbf{F} = q(\mathbf{E} + \mathbf{v} \times \mathbf{B}), \quad (1.27)$$

where \mathbf{v} is the velocity of the moving charged particle q . Eqs. (1.23)-(1.26), along with the Lorentz force (1.27) summarise the whole theoretical milieu of classical electrodynamics and describe all its phenomena. At first glance, one notices that Maxwell's equations are nothing

else but differential equations, and as such, they must be accompanied by the appropriate boundary conditions, reflecting the physics of the problem at hand [26]. Note though that here the problem of self-consistency arises, in the sense that the motions of the charged particles (sources) generate extra fields that are to be taken into account in Maxwell equations. Hence, it becomes quite clear that one needs a self-consistent theory that describes the interaction between matter and electromagnetic fields. Plasma physics aims to bridge this gap, by providing such self-consistent frameworks for the plasma, while ensuring closure for the system of equations at hand. Below we present the most notable categories of plasma models, along with the Hall Magnetohydrodynamics (Hall MHD) model that will be used extensively in the current thesis.

1.4.1 From kinetic to fluidistic description

Owing to the collective behaviour and the large number of charged particles that comprise plasmas, it is evident that keeping track of every single particle motion is practically impossible. Furthermore, it is clear that in this case the initial conditions cannot be known with sufficient accuracy [28]. For these reasons we may adopt a statistical model of description that relies on the *distribution function* $f_\alpha(\mathbf{r}, \mathbf{v}, t)$ for each of the particle species α that comprise the plasma. This function contains information about how the particles distribute in the 6-dimensional phase space (\mathbf{r}, \mathbf{v}) at a given instance t . The evolution of the distribution function is given by the so-called Vlasov equation [29], [30]:

$$\frac{\partial f_\alpha}{\partial t} + \mathbf{v} \cdot \nabla_{\mathbf{x}} f_\alpha + \frac{q_\alpha}{m_\alpha} (\mathbf{E} + \mathbf{v} \times \mathbf{B}) \cdot \nabla_{\mathbf{v}} = 0, \quad (1.28)$$

which is a direct consequence of the Liouville theorem [31]. If collisions are present, relation (1.28) is modified to the so-called Boltzmann equation [2], [31]:

$$\frac{\partial f_\alpha}{\partial t} + \mathbf{v} \cdot \nabla_{\mathbf{x}} f_\alpha + \frac{q_\alpha}{m_\alpha} (\mathbf{E} + \mathbf{v} \times \mathbf{B}) \cdot \nabla_{\mathbf{v}} = \mathcal{C}[f_\alpha], \quad (1.29)$$

where $\mathcal{C}[f_\alpha]$ is the collision operator that is associated with the evolution of the distribution function due to the particle collisions [2], [28], [31]. The sources (charge and current densities) are found as

$$s(\mathbf{r}, t) = \sum_{\alpha} q_\alpha n_\alpha, \quad \text{and} \quad \mathbf{J}(\mathbf{r}, t) = \sum_{\alpha} q_\alpha n_\alpha \mathbf{v}_\alpha, \quad (1.30)$$

while the number density of the species α is given from the distribution function

$$n_\alpha(\mathbf{r}, t) = \int f_\alpha(\mathbf{r}, t) d^3v. \quad (1.31)$$

Solving the system of equations (1.23)-(1.26) along with (1.30), (1.31) and either (1.28) or (1.29) is by all means a very complicated task to be carried out, even via exploiting numerical schemes. Therefore, we usually resort to simplified models of description, such as the fluid ones. In fact, by taking the velocity moments of the Vlasov equation we end up at the well-known two-fluid equations [28]. By performing this reduction, the microscopic motions are eliminated by averaging out all of the physical quantities. This is an ample approximation when we study most laboratory or astrophysical plasmas. On the other hand, in spite of the adequacy of the fluid models, one may have to resort to kinetic descriptions, since Vlasov equation provides a proper basis for studying wave-particle interactions [32], [33], plasmas in astrophysical environments [31], weakly magnetised, high temperature plasmas [28], [34], [35] etc. The subsection that follows moves on to consider the importance and present the basic principles of the Magnetohydrodynamics model.

1.4.2 The Magnetohydrodynamics (MHD) model

In a fully ionised plasma where low characteristic frequencies are involved, both electrons and ions can respond simultaneously at any change in the kinetic state of the plasma, and hence the motions of ions and electrons are coupled. In that case, we may consider the plasma to behave as a single, magnetised, electrically conducting fluid (Magnetohydrodynamics - MHD). MHD can be derived from the two-fluid theory (model) which in turn is less fundamental than kinetic theory. Its detailed derivation is given in [8] - here we will content ourselves with presenting its basic assumptions and equations. The reason behind this is to generalise the MHD model later for the needs of the current thesis.

1.4.2.1 Basic assumptions and formulation

MHD provides a proper framework for the study of many astrophysical and even laboratory plasmas. This is indeed the case, when:

1. The characteristic length scale L of our system is much larger than the Debye length and other microscopic lengths such as the the ion and electron Larmor radii and skin depths: $L \gg \lambda_D, r_{Ls}, d_s$, where $s = i, e$.
2. The characteristic time scales involved are much longer than the inverses of the plasma and Larmor frequencies: $\tau \gg \omega_{ps}^{-1}, \omega_{cs}^{-1}$, where $s = i, e$.
3. The characteristic speed (and thus the Alfvén speed) is small compared to the speed of light: $v_A \ll c$, and hence the displacement current in Ampère-Maxwell law (1.26) can be neglected.

It is evident that the assumption $L \gg \lambda_D$ implies quasineutrality, as discussed in Section 1.2.1, while $L \gg r_{Ls}, d_s$ and the second assumption are necessary in order that two-fluid effects can be neglected. The reason why the third assumption implies the neglect of the displacement current can be seen by making an order-of-magnitude estimate for the different terms in (1.26), considering the characteristic length and time scales, L and T respectively:

$$\mu_0 \epsilon_0 \frac{\partial E}{\partial t} = \frac{1}{c^2} \frac{\partial E}{\partial t} \sim \frac{1}{c^2} \frac{L v B}{T L} \sim \left(\frac{v}{c}\right)^2 \frac{B}{L} \ll |\nabla \times \mathbf{B}| \sim \frac{B}{L}, \quad (1.32)$$

[8], [28]. The third assumption is also interconnected with quasineutrality, which is discussed in [28]. The above assumptions end up at the following equations

$$\frac{\partial \rho}{\partial t} + \nabla \cdot (\rho \mathbf{v}) = 0 \quad (\text{Equation of continuity}), \quad (1.33)$$

$$\rho \left[\frac{\partial \mathbf{v}}{\partial t} + (\mathbf{v} \cdot \nabla) \mathbf{v} \right] = \mathbf{J} \times \mathbf{B} - \nabla P + \rho \mathbf{g} \quad (\text{Momentum equation}), \quad (1.34)$$

$$\mathbf{E} + \mathbf{v} \times \mathbf{B} = \eta \mathbf{J} \quad (\text{Ohm's law}), \quad (1.35)$$

$$\nabla \cdot \mathbf{B} = 0 \quad (\text{Absence of magnetic monopoles}), \quad (1.36)$$

$$\nabla \times \mathbf{B} = \mu_0 \mathbf{J} \quad (\text{Ampère's law}), \quad (1.37)$$

$$\nabla \times \mathbf{E} = -\frac{\partial \mathbf{B}}{\partial t} \quad (\text{Faraday's law}), \quad (1.38)$$

$$\text{Equation of state: } \begin{cases} P \propto \rho^\gamma & (\text{Adiabatic}), \\ P \propto \rho & (\text{Isothermal}) \end{cases}. \quad (1.39)$$

Eqs. (1.33)-(1.39) describe a single-fluid plasma of mass density ρ and velocity \mathbf{v} , with an isotropic (i.e. zeroth order tensor - scalar) pressure P . The gravitational force per unit volume $\rho \mathbf{g}$ will be henceforth omitted since it is insubstantial for laboratory plasmas. We also stress that eqs. (1.39), along with the incompressibility condition of the velocity field, are just

simplifications for isentropic processes, useful in the scope of analytic approaches. In the case where one wishes to be more precise, as in numerical calculations, an *energy equation* should be taken into account, that describes the conservation of entropy [8]. Last but not least, the behaviour of the plasma specific resistivity η is examined in detail in Section 1.4.2.2.

It is also worth mentioning that we may combine Faraday's law (1.38) with Ohm's law (1.35), to end up at an equation that describes the temporal variation of the magnetic field. Truly, after some basic vector calculus manipulations, we end up at

$$\boxed{\frac{\partial \mathbf{B}}{\partial t} = \frac{\eta}{\mu_0} \nabla^2 \mathbf{B} + \nabla \times (\mathbf{v} \times \mathbf{B})}, \quad (1.40)$$

which is the so-called *induction equation* for the magnetic field [5]. This equation is very important since it describes the ways in which the magnetic field \mathbf{B} can change, as a result of its interaction with the plasma. On the one hand, the first term of the RHS of relation (1.40) links the temporal change of the magnetic field with the spacial change of the field and the plasma conductivity, and is known in the literature as the *diffusion term*. On the other hand, the second term of the RHS of the equation in question shows us that the the magnetic field may vary in time due to plasma motions [5].

The equations of Magnetohydrodynamics (1.33)-(1.39) are a system of 7 coupled differential equations with partial derivatives, which describe non-relativistic phenomena in low-frequency plasmas and must be solved self-consistently [8].

1.4.2.2 Spitzer's law - Ideal Magnetohydrodynamics

As we saw in the previous section, the specific resistivity of plasma emerges in Ohm's law. Being already aware of the behaviour of the resistivity in metal conductors, one would expect intuitively that as we increase the temperature, the resistivity will also increase. This picture is reversed in the plasma, where in fact the opposite is true - *the specific resistance decreases with temperature*. This behaviour is described by Spitzer's law [36], [37]:

$$\eta \approx \frac{\pi e^2 m_e^{1/2}}{(4\pi\epsilon_0)^2 (k_B T_e)^{3/2}} \ln \Lambda, \quad (1.41)$$

where $\ln \Lambda$ is a constant called the *Coulomb logarithm* [8]. More simply, we may write

$$\eta \propto T_e^{-3/2}. \quad (1.42)$$

We can attribute this resistivity behaviour to the Coulomb scattering that takes place between electrons and ions in the plasma. Relation (1.41) informs us that as the plasma heats up, the Coulomb scattering cross section decreases and as a result the resistivity decreases relatively rapidly with increasing temperature. For sufficiently large temperatures, we have in essence a collisionless plasma and hence we can set $\eta \simeq 0$. Because of this resistivity behavior, it is impossible to heat the plasma ohmically (i.e., with currents) at very high temperatures, because as we increase the temperature, the plasma becomes collisionless. In particular, for temperatures from 1 keV and above the plasma becomes such a good conductor that ohmic heating is a slow and inefficient process [2].

So in the case where sufficiently high temperatures prevail, which as we saw are necessary for thermonuclear fusion reactions to take place, the plasma is sufficiently conductive and thus we can set the resistivity equal to zero. Ohm's law then becomes

$$\mathbf{E} + \mathbf{v} \times \mathbf{B} = 0, \quad (1.43)$$

and then the model is called **Ideal Magnetohydrodynamics (Ideal MHD)** [8].

1.4.2.3 Alfvén’s theorem - Comparing ideal with non-ideal models

The behaviour of the plasma resistivity at thermonuclear temperatures - besides setting the right-hand side of (1.35) equal to zero - has another unexpected consequence, which is summarised in the so-called **Alfvén’s theorem**: “In a fluid with infinite electrical conductivity, the magnetic field lines are ‘frozen-in’ the fluid and move with it.” [38]. In fact, Alfvén in 1943 argued that “in view of the infinite conductivity, every motion (perpendicular to the field) of the liquid in relation to the lines of force is forbidden because it would give infinite eddy currents”. This means that, given a surface \mathcal{S} , the magnetic flux Φ_B passing through it is constant as the surface moves with the plasma:

$$\frac{d\Phi_B}{dt} = 0 \Leftrightarrow \int_{\mathcal{S}} \mathbf{B} \cdot d\mathbf{S} = \text{const.} \quad (1.44)$$

The qualitative interpretation of eq. (1.44) is that two scenarios may occur: either the plasma will move parallel to the magnetic field lines (when the energy density of the plasma is much lower than the energy density of the magnetic field), or the plasma will drag and deform the field lines as it moves (in the opposite case) [5]. Due to Spitzer’s law, (1.42), this property of “frozen-in” field lines is better satisfied the higher the temperature. In fusion plasmas with temperatures of the order of 10 keV the above-mentioned “freezing” is an extremely good approximation, which is why Ideal MHD satisfactorily describes much of the phenomena occurring in it. As the temperature decreases however, the magnetic field acquires an independent motion and the above constraint is removed. Then, the magnetic field lines can break and reconnect through the process of **magnetic reconnection** [4], [5]. This very important physical process is depicted in Figure 1.12, where we see the magnetic field lines breaking and reconnecting when a localised diffusion region (shaded) causes a shift in plasma element connectivity (AB to AC). In most reconnection scenarios, the crucial parameter is the so-called *reconnection rate*. Many models have been proposed that address this issue, in the context of solar flares, Coronal Mass Ejections (CMEs), magnetic flux emergence etc. [39], [40], [41]. In the case when reconnection occurs, one should use MHD with finite resistivity (also called *resistive MHD*), that takes into account the $\eta \mathbf{J}$ term in the RHS of Ohm’s law (1.35) as well as the diffusion term in the induction equation (1.40).

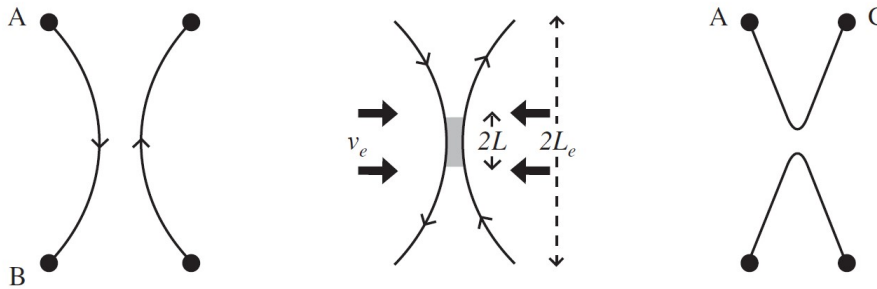


Figure 1.12: Schematic representation of the magnetic reconnection process on a typical scale of $2L_e$. $2L$ is the scale of the diffusion region (shaded), while v_e is the inflow plasma velocity [5].

The above finding (1.44) is remarkable, because it guarantees that the topology of the magnetic field cannot change during any physically allowed ideal MHD motion. In this thesis we will adopt the above assumption as it is satisfactory for the high temperatures that are necessary for fusion reactions.

Before closing this section, we wish to stress another important aspect stemming from the plasma resistivity. More specifically, it is evident that the inclusion of the resistivity term $\eta \mathbf{J}$ in Ohm’s law (1.35), provides a means for the energy to *dissipate*; namely, via ohmic heating.

There are many such mechanisms in laboratory and astrophysical plasmas that lead to energy dissipation, such as Landau damping⁷ [2], turbulence, described by Kolomgorov theory and further generalised for the case of MHD [42], [43], shock waves [4], [5], wave-particle interactions [32], [33], etc. Nonetheless, due to the severe complexity introduced, in the current thesis we will refrain from assuming that such mechanisms are present.

1.4.3 The Hall Magnetohydrodynamics (Hall MHD) model

MHD is a very popular and a widely employed model; it describes pretty satisfactorily the majority of phenomena that involve plasma in our universe. Nevertheless, it is apparent that when one omits the two-fluid nature of plasma and treats the latter as *one* electrically conducting fluid, much of its physics and interesting effects are lost upon this simplification. To make this better understood, in the subsections that follow we will generalise the ordinary MHD model so as to incorporate two-fluid effects. Afterwards, we will introduce the normalization scheme that will be used exclusively thereafter and finally we will deduce the Hall MHD model - which is the key model of description of this thesis - from the more generic Extended MHD (XMHD) model.

1.4.3.1 Two-fluid generalisation of the ideal MHD model

Instead of writing down the two-fluid equations, we may take the first step towards establishing a two-fluid generalisation of ideal MHD by defining a center of mass velocity for our **quasineutral** (1.7) plasma, which is characterised by a mass $m = m_i + m_e$ and a mass density $\rho = nm = n(m_i + m_e)$

$$\mathbf{v} = \frac{1}{\rho} (n_i m_i \mathbf{v}_i + n_e m_e \mathbf{v}_e) \stackrel{(1.7)}{=} \frac{m_i \mathbf{v}_i + m_e \mathbf{v}_e}{m_i + m_e}, \quad (1.45)$$

which is similar conceptually with the respective MHD one-fluid velocity. The current density of the plasma reads

$$\mathbf{J} = en(\mathbf{v}_i - \mathbf{v}_e). \quad (1.46)$$

Note that although the quantities m , ρ and \mathbf{v} are one-fluid ones, they actually refer to a *two-fluid plasma*. If we now multiply the two-fluid continuity equations with the corresponding masses, then add the results and use eq. (1.45), we end up at a single fluid continuity equation of the form

$$\frac{\partial \rho}{\partial t} + \nabla \cdot (\rho \mathbf{v}) = 0, \quad (1.47)$$

which describes the conservation of fluid mass. The way to proceed to a single-fluid momentum equation is to notice that

$$\mathbf{v}_e = \mathbf{v} - \frac{m_i}{m} \frac{\mathbf{J}}{en}, \quad (1.48)$$

$$\mathbf{v}_i = \mathbf{v} + \frac{m_e}{m} \frac{\mathbf{J}}{en}, \quad (1.49)$$

which are found by combining eqs. (1.45) and (1.46). If we further add the two-fluid momentum equations, the result reads

$$\frac{\partial \mathbf{v}}{\partial t} = \mathbf{v} \times (\nabla \times \mathbf{v}) + \frac{m_i m_e}{m^2} \frac{\mathbf{J}}{en} \times \nabla \times \frac{\mathbf{J}}{en} - \nabla \left(P + \frac{|\mathbf{v}|^2}{2} + \frac{m_i m_e}{2m^2} \left| \frac{\mathbf{J}}{en} \right|^2 \right) + (mn)^{-1} \mathbf{J} \times \mathbf{B}, \quad (1.50)$$

⁷Yet this dissipation mechanism is *collisionless*.

where $P = P_i + P_e$ is the total pressure of the plasma, given by Dalton's law. The next equation of this generalised two-fluid model is obtained if we multiply the ion momentum equation by m_e and the electron momentum equation by m_i and then subtract the resulting equations. We find

$$\begin{aligned} E + v \times B^* &= \frac{m_i m_e}{em} \left[\frac{\partial}{\partial t} \left(\frac{J}{en} \right) - \right. \\ &- \frac{J}{en} \times (\nabla \times v) + \nabla \left(\frac{v \cdot J}{en} + \frac{m_e^2 - m_i^2}{2m^2} \left| \frac{J}{en} \right|^2 \right) \left. \right] - \\ &- \frac{m_e^2 - m_i^2}{m^2} \left(\frac{J}{en} \times B^* \right) + \frac{1}{men} \nabla (m_e P_i - m_i P_e), \end{aligned} \quad (1.51)$$

where B^* is a "generalised magnetic field", modified by electron inertia

$$B^* = B + \frac{m_i m_e}{em} \left(\nabla \times \frac{J}{en} \right). \quad (1.52)$$

Eq. (1.51) is essentially a generalised Ohm's law, since it relates the electric field E with the current density J . We can also deduce an induction equation, similar to (1.40), by combining the generalised form of Ohm's law (1.51) with Faraday's law (1.25)

$$\begin{aligned} \frac{\partial B^*}{\partial t} &= \nabla \times \left[v \times B^* + \frac{m_i m_e}{em} \frac{J}{en} \times (\nabla \times v) + \frac{m_e - m_i}{m} \frac{J}{en} \times B^* \right] + \\ &+ \frac{1}{emn^2} \nabla n \times (m_e \nabla P_i - m_i \nabla P_e). \end{aligned} \quad (1.53)$$

1.4.3.2 Alfvén normalisation scheme

The above equations comprise the so-called **Extended Magnetohydrodynamics (XMHD) model**, and describe a *two-fluid* quasineutral plasma in a similar fashion as the MHD model does [28]; however with significantly greater complexity. In most cases, we are interested in a reduced form of the above model, depending of the system that we examine. In order to perform such a reduction, it is often preferable to normalise the equations in question. For this scope, we will employ the so-called Alfvén normalisation scheme, that reads as follows

$$\begin{aligned} \bar{B} &= B/B_0, \quad \bar{v} = v/v_A, \quad \bar{J} = J/(B_0/L_0\mu_0), \quad \bar{E} = E/(v_A B_0), \\ \bar{\nabla} &= L_0 \nabla, \quad \bar{R} = R/L_0, \quad \bar{Z} = Z/L_0, \quad \bar{P} = P/(B_0^2/\mu_0), \\ \bar{t} &= t/\tau_A, \quad \bar{n} = n/n_0, \end{aligned} \quad (1.54)$$

where L_0 is the reference length scale, B_0 is the reference magnetic field, n_0 is the reference number density of the quasineutral plasma, $v_A = B_0/\sqrt{\mu_0 m n_0}$ is the Alfvén speed and finally $\tau_A = L_0/v_A$ is the Alfvén time. Quantities with bars are dimensionless, while the physical ones (viz. with dimensions) are without bars. Henceforth, we will omit the bars for notational economy, on the understanding that all appearing quantities are normalized as described above.

Thus, eqs. (1.50) and (1.51) are modified [28] after the prescribed normalisation (1.54) as

$$\frac{\partial v}{\partial t} = -\nabla \left(P + \frac{|v|^2}{2} - \frac{d_e^2 |J|^2}{2 \rho^2} \right) + v \times (\nabla \times v) + J \times B^*, \quad (1.55)$$

$$\begin{aligned} E + v \times B &= d_i \frac{J \times B^*}{\rho} - d_i \frac{\nabla P_e}{\rho} + \\ &+ d_e^2 \left[\frac{\partial}{\partial t} \left(\frac{J}{\rho} \right) - \rho^{-1} J \times (\nabla \times v) + \nabla \left(\frac{v \cdot J}{\rho} - \frac{d_i |J|^2}{2 \rho^2} \right) \right]. \end{aligned} \quad (1.56)$$

The induction equation (1.53) can also be normalised, considering that the pressure only depends on the mass density (barotropic plasma), as

$$\frac{\partial \mathbf{B}^*}{\partial t} = \nabla \times \left(\mathbf{v} \times \mathbf{B}^* - d_i \frac{\mathbf{J} \times \mathbf{B}^*}{\rho} + d_e^2 \frac{\mathbf{J} \times \nabla \times \mathbf{v}}{\rho} \right), \quad (1.57)$$

where the generalised magnetic field now reads

$$\mathbf{B}^* = \mathbf{B} + d_e^2 \nabla \times \frac{\mathbf{J}}{\rho}. \quad (1.58)$$

At this point it is evident that the normalisation of the equations has shed light to another important aspect of the XMHD model; *the new terms that have appeared in the RHS of (1.56) compared to the simpler ideal MHD form of Ohm's law (1.43) give rise to new physics in our system.* More specifically, the first term in the RHS of (1.56) is the so-called **Hall term**, and is intimately connected with the Hall effect that occurs when we place a flow of charges (that is, a current \mathbf{J}) in a magnetic field \mathbf{B} . The second term is the electron pressure term, while the last term is related to electron inertia⁸. It is further noteworthy that *each of these terms "enter in" at a different length scales*: the first two terms enter in at the so-called (normalised) **ion skin depth**⁹ d_i

$$d_i = \frac{c}{\omega_{p_i} L_0}, \quad \text{where} \quad \omega_{p_i} = \left(\frac{n_0 e^2}{\epsilon_0 m_i} \right)^{1/2} \quad \text{is the plasma frequency for the ions,} \quad (1.59)$$

and is the characteristic length scale for ions to be accelerated by electromagnetic forces in a plasma. On the other hand, the last term at the RHS of eq. (1.56) enters in at the (normalised) **electron skin depth** d_e , defined in a similar fashion as

$$d_e = \frac{c}{\omega_{p_e} L_0}, \quad \text{where} \quad \omega_{p_e} = \left(\frac{n_0 e^2}{\epsilon_0 m_e} \right)^{1/2} \quad \text{is the plasma frequency for the electrons.} \quad (1.60)$$

In the case where $L_0 \lesssim d_i$, the ion fluid becomes detached from the electron one and attains a separate motion with velocity \mathbf{v}_i . The magnetic field however remains frozen in the electron fluid, so Alfvén's theorem holds for the latter. This model is known as **Hall Magnetohydrodynamics (Hall MHD)** and is one of the simplest two-fluid models for describing plasmas [2], [45], [46]. In the even more extreme case concerning length scales $L_0 \lesssim d_e$, then even the electron fluid becomes detached from the magnetic field. This is the case in **Extended Magnetohydrodynamics (XMHD)** where we further incorporate the inertia of electrons [28].

1.4.3.3 Reduction to Hall MHD

At this point we may take a step to further restrict our study in the scope of Hall MHD. In this regard, we will assume that the electron inertia term is negligible (massless electrons), which translates to $m_e \rightarrow 0$ or in view of the normalised equations as $d_e \rightarrow 0$. This is usually a very good approximation, since $d_i \approx 43 d_e$ [45]. In this case, owing to (1.49), the velocity of the ion fluid is equivalent to the center of mass velocity: $\mathbf{v}_i \equiv \mathbf{v}$. Furthermore, only the ion fluid contributes to the total mass: $m \equiv m_i$, and as concerns the normalised densities, one can notice that $\rho \equiv n$. Moreover, the "generalised magnetic field" due to electron inertia reduces to our ordinary magnetic field \mathbf{B} . In view of these assumptions, the generalised Ohm's law (1.56) reduces to

$$\mathbf{E} + \mathbf{v} \times \mathbf{B} = \frac{d_i}{\rho} (\mathbf{J} \times \mathbf{B} - \nabla P_e). \quad (1.61)$$

⁸A relative comparison between the different terms of the generalised Ohm's law is carried out in [44].

⁹Also called ion inertial length.

For the needs of the current thesis, we will also assume that the density is constant: $\rho = 1$ and then the above equation (1.61) further reduces to

$$E + v \times B = d_i(J \times B - \nabla P_e) \quad (\text{Ohm's law}). \quad (1.62)$$

Furthermore, equations (1.55) and (1.57) reduce respectively to

$$\frac{\partial v}{\partial t} = -\nabla \left(P + \frac{|v|^2}{2} \right) + v \times (\nabla \times v) + J \times B \quad (\text{Momentum equation}), \quad (1.63)$$

and

$$\frac{\partial B}{\partial t} = \nabla \times [v \times B - d_i(J \times B)] \quad (\text{Induction equation}). \quad (1.64)$$

Finally, in view of the continuity equation (1.47), a constant density $\rho = 1$ automatically implies incompressibility of the ion velocity field, viz.

$$\nabla \cdot v = 0 \quad (\text{Incompressible ion flow}). \quad (1.65)$$

Equations (1.62)-(1.65), along with the Maxwell equations (1.36) and (1.37) are the building blocks of our model, and govern the physics of the phenomena that are to be studied in the current thesis.

1.5 Motivation and aim

From the previous sections it has been established that the Hall MHD model is employed - as a "zeroth-order approximation" - when we want to distinguish the electron from the ion fluid in our plasma. A more thorough approach would however be to examine whether the criterion for the validity of our model is satisfied for our physical system in question, that is fusion plasmas. In order for this framework to be consistent, the necessary condition is to encounter length scales of the order of the ion skin depth d_i (1.59), as mentioned above. Therefore, one may justifiably wonder whether such length scales could be sought in fusion devices. The answer to this is positive, for there exist numerous scenarios where small length scales are involved; many of those phenomena concern strong gradients of physical quantities and even play a leading role in the successful confinement of plasma. Perhaps the most notable example is the so-called Low-to-High-confinement mode transition (L-H transition) [47], [48], first observed experimentally in the ASDEX Tokamak in 1982. This transition occurs when a fusion plasma is heated by neutral beams and a specific power threshold is exceeded. The result is a significant decrease in the outward radial diffusion of the plasma and a subsequent increase in the energy confinement time¹⁰. This improvement is related to the creation of a transport barrier (also known as *pedestal*) near the plasma boundary, wherein sheared poloidal flows [49], [50] have been observed, associated with the development of a spontaneous radial electric field. Accordingly, the plasma pressure remains almost constant in the inner regime and decreases steeply in the pedestal region, thus a strong pressure gradient is formed therein. It was also observed that the plasma was lost in bursts called Edge Localised Modes (ELMs), a kind of instability that still remains not well understood [2]. It is now clear that if one wishes to examine ELMs or steep pressure gradients - like the ones developing in L-H transitions - it is imperative to resort to the Hall MHD model since the gradient length scales are of the order

¹⁰In fact, most Tokamaks today operate in the H-mode regime [2].

of the ion skin depth. Moreover, it should be noted that Hall effects are capable of causing the so-called tearing mode instability [51], which occurs in both laboratory and astrophysical environments. From a more general point of view, this model is also suitable for the study of transport in fusion plasmas, like neoclassical diffusion [2], [52].

To further acknowledge the importance of the Hall MHD model in controlled thermonuclear fusion, we stress that the neglect of the Hall term in magnetic confinement devices has been previously criticised in [53], by stating that “the Hall-current effect is much more important than the electrical resistivity whenever the magnetic field is so large that the gyro-frequency of electrons greatly exceeds their collision frequency”. A similar argument concerning ion inertial terms has been raised in [54], where it is explicitly noted that the Hall term cannot be neglected in Tokamaks.

Finally, the Hall MHD model consists an adequate - and sometimes mandatory! - framework for the description of several phenomena in astrophysical plasmas. More specifically, Hall MHD has shed light to the interpretation of fast magnetic reconnection in astrophysical plasmas, particularly in solar flares and planetary magnetospheres [5], [45], [55]. The fact that magnetic reconnection is described by a two-fluid plasma model was also corroborated by in situ measurements of the magnetic reconnection that takes place in Earth’s magnetosphere [56]. The usefulness of Hall MHD is not limited to the above examples; the interested reader is referred to [57] for even more examples of astrophysical systems described by Hall MHD, like dense molecular clouds, protostellar disks and neutron stars, to name only a few.

For the successful confinement of plasma in thermonuclear temperatures, an equilibrium state for the plasma is a very important necessary condition. For the construction of such, many conventional schemes have been employed, which mainly start from the equilibrium equations of MHD (that is, the MHD equations (1.33)-(1.39) with vanishing temporal derivatives), and then end up in equations of the Grad-Shafranov type [58], [59] by exploiting the geometry of the confinement device in question. Nevertheless, another intriguing approach is to exploit the non-canonical Hamiltonian structure that ideal Hall MHD possesses, with the aim of utilising several variational principles for deducing equilibrium states. In that scope, one can produce more general equilibrium equations and even carry out a stability analysis, as per [28]. The identification of the Hamiltonian structure of the model in question is of utmost importance, since it automatically ensures a correct interpretation for the variational principle that one utilises. In the early times of theoretical plasma physics, most variational principles were introduced in an ad hoc manner, based on physical arguing and conjectures. Not until the development of non-canonical Hamiltonian theory was a rigorous mathematical justification for these methods given.

In the present thesis we aim to construct equilibrium states for fusion plasmas in the framework of Hall MHD, by exploiting the so-called **Energy-Casimir variational principle**. It will be seen at a later chapter that not only our model of description gives rise to new physics in our system, but that it even provides us with more ways of constructing realistic equilibrium states that may be applicable for modern fusion devices, compared to the conventional and widely employed ideal MHD model.

1.6 Thesis outline

This thesis is organised as follows: in the second chapter we present the key-principles of the Hamiltonian formalism in the scope of ideal fluid models, with particular focus on the non-canonical Hamiltonian structure that Hall MHD possesses. In light of the Energy-Casimir variational principle, we then deduce equilibrium equations for axisymmetric two-fluid plasmas with incompressible ion flows. In the third chapter, we proceed to seek solutions to the said equilibrium equations using a variety of mathematical tools and we also examine their main traits. In the fourth chapter, we eventually apply the constructed solutions to Tokamaks and FRCs using ITER and PFRC numerical values respectively. The construction of Tokamak-

relevant equilibria is done by means of proper shaping methods, while for the Solovév type of equilibrium we follow the footsteps of the respective static case. In the fifth, final chapter we summarise the present study by presenting its basic conclusions, discussing possible applications of the solutions to realistic scenarios and finally by proposing certain future research prospects.

2

Equilibria construction via the Energy-Casimir variational principle

Why look at fluid mechanics from a Hamiltonian perspective? The simple answer is because it is there and it is beautiful.

Philip J. Morrison

2.1 Hamiltonian formulation for ideal fluid models

Hamiltonian mechanics have been used extensively over the last two centuries and have provided the necessary machinery for the establishment of many fields of physics, ranging from particle motions to quantum mechanics and modern field theories. Its foundations lie in the so-called Hamiltonian function of a physical system, which under certain conditions [60] coincides with the total energy of the system, expressed in terms of generalised coordinates and momenta, that describe the state of the system. This description sheds light to the system's dynamical structure, since it helps us to identify constants of motion (also known as *integrals of motion*) and provides a geometric interpretation of the dynamics that facilitate the study of dynamical properties and phase-space structure. Below we start with presenting the standard, *canonical* Hamiltonian formalism for systems with finite degrees of freedom and then we proceed with a generalisation to systems that are described by *non-canonical* variables. The reason for this generalisation is our desire to create a proper formulation for the ideal Hall MHD model (Section 1.4.3.3) in the Eulerian fluid description, in the scope of constructing axisymmetric equilibrium states for fusion plasmas as the non-canonical Hamiltonian formulation in the Eulerian picture provides a powerful variational method for deriving equilibrium and stability conditions, namely the *Energy-Casimir* method which will be discussed later in this chapter.

2.1.1 Canonical Hamiltonian description

Imagine that we are studying a dynamical system with N degrees of freedom, with coordinates (q^i, p_i) , where $i = 1, 2, \dots, N$. It is said that the (independent) quantities (q^i, p_i) constitute a set of *canonically conjugate pairs* that inhabit our system's $2N$ -dimensional¹ *phase space* \mathcal{X} , with q^i being the (contravariant) canonical coordinate and p_i being the (covariant) canonical momentum. The covariant formalism has been employed here, in order to demonstrate

¹It is therefore evident that a single degree of freedom corresponds to each (q, p) pair.

the behaviour of these variables under coordinate transformations. Our system's dynamics is described by the well-known Hamilton's equations, viz.

$$\dot{q}^i = \{q^i, \mathcal{H}\} = \frac{\partial \mathcal{H}}{\partial p_i}, \quad \dot{p}_i = \{p_i, \mathcal{H}\} = -\frac{\partial \mathcal{H}}{\partial q^i}, \quad (2.1)$$

where $\mathcal{H} = \mathcal{H}(q^i, p_i, t)$ is the Hamiltonian of our dynamical system and the dot is a shorthand notation for temporal derivatives. In equations (2.1), we implicitly used the so-called *Poisson brackets*, defined as

$$\{F, G\} = \frac{\partial F}{\partial q^i} \frac{\partial G}{\partial p_i} - \frac{\partial F}{\partial p_i} \frac{\partial G}{\partial q^i}, \quad (2.2)$$

for two arbitrary functionals² F and G [61]. Note that here and henceforth repeated indices are to be summed³ (Einstein summation convention). Poisson brackets have certain properties, namely they are bilinear, antisymmetric, they obey the Leibniz rule and finally they satisfy the *Jacobi identity*, namely

$$\{F, \{G, H\}\} + \{H, \{F, G\}\} + \{G, \{H, F\}\} = 0, \quad (2.3)$$

where H is another arbitrary functional, not to be confused with the Hamiltonian \mathcal{H} [28]. Poisson brackets are very important for the study of Hamiltonian systems because *they control the temporal evolution of any functional*, say F . Truly, it can be corroborated [62] using the chain rule that the rate of change of $F(q^i, p_i, t)$ is

$$\frac{dF}{dt} = \frac{\partial F}{\partial t} + \frac{\partial F}{\partial q^i} \dot{q}^i + \frac{\partial F}{\partial p_i} \dot{p}_i = \frac{\partial F}{\partial t} + \{F, \mathcal{H}\}, \quad (2.4)$$

in view of Hamilton's equations (2.1) and the definition (2.2). In the case where there is no explicit dependence from time t , the above result simply reads

$$\frac{dF}{dt} = \{F, \mathcal{H}\}. \quad (2.5)$$

From relation (2.5) it can be seen that the Hamiltonian \mathcal{H} is in fact the *generator of time translations*.

It is also interesting that Hamilton's equations (2.1) can be put in *symplectic* form, by defining the coordinates in the phase space \mathcal{Z} as follows

$$z^i = \begin{cases} q^i & \text{for } i = 1, 2, \dots, N, \\ p_{i-N} & \text{for } i = N + 1, \dots, 2N. \end{cases} \quad (2.6)$$

Then, eqs. (2.1) read

$$\dot{z}^i = \mathcal{J}_c^{ij} \frac{\partial \mathcal{H}}{\partial z^j} = \{z^i, \mathcal{H}\}, \quad (2.7)$$

where the Poisson bracket is now defined as

$$\{F, G\} = \frac{\partial F}{\partial z^i} \mathcal{J}_c^{ij} \frac{\partial G}{\partial z^j}, \quad (2.8)$$

with

$$\mathcal{J}_c^{ij} = \begin{pmatrix} 0_N & \mathbb{1}_N \\ -\mathbb{1}_N & 0_N \end{pmatrix} \quad (2.9)$$

²A functional is essentially a function that takes other functions as arguments. Square brackets denote functional dependence.

³In the case where our system possesses infinite degrees of freedom, i.e. $N \rightarrow \infty$, then the summation is replaced by an integral over the phase space. This will be the case later in non-canonical Hamiltonian description.

being the *co-symplectic form*⁴, also known as the *Poisson operator*, where $\mathbb{1}_N$ is the $N \times N$ identity matrix and 0_N is a $N \times N$ matrix of zeroes [28], [61]. This completes the basis of the canonical Hamiltonian description.

2.1.2 Non-canonical Hamiltonian description

Canonically conjugate pairs are not always the most physically compelling kind of variables for studying physical systems; many theories are structured in *non-canonical* coordinates, with fluid mechanics and plasma physics being two notable cases. For both, the Eulerian description is almost always employed, since it allows one to examine the motion of the fluid in a convenient way considering fixed points in space, compared to the Lagrangian one, which follows a fluid element through space and time. The latter specification is expressed entirely in terms of canonical coordinates, while the former relies on *fields*, which comprise a set of non-canonical variables. Hence, the question of how the formalism in Section 2.1.1 can be generalised for fields in place of coordinates is raised. Such fields may be the velocity field v or the magnetic field B of the Hall MHD model, presented in Section 1.4.3.3, etc. To illustrate this generalisation considering a system with finite degrees of freedom, let us assume a coordinate transformation

$$z^i \rightarrow u^i = u^i(z^i) \quad (2.10)$$

in an N -dimensional phase space \mathcal{Z} . Because for continua, like plasma, the phase space is infinite dimensional (viz. $N \rightarrow \infty$), a further generalisation will be given later. Under such a coordinate transformation, the Hamiltonian transforms as a scalar, i.e.

$$\tilde{\mathcal{H}}[u^i] = \mathcal{H}[z^i]. \quad (2.11)$$

In order to deduce Hamilton's equations in non-canonical coordinates, we proceed by seeking the time derivative of eq. (2.10)

$$\dot{u}^m = \frac{\partial u^m}{\partial z^i} \dot{z}^i \stackrel{(2.7)}{=} \frac{\partial u^m}{\partial z^i} \mathcal{J}_c^{ij} \frac{\partial \mathcal{H}}{\partial z^j} = \left[\frac{\partial u^m}{\partial z^i} \mathcal{J}_c^{ij} \frac{\partial u^n}{\partial z^j} \right] \frac{\partial \mathcal{H}}{\partial u^n}. \quad (2.12)$$

If we define

$$\mathcal{J}^{mn} = \frac{\partial u^m}{\partial z^i} \mathcal{J}_c^{ij} \frac{\partial u^n}{\partial z^j}, \quad (2.13)$$

relation (2.12) becomes

$$\dot{u}^m = \mathcal{J}^{mn} \frac{\partial \mathcal{H}}{\partial u^n}. \quad (2.14)$$

One immediately observes that Hamilton's equations have *the same form* and as a matter of fact, they are manifestly covariant. Furthermore, from eq. (2.13), one can see that the co-symplectic operator transforms as a contravariant tensor of second rank; however in the non-canonical Hamiltonian description, it is evident that the new Poisson operator (2.13) now may depend on the non-canonical variables: $\mathcal{J}^{mn} = \mathcal{J}^{mn}[u^i]$. In this frame, the non-canonical Poisson brackets are defined as

$$\{F, G\} = \frac{\partial F}{\partial u^i} \mathcal{J}^{ij} \frac{\partial G}{\partial u^j}, \quad (2.15)$$

for arbitrary functionals F and G . Finally, the temporal evolution of a functional has the same form as eq. (2.5).

⁴The subscript c of J_c indicates that we have used *canonical* coordinates for describing our system.

Since fluid models involve an infinite number of degrees of freedom, we shall resort to a generalisation upon introducing the functional Poisson bracket

$$\{F, G\} = \int dv \frac{\delta F}{\delta u^i} \mathcal{J}^{ij} \frac{\delta G}{\delta u^j}, \quad (2.16)$$

where v denotes spatial or in general Eulerian coordinates. For this generalisation it is necessary to define the *functional derivative* $\frac{\delta F}{\delta u}$ through the *first variation* δF , as

$$\delta F = \lim_{\epsilon \rightarrow 0} \frac{F[u + \epsilon \delta u] - F[u]}{\epsilon} = \int dv \frac{\delta F}{\delta u} \delta u. \quad (2.17)$$

The functional derivative is in essence the rate of change of a functional F for a change on the function on which F depends on, δu . We also state that the properties of antisymmetry, bilinearity and the Jacobi identity (2.3) still hold for infinite degrees of freedom [28], [61].

2.1.3 The Energy-Casimir variational principle

Let us suppose that we study a N -degree of freedom system for which there exist N independent conserved quantities, hence its dynamical evolution can be determined analytically. Systems of this kind are known in the literature [63], [64] as *integrable Hamiltonian systems*, and in this case, it has been established [61] that the motion takes place on an N -dimensional manifold, known as N -torus⁵ immersed in the $2N$ -dimensional phase space \mathcal{X} . In general, the trajectories of the system lie on the leaves of the foliation, i.e., they move within a given level set of the Hamiltonian function \mathcal{H} . In the framework of non-canonical Hamiltonian description, the previously mentioned dependence of the Poisson operator on the variables of our system gives rise to a class of invariant quantities that are built in \mathcal{X} and induce a foliation of the phase-space into sub-manifolds (*Casimir leaves*) whereon they are constant. Those quantities are known as **Casimir invariants** [61], and their gradients span the null space of the Poisson operator. In other words,

$$\mathcal{J}^{ij} \frac{\delta \mathcal{C}^k}{\delta u^j} = 0. \quad (2.18)$$

Owing to the property (2.18), it can be readily seen from the very definition of the Poisson brackets (2.15) that the Casimir invariants commute with *any* arbitrary functional F , i.e. $\{\mathcal{C}^k, F\} = 0 \forall F$. This in turn means that **the Casimir invariants are kinematic constants of motion**, since

$$\dot{\mathcal{C}}^k = \{\mathcal{C}^k, \mathcal{H}\} = \int dv \frac{\delta \mathcal{C}^k}{\delta u^i} \mathcal{J}^{ij} [u^i] \frac{\delta \mathcal{H}}{\delta u^j} = 0, \quad (2.19)$$

for every Hamiltonian \mathcal{H} . At this point it becomes apparent that the Casimir invariants \mathcal{C}^k confine the system's trajectories in the phase space \mathcal{X} on surfaces where $\mathcal{C}^k = \text{const.}$, and that they play a crucial role in the dynamical evolution of our system [28], [61]. Their usefulness is not exhausted there; if one seeks equilibrium points for a functional F , that is points where $\dot{F} = 0$, then in view of relations (2.5) and (2.16), it follows that

$$\mathcal{J}^{ij} \frac{\delta \mathcal{H}}{\delta u^j} = 0. \quad (2.20)$$

⁵This kind of systems is the counterpart of chaotic ones, for which the trajectories "wander in a seemingly random way" and the N -tori cease to exist. They are characterised by a sensitive dependence on initial conditions [61].

However, owing to relation (2.18), equation (2.20) does not give us all the possible equilibrium points since

$$\mathcal{J}^{ij} \frac{\delta}{\delta u^j} \left(\mathcal{H} + \sum_k C_k \right) = 0, \quad (2.21)$$

is also satisfied. A solution to (2.21) is

$$\delta(\mathcal{H} + \sum_k C_k) = 0. \quad (2.22)$$

One may introduce some arbitrary Lagrange multipliers μ_k to the above equation. Then, any point \mathbf{u}_e that satisfies

$$\delta(\mathcal{H} - \sum_k \mu_k C_k)[\mathbf{u}_e] = 0. \quad (2.23)$$

is an equilibrium point. Equation (2.23) is the **Energy-Casimir variational principle** [28], [61], [65]. Note however that *this condition is sufficient but not necessary for equilibrium*, viz. there exist equilibrium points $\tilde{\mathbf{u}}_e$ that do not satisfy (2.23). This variational principle comprises the cornerstone of the current thesis, and will be used in the next section for the deduction of equilibrium states in the framework of the ideal Hall MHD model.

2.2 Axisymmetric Hall MHD equilibria

On the basis of the Energy-Casimir variational principle presented in the previous section, we may proceed at this point to the construction of Hall MHD equilibrium states for axisymmetric confinement devices. Also, recall that we are interested in equilibrium states with constant density, i.e. $\rho = 1$, which - albeit a crude approximation - significantly simplifies our computations. In this scope, we write down the Hamiltonian in the frame of Alfvén units, per Section 1.4.3.2, as

$$\mathcal{H} = \frac{1}{2} \int_{\mathcal{S}} d^2x (\rho v^2 + B^2), \quad (2.24)$$

where \mathcal{S} is our computational domain, which in our case is a cross section of the toroidal system [28]. The key assumption here is that of *axisymmetry*, which is summarised by relation (1.20) and was thoroughly discussed in Section 1.3.2.1. Axisymmetry limits our analysis to a specific cross section of the toroidal system⁶, and it allows us to exploit the so-called poloidal representations for our two fields of interest, viz. the magnetic field \mathbf{B} and the ion fluid velocity \mathbf{v} , which read

$$\mathbf{B} = RB_\phi \nabla\phi + \nabla\Psi \times \nabla\phi, \quad \text{and} \quad (2.25)$$

$$\mathbf{v} = Rv_\phi \nabla\phi + \nabla\mathcal{X} \times \nabla\phi, \quad (2.26)$$

where Ψ is the flux function for the magnetic field, already defined in Section 1.3.2.1; however, the ion velocity \mathbf{v} is also a key-component of the Hall MHD model and thus it will be described by another flux function \mathcal{X} , to which we attribute a similar physical interpretation with Ψ . In

⁶Since the topology of the magnetic surfaces does not change from one cross section to another.

addition, we used the shorthand notation of $\nabla\phi = e_\phi/R$. Substituting the representations (2.25) and (2.26) in (2.24) results in

$$\mathcal{H} = \frac{1}{2} \int_S d^2x \left(\rho v_\phi^2 + B_\phi^2 + \frac{|\nabla\Psi|^2}{R^2} + \rho \frac{|\nabla\mathcal{X}|^2}{R^2} \right). \quad (2.27)$$

In the presence of axisymmetry, the Hall MHD Casimir invariants have been previously found in [66] and read

$$\begin{aligned} C_1 &= \int_S d^2x (R^{-1}B_\phi + d_i\Omega)\mathcal{F}(\Phi), & C_2 &= \int_S d^2x R^{-1}B_\phi\mathcal{G}(\Psi), \\ C_3 &= \int_S d^2x \rho\mathcal{M}(\Phi), & \text{and } C_4 &= \int_S d^2x \rho\mathcal{N}(\Psi), \end{aligned} \quad (2.28)$$

where \mathcal{F} , \mathcal{G} , \mathcal{M} and \mathcal{N} are free functions and $\Omega = (\nabla \times v_p) \cdot \nabla\phi = -\frac{1}{R^2}\Delta^*\mathcal{X}$, with $v_p = \nabla\mathcal{X} \times \nabla\phi$ being the poloidal component of the velocity field and $\Delta^* \equiv R^2\nabla \cdot (\nabla/R^2)$ is the so-called Shafranov operator. It turns out that it is convenient to write \mathcal{H} and C_1 in terms of v_p rather than \mathcal{X} , although the two representations are completely equivalent. We also defined another flux function, Φ , as

$$\boxed{\Phi = \Psi + d_i R v_\phi.} \quad (2.29)$$

In Section 1.4.3.2, we thoroughly discussed the separation of the ion fluid from the electron one, which is introduced in the framework of the Hall MHD model. It transpires that, apart from the electron fluid, which is described by the so-called *magnetic surfaces* (see Section 1.3.2.1), the ion fluid - which has different properties from the electron one - can also be described by another flux function, apart from \mathcal{X} . That function is no other than Φ . With that being said, we expect to notice another kind of surfaces in our computations, namely *ion velocity field surfaces*, which will become clear in Chapter 4.

For the deduction of the equilibrium equations we shall employ the Energy- Casimir variational principle (2.23), with the addition of the plasma pressure as a Lagrange multiplier in such a manner, that the restriction of $\rho = 1$ follows directly from the variation, or:

$$\delta \left[\mathcal{H} - \sum_i C_i + \int_S d^2x P(\rho - 1) \right] = 0. \quad (2.30)$$

With that being said, a direct substitution of eqs. (2.27) and (2.28) to (2.30) yields

$$\begin{aligned} \delta \int_S d^2x \left\{ \rho \frac{v_\phi^2}{2} + \frac{B_\phi^2}{2} + \frac{|\nabla\Psi|^2}{2R^2} + \rho \frac{|v_p|^2}{2} - (R^{-1}B_\phi + d_i\Omega)\mathcal{F}(\Phi) - \right. \\ \left. - R^{-1}B_\phi\mathcal{G}(\Psi) - \rho\mathcal{M}(\Phi) - \rho\mathcal{N}(\Psi) + P(\rho - 1) \right\} = 0. \end{aligned} \quad (2.31)$$

If we impose that the field-variables $(\Psi, B_\phi, v_\phi, v_p, P, \rho)$ vary up to first order, eq. (2.31) is

modified, after employing some vector analysis manipulations, to

$$\begin{aligned}
 \int_S d^2x \left\{ \rho v_\phi \delta v_\phi + \frac{v_\phi^2}{2} \delta \rho + B_\phi \delta B_\phi + \frac{1}{R^2} \nabla \Psi \cdot \nabla \delta \Psi + \rho v_p \cdot \delta v_p + \frac{|v_p|^2}{2} \delta \rho \right. \\
 - R^{-1} \mathcal{F} \delta B_\phi - d_i (\nabla \times \delta v_p) \cdot (\mathcal{F} \nabla \phi) - R^{-1} \mathcal{G} \delta B_\phi - \\
 - R^{-1} B_\phi \mathcal{G}' \delta \Psi - [R^{-1} B_\phi + d_i (\nabla \times v_p) \cdot \nabla \phi] \mathcal{F}' \delta \Psi - \\
 - [R^{-1} B_\phi + d_i (\nabla \times v_p) \cdot \nabla \phi] d_i R \mathcal{F}' \delta v_\phi - \\
 \left. - \rho \mathcal{M}' \delta \Psi - d_i R \rho \mathcal{M}' \delta v_\phi - \rho \mathcal{N}' \delta \Psi - \mathcal{M} \delta \rho - \mathcal{N} \delta \rho + P \delta \rho + (\rho - 1) \delta P \right\} = 0,
 \end{aligned} \tag{2.32}$$

where we used the commutativity of the operators ∇ and δ and the chain rule as well. The prime denotes differentiation with respect to either Ψ or Φ - depending on the free function. Our goal is to factorise relation (2.32) in terms of the different variations, in order to collect terms and subsequently perform integrations by parts wherever it is necessary so that the variations of the field variables appear outside operators, namely

$$\begin{aligned}
 \int_S d^2x \left\{ [\rho v_\phi - (R^{-1} B_\phi + d_i \Omega) d_i R \mathcal{F}' - d_i r \rho \mathcal{M}'] \delta v_\phi + \right. \\
 + [B_\phi - R^{-1} \mathcal{F} - R^{-1} \mathcal{G}] \delta B_\phi + [\rho v_p - d_i \nabla \mathcal{F} \times \nabla \phi] \cdot \delta v_p - \\
 - \left[\nabla \cdot \left(\frac{\nabla \Psi}{R^2} \right) + R^{-1} B_\phi \mathcal{G}' + (R^{-1} B_\phi + d_i \Omega) \mathcal{F}' + \rho \mathcal{M}' + \rho \mathcal{N}' \right] \delta \Psi + \\
 + \left[\frac{v_\phi^2}{2} + \frac{|v_p|^2}{2} - \mathcal{M} - \mathcal{N} + P \right] \delta \rho + \\
 \left. + (\rho - 1) \delta P \right\} + \oint_{\partial S} f(\delta \Psi, \delta v_p) \cdot d\ell = 0.
 \end{aligned} \tag{2.33}$$

The second line integral in (2.33) is evaluated at the boundary ∂S of our domain and is equal to zero if we impose appropriate boundary conditions in the variations $\delta \Psi$ and δv_p such, that the boundary terms stemming from the integration by parts vanish. The first surface integral in (2.33) equals to zero for arbitrary and independent variations $\delta \Psi$, δB_ϕ , δv_ϕ , δv_p , $\delta \rho$ and δP , only if the coefficients of the variations vanish identically. In other words,

$$\delta v_\phi : \quad \rho v_\phi - d_i R (R^{-1} B_\phi + d_i \Omega) \mathcal{F}' - d_i R \rho \mathcal{M}' = 0, \tag{2.34}$$

$$\delta B_\phi : \quad B_\phi - R^{-1} \mathcal{F} - R^{-1} \mathcal{G} = 0, \tag{2.35}$$

$$\delta \Psi : \quad \nabla \cdot \left(\frac{\nabla \Psi}{R^2} \right) + R^{-1} B_\phi \mathcal{G}' + (R^{-1} B_\phi + d_i \Omega) \mathcal{F}' + \rho (\mathcal{M}' + \mathcal{N}') = 0, \tag{2.36}$$

$$\delta v_p : \quad \rho v_p - d_i \nabla \mathcal{F} \times \nabla \phi = 0, \tag{2.37}$$

$$\delta \rho : \quad P = \mathcal{M} + \mathcal{N} - \frac{v^2}{2} \tag{2.38}$$

$$\delta P : \quad \rho = 1. \tag{2.39}$$

Therefore we can set $\rho = 1$ for our calculations, in view of (2.39). From equation (2.35), we immediately obtain

$$\boxed{B_\phi = R^{-1} (\mathcal{F} + \mathcal{G})}. \tag{2.40}$$

We can also recover a similar expression for the toroidal component of the velocity field, by exploiting relation (2.29)

$$v_\phi = \frac{\Phi - \Psi}{d_i R}. \quad (2.41)$$

The poloidal fields B_p , v_p are essentially the second terms in the RHS of the representations (2.25), (2.26). In addition, from eq. (2.37) we obtain

$$v_p = \nabla \mathcal{X} \times \nabla \phi = d_i \nabla \mathcal{F} \times \nabla \phi \Rightarrow \mathcal{X} = d_i \mathcal{F}, \quad (2.42)$$

up to an integration constant which we set equal to zero, due to the arbitrariness of \mathcal{F} . If we now recall that

$$\Omega = (\nabla \times v_p) \cdot \nabla \Psi = -\Delta^* \mathcal{X} / R^2 = \nabla \cdot (\nabla \mathcal{X} / R^2), \quad (2.43)$$

and use eq. (2.42) in conjunction with (2.40), relation (2.34) becomes

$$v_\phi - d_i R^{-1} (\mathcal{F} + \mathcal{G}) \mathcal{F}' + d_i^3 R \mathcal{F}' \nabla \cdot \left(\frac{\nabla \mathcal{F}}{R^2} \right) - d_i R \mathcal{M}' = 0. \quad (2.44)$$

Then, eq. (2.44) leads to the first Grad-Shafranov equation

$$d_i^2 \mathcal{F}'(\Phi) R^2 \nabla \cdot \left[\mathcal{F}'(\Phi) \frac{\nabla \Phi}{R^2} \right] - [\mathcal{F}(\Phi) + \mathcal{G}(\Psi)] \mathcal{F}'(\Phi) - \mathcal{M}'(\Phi) R^2 + \frac{\Phi - \Psi}{d_i^2} = 0, \quad (2.45)$$

where the chain rule $\nabla \mathcal{F} = \mathcal{F}' \nabla \Phi$ has been used. Furthermore, from eqs. (2.36) and (2.40), we have

$$\nabla \cdot \left(\frac{\nabla \Psi}{R^2} \right) + R^{-2} (\mathcal{F} + \mathcal{G}) \mathcal{G}' + \mathcal{M}' + \mathcal{N}' + (R^{-1} B_\phi + d_i \Omega) \mathcal{F}' = 0, \quad (2.46)$$

which, in the light of equation (2.34), leads to the second Grad-Shafranov equation

$$\Delta^* \Psi + [\mathcal{F}(\Phi) + \mathcal{G}(\Psi)] \mathcal{G}'(\Psi) + \mathcal{N}'(\Psi) R^2 + \frac{\Phi - \Psi}{d_i^2} = 0. \quad (2.47)$$

The pressure inside the axisymmetric fusion device is given from (2.38), or

$$P = \mathcal{M}(\Phi) + \mathcal{N}(\Psi) - \frac{v^2}{2}. \quad (2.48)$$

Relations (2.45), (2.47) and (2.48) comprise a **Grad-Shafranov Bernoulli (GS-Bernoulli) system**. For the rest of the current thesis, we shall concern ourselves with the self-consistent solution of the system of equations (2.45) and (2.47), which are second-order partial differential equations of the elliptic type. The total plasma pressure P inside the fusion device is given by relation (2.48), from which one can notice that P has two contributions; one from the dynamical pressure $v^2/2$ that is attributed to the velocity v of the ion fluid, as well as a contribution from the free functions $\mathcal{M}(\Phi)$ and $\mathcal{N}(\Psi)$ introduced in the framework of the Hall MHD model. At this point, it is becoming evident why we chose the Hall MHD model (among other reasons, discussed extensively in Section 1.5): for the freedom it gives us for the construction of the desired pressure profile in magnetic confinement fusion. Such a pressure profile is peaked on the magnetic axis, which in turns means that the temperature has a maximum in the centre of the formation, and therefore the cross-section of thermonuclear reactions is sufficiently high.

2.3 Ansatz for the free functions - Equilibria cases

The GS-Bernoulli system (2.45), (2.47) and (2.48) contains 4 functions $\mathcal{F}, \mathcal{G}, \mathcal{M}, \mathcal{N}$ that are completely arbitrary, in the sense that the Hall MHD model does not provide us with any insight whatsoever about their form; in order to proceed, one shall make a choice (ansatz) for them. Furthermore, it becomes apparent that the ansatz that we make will be crucial for the topology and the characteristics of the equilibrium, as well as the construction of a desired pressure profile, as discussed above. Henceforward, we will adopt the following general ansatz for our free functions

$$\mathcal{F}(\Phi) = f_0 + f_1 \Phi, \quad (2.49)$$

$$\mathcal{G}(\Psi) = g_0 + g_1 \Psi, \quad (2.50)$$

$$\mathcal{M}(\Phi) = m_0 + m_1 \Phi + \frac{1}{2} m_2 \Phi^2, \quad (2.51)$$

$$\mathcal{N}(\Psi) = n_0 + n_1 \Psi + \frac{1}{2} n_2 \Psi^2, \quad (2.52)$$

where $f_0, f_1, g_0, g_1, m_0, m_1, m_2, n_0, n_1, n_2 \in \mathbb{R}$ are free constant parameters⁷. It is noteworthy that f_0 and g_0 are related to the *vacuum toroidal magnetic field*, i.e. the toroidal magnetic field needed for confinement in the absence of plasma⁸. A selection such that $f_0 + g_0 \neq 0$ results in a Tokamak-relevant configuration, while a selection for which $f_0 + g_0 = 0$ results in a Spheromak-like one. Moreover, m_0 and n_0 are used in the determination of the pressure profile, while the rest of the parameters $f_1, g_1, m_1, m_2, n_1, n_2$ come into play for the calculation of the vector fields, like \mathbf{B}, \mathbf{v} , etc.

The general ansatz (2.49)-(2.52) gives us a lot of flexibility for the choice of the free parameters, since many different types of equilibria arise. On this basis, we briefly list some notable cases of equilibrium that will be studied rigorously in the chapter to follow:

1. **Equilibria with $m_1 \neq 0, n_1 \neq 0, m_2 = n_2 = 0$:** A Double Beltrami system of coupled Grad-Shafranov equations is recovered. The solution for the flux functions is written as a superposition of Beltrami fields.
2. **Equilibria with $m_1 \neq 0, n_1 \neq 0, m_2 \neq 0, n_2 \neq 0$ and $g_1 = -1/(d_i^2 f_1)$:** This selection for the free parameter g_1 decouples the system of the two Grad-Shafranov equations (2.45) and (2.47). The solution for each homogeneous equation is expressed in terms of the Whittaker functions. The particular solution for the non-homogeneous equation can be found by a similarity reduction procedure, as per [67], and a certain constraint must hold for the coefficients in order for each particular solution to satisfy both of the two non-homogeneous Grad-Shafranov equations. For the special case of $m_1 = n_1 = 0$, we derive equilibria that correspond to Spheromak configurations.
3. **Equilibria with $m_1 \neq 0, n_1 \neq 0, m_2 = n_2 = 0, f_1 = 1/d_i = -g_1$:** Solovév type of equilibrium [68] for both flux functions Ψ and Φ . The solution has two up-down symmetric saddle points (*X-points*). The free parameters should be chosen - if possible - in such a manner that the X-points which correspond to Ψ and Φ coincide.
4. **Generic equilibria with $m_1 \neq 0, n_1 \neq 0, m_2 \neq 0, n_2 \neq 0$:** Notwithstanding the generality of this case, the GS-Bernoulli system remains analytically tractable, and configurations with closed magnetic and ion velocity surfaces can be recovered when some specific criteria are met for the free parameters.

⁷Due to the normalisation scheme of Section 1.4.3.2, these free parameters are also *dimensionless*.

⁸To be exact, the vacuum toroidal magnetic field is equal to $(f_0 + g_0)/R$, see relation (2.40).

3

A family of analytic solutions to the Grad-Shafranov-Bernoulli system

Equilibrium is the essence of a thermodynamic system. The system seeks it, strives for it, tends towards it; in the process, it evolves towards higher levels of organization.

Ilya Prigogine

Having presented four notable types of axisymmetric Hall MHD equilibrium in Section 2.3, we now proceed to seek solutions for each of the said cases. Owing to this diversity of solutions, we will exploit various mathematical tools in each of the following sections in order to solve the systems of differential equations that arise. We will also discuss the general behaviour of the solutions in question with the aim of applying the latter in axisymmetric fusion devices.

3.1 Double Beltrami equilibria

3.1.1 Direct derivation of the double Beltrami system via the Energy-Casimir variational principle

We begin by examining the first kind of solutions that satisfy the system of equations (2.45) and (2.47). It will be readily seen that this kind of solutions is closely related to vector fields \mathcal{A} that are eigenvectors of the curl operator. In other words,

$$\nabla \times \mathcal{A} = \lambda_i \mathcal{A}, \quad (3.1)$$

where λ_i are the respective eigenvalues. This kind of fields are known in the literature as **Beltrami fields** [69], [70], and for an ideal MHD plasma they are homonymous to the so-called *force-free* [71] states, i.e. states where the Lorentz force (1.27) vanishes. Those states are widely employed in Solar Physics [72], for the needs of *magnetic field extrapolations* in the solar corona. It has been established by Woltjer in 1958 [73] that plasmas tend to relax, or *self-organise* to such states when the total plasma energy is conserved under the constraint that the magnetic helicity remains constant. He proved that in the scope of ideal MHD, the magnetic helicity is conserved locally, while Taylor [74] conjectured that in a plasma with some kind of dissipation, although the magnetic helicity is not conserved locally, it is conserved globally. This is the well-known *Taylor conjecture* and those states are known in the literature as *Taylor states*. It should be stressed however, that self-organisation into Taylor states is not a general tendency of plasmas, and it only occurs under very specific conditions [75].

In our case, we aim to repeat this process for two-fluid (Hall MHD) plasmas in the light of the Energy-Casimir variational principle (2.23), in order to deduce the **double Beltrami states**, which are essentially superpositions of the ordinary Beltrami ones (3.1). This derivation demonstrates the sheer power this variational principle possesses. We start by considering the standard Hamiltonian (2.24) of our model for $\rho = 1$; however, the Casimir invariants will now be the the *helicity* of the magnetic field [4], [5]:

$$C_1 = \frac{1}{2} \int_S \mathbf{A} \cdot \mathbf{B} \, d^2x, \quad (3.2)$$

where \mathbf{A} is the vector potential, and the so-called *ion helicity* [76], which intertwines the topological properties of the magnetic and the velocity field:

$$C_2 = \frac{1}{2} \int_S (\mathbf{A} + d_i \mathbf{v}) \cdot (\mathbf{B} + d_i \nabla \times \mathbf{v}) \, d^2x. \quad (3.3)$$

This derivation was motivated by the work presented in [75], [76], [77] where multi-Beltrami states are treated in the context of ad hoc variational principles for two-fluid plasmas. A discussion for the proper functional that has to be minimised (*target functional*) is also done, which however does not concern us in the present work since we are working in the scope of the Energy-Casimir variational principle, which already provides us with a basis to interpret the variation correctly in terms of the physics that govern the system in question.

With that being said, we proceed by substituting the two Casimir invariants (3.2) and (3.3) to (2.23) and varying only the vector potential, \mathbf{A} and the ion velocity field, \mathbf{v} as follows

$$\begin{aligned} \delta \int_S d^2x \left[\frac{(\nabla \times \mathbf{A})^2}{2} + \frac{v^2}{2} - \frac{\mu_1}{2} (\mathbf{A} \cdot \nabla \times \mathbf{A}) - \frac{\mu_2}{2} (\mathbf{A} + d_i \mathbf{v}) \cdot (\nabla \times \mathbf{A} + d_i \nabla \times \mathbf{v}) \right] &= 0 \\ \Rightarrow \int_S d^2x \left[\underbrace{(\nabla \times \mathbf{A}) \cdot (\nabla \times \delta \mathbf{A})}_{\textcircled{1}} + \mathbf{v} \cdot \delta \mathbf{v} - \frac{\mu_1}{2} (\delta \mathbf{A} \cdot \nabla \times \mathbf{A} + \mathbf{A} \cdot \nabla \times \delta \mathbf{A}) - \right. \\ &- \frac{\mu_2}{2} (\delta \mathbf{A} \cdot \nabla \times \mathbf{A} + \mathbf{A} \cdot \nabla \times \delta \mathbf{A} + d_i \delta \mathbf{A} \cdot \nabla \times \mathbf{v} + d_i \mathbf{A} \cdot \nabla \times \delta \mathbf{v} + d_i \delta \mathbf{v} \cdot \nabla \times \mathbf{A} + \\ &\left. d_i \mathbf{v} \cdot \nabla \times \delta \mathbf{A} + d_i^2 \delta \mathbf{v} \cdot \nabla \times \mathbf{v} + d_i^2 \mathbf{v} \cdot \nabla \times \delta \mathbf{v}) \right] = 0 \end{aligned} \quad (3.4)$$

The first term in the second equation of (3.4) can be written as

$$\textcircled{1} = \int_S d^2x [(\nabla \times \mathbf{A}) \cdot (\nabla \times \delta \mathbf{A})] = \int_S d^2x \mathbf{B} \cdot (\nabla \times \delta \mathbf{A}). \quad (3.5)$$

Using the vector identity: $\nabla \cdot (\mathbf{a} \times \mathbf{b}) = \mathbf{b} \cdot (\nabla \times \mathbf{a}) - \mathbf{a} \cdot (\nabla \times \mathbf{b})$, one gets

$$\textcircled{1} = \int_S d^2x [\nabla \cdot (\delta \mathbf{A} \times \mathbf{B}) + \delta \mathbf{A} \cdot (\nabla \times \mathbf{B})] = \oint_{\partial S} (\delta \mathbf{A} \times \mathbf{B}) \cdot d\mathbf{S} + \int_S d^2x \delta \mathbf{A} \cdot (\nabla \times \mathbf{B}). \quad (3.6)$$

If we further suppose that the variation on the boundary ∂S vanishes, i.e. $\delta \mathbf{A}|_{\partial S} = 0$, then the surface term has no contribution whatsoever and therefore

$$\textcircled{1} = \int_S d^2x \delta \mathbf{A} \cdot (\nabla \times \mathbf{B}). \quad (3.7)$$

Working similarly for the other five terms, we find similar results. Our goal is to factorize the integral in (3.4), with the two variations as common factors. More specifically we end up at

$$\int_S d^2x \{ [\nabla \times \mathbf{B} - (\mu_1 + \mu_2)\mathbf{B} - \mu_2 d_i(\nabla \times \mathbf{v})] \cdot \delta \mathbf{A} + [\mathbf{v} - \mu_2 d_i \mathbf{B} - \mu_2 d_i^2(\nabla \times \mathbf{v})] \cdot \delta \mathbf{v} \} = 0. \quad (3.8)$$

Given that the above equation must hold for arbitrary and independent variations $\delta \mathbf{A}$ and $\delta \mathbf{v}$, we have:

$$\nabla \times \mathbf{B} - (\mu_1 + \mu_2)\mathbf{B} - \mu_2 d_i(\nabla \times \mathbf{v}) = 0 \quad (3.9)$$

$$\mathbf{v} - \mu_2 d_i \mathbf{B} - \mu_2 d_i^2(\nabla \times \mathbf{v}) = 0. \quad (3.10)$$

By solving relation (3.10) with respect to \mathbf{B} , we find:

$$\mathbf{B} = \frac{1}{\mu_2 d_i} \mathbf{v} - d_i(\nabla \times \mathbf{v}). \quad (3.11)$$

Owing to (3.11), the two equations (3.9) and (3.10) can be easily decoupled. We observe that the two fields satisfy in fact the **same** differential equation:

$$\nabla \times \nabla \times \mathcal{V} + b_1(\nabla \times \mathcal{V}) + b_2 \mathcal{V} = 0, \quad (3.12)$$

where \mathcal{V} is either the magnetic field \mathbf{B} or the velocity field \mathbf{v} and:

$$b_1 = -\mu_1 - \frac{1}{\mu_2 d_i^2} \quad \text{and} \quad b_2 = \frac{\mu_1 + \mu_2}{\mu_2 d_i^2} \quad (3.13)$$

are constants. Eq. (3.12) is known in the literature as the "double Beltrami equation", since the double curl operator appears. Although \mathbf{B} and \mathbf{v} satisfy the same differential equation, we must stress that they are *different* entities as vector fields, since they are interconnected by equation (3.11), which is compatible with (3.12).

3.1.2 Double Beltrami system in terms of the flux functions

In order to solve the system of equations (3.9) and (3.10), we need to express the later in terms of the flux functions Ψ and \mathcal{X} . For that, we will need the poloidal representations of the two fields, given by relations (2.25) and (2.26). Substituting these and their curls:

$$\nabla \times \mathbf{B} = \nabla(RB_\phi) \times \nabla\phi - \Delta^* \Psi \nabla\phi, \quad (3.14)$$

$$\nabla \times \mathbf{v} = \nabla(Rv_\phi) \times \nabla\phi - \Delta^* \mathcal{X} \nabla\phi \quad (3.15)$$

into eqs. (3.9) and (3.10) results in

$$-\Delta^* \Psi \nabla\phi + \nabla(RB_\phi) \times \nabla\phi = \mu_1 RB_\phi \nabla\phi + \mu_1 \nabla\Psi \times \nabla\phi + \frac{1}{d_i} (Rv_\phi \nabla\phi + \nabla\mathcal{X} \times \nabla\phi), \quad (3.16)$$

$$\Delta^* \mathcal{X} \nabla\phi - \nabla(Rv_\phi) \times \nabla\phi = -\frac{1}{d_i^2 \mu_2} (Rv_\phi \nabla\phi + \nabla\mathcal{X} \times \nabla\phi) + \frac{1}{d_i} (RB_\phi \nabla\phi + \nabla\Psi \times \nabla\phi). \quad (3.17)$$

By projecting equations (3.16) and (3.17) to the directions parallel and perpendicular to $\nabla\phi$ and substituting back the results, we find

$$\Delta^* \Psi = -\mu_1 \left(\mu_1 \Psi + \frac{1}{d_i} \mathcal{X} + \gamma \right) - \frac{1}{d_i} \left(\frac{1}{d_i^2 \mu_2} \mathcal{X} - \frac{\Psi}{d_i} + \delta \right), \quad (3.18)$$

$$d_i \mu_2 \Delta^* \mathcal{X} = -\frac{1}{d_i} \left(\frac{1}{d_i^2 \mu_2} \mathcal{X} - \frac{1}{d_i} \Psi + \delta \right) + \mu_2 \left(\frac{1}{d_i} \mathcal{X} + \mu_1 \Psi + \gamma \right), \quad (3.19)$$

where γ and δ are two integration constants which we have the freedom to set equal to zero. By arranging terms, we end up at

$$\Delta^* \Psi = - \left(\mu_1^2 - \frac{1}{d_i^2} \right) \Psi - \left(\frac{\mu_1}{d_i} + \frac{1}{d_i^3} \right) \mathcal{X}, \quad (3.20)$$

$$d_i \mu_2 \Delta^* \mathcal{X} = \left(\mu_1 \mu_2 + \frac{1}{d_i^2} \right) \Psi + \frac{1}{d_i} \left(\mu_2 - \frac{1}{d_i^2 \mu_2} \right) \mathcal{X}. \quad (3.21)$$

Let us now return to the initial system of equations (2.45) and (2.47), and adopt the ansatz (2.49)-(2.52) for $m_2 = n_2 = 0$. Then the system in question reduces to

$$\Delta^* \Psi = -g_1(f_0 + g_0) - g_1(f_1 \Phi + g_1 \Psi) - n_1 R^2 - \frac{\Phi - \Psi}{d_i^2}, \quad (3.22)$$

$$d_i^2 f_1^2 \Delta^* \Phi = f_1(f_0 + g_0) + f_1(f_1 \Phi + g_1 \Psi) + m_1 R^2 - \frac{\Phi - \Psi}{d_i^2}. \quad (3.23)$$

For the purposes of this section, we will use the flux function \mathcal{X} instead of Φ . Both describe the ion velocity field and are interconnected through relation (2.42). Thus we can substitute $\Phi = \frac{\mathcal{X} - d_i f_0}{d_i f_1}$ on eqs. (3.22), (3.23) and end up at

$$\Delta^* \Psi = - \left(g_1^2 - \frac{1}{d_i^2} \right) \Psi - \left(\frac{g_1}{d_i} + \frac{1}{f_1 d_i^3} \right) \mathcal{X} - \left(g_0 g_1 - \frac{f_0}{d_i^2 f_1} \right) - n_1 R^2, \quad (3.24)$$

$$d_i f_1 \Delta^* \mathcal{X} = \left(f_1 g_1 + \frac{1}{d_i^2} \right) \Psi + \left(\frac{f_1}{d_i} - \frac{1}{f_1 d_i^3} \right) \mathcal{X} + \left(f_1 g_0 + \frac{f_0}{d_i^2 f_1} \right) + m_1 R^2. \quad (3.25)$$

Notice that the homogeneous system of equations (3.24) and (3.25) is identical to the system of eqs. (3.20) and (3.21), for $f_1 = \mu_2$ and $g_1 = \mu_1$. Hence, relations (3.24) and (3.25) describe the equilibrium state of a double Beltrami system. We will initially seek a general solution to the homogeneous counterpart of eqs. (3.24) and (3.25), and then we shall proceed to find a particular solution to the respective non-homogeneous system. There exist two ways (among many others) to solve the homogeneous system; either by expressing the two fields as superpositions of Beltrami fields, or by exploiting the eigenvectors of the Shafranov operator. The first way is discussed here, while the latter is presented in Appendix A.

3.1.3 Solution to the double Beltrami equations

3.1.3.1 Homogeneous system

Let \mathcal{A} be a Beltrami field, viz. a field that satisfies relation (3.1). We require that the Beltrami field \mathcal{A} satisfies the Double Beltrami equation (3.12). Direct substitution of relation (3.1) at (3.12), along with the requirement that \mathcal{A} is other than the zero vector, yields the quadratic equation:

$$\lambda^2 + b_1 \lambda + b_2 = 0, \quad (3.26)$$

from which we deduce the two eigenvalues of the curl operator

$$\lambda_{\pm} = \frac{-b_1 \pm \sqrt{b_1^2 - 4b_2}}{2}. \quad (3.27)$$

These two eigenvalues correspond to two Beltrami vectors, \mathcal{A}_{\pm} , respectively. The main notion which we will adopt to solve the system of the two double Beltrami equations is that the two fields \mathbf{B} and \mathbf{v} can be written as a linear combination of the two Beltrami fields \mathcal{A}_{\pm} . For the velocity field, we suppose that

$$\mathbf{v} = c_+ \mathcal{A}_+ + c_- \mathcal{A}_-, \quad (3.28)$$

where c_{\pm} are two arbitrary constants. The magnetic field¹ is found via eqs. (3.11) and (3.28):

$$\mathbf{B} = c_+ \left(\frac{1}{f_1 d_i} - d_i \lambda_+ \right) \mathcal{A}_+ + c_- \left(\frac{1}{f_1 d_i} - d_i \lambda_- \right) \mathcal{A}_-. \quad (3.29)$$

The introduction of the two Beltrami vectors \mathcal{A}_{\pm} has a very interesting consequence; instead of trying to specify the two vector fields \mathbf{B} and \mathbf{v} , it prompts us to try to derive a Grad-Shafranov equation for the vectors \mathcal{A}_{\pm} . Having they been specified, one can easily find the magnetic and the velocity fields via eqs. (3.29) and (3.28). Although the following analysis concerns an axisymmetric system, a generalisation for helical symmetry can be found in Appendix B.

Axisymmetry allows one to exploit the poloidal representations for the Beltrami vectors \mathcal{A}_{\pm} as

$$\mathcal{A}_{\pm} = R \mathcal{A}_{\pm\phi} \nabla\phi + \nabla\Psi_{\pm} \times \nabla\phi, \quad (3.30)$$

where Ψ_{\pm} are the flux functions describing the two Beltrami vectors. The curl of (3.30) is written as

$$\nabla \times \mathcal{A}_{\pm} = -\Delta^* \Psi_{\pm} \nabla\phi + \nabla(R \mathcal{A}_{\pm\phi}) \times \nabla\phi. \quad (3.31)$$

Nevertheless, since \mathcal{A}_{\pm} are Beltrami vectors, then by their very definition eq. (3.1) should hold as well. Therefore, equating relations (3.1) and (3.31) results in

$$-\Delta^* \Psi_{\pm} \nabla\phi + \nabla(R \mathcal{A}_{\pm\phi}) \times \nabla\phi = \lambda_{\pm} R \mathcal{A}_{\pm\phi} \nabla\phi + \lambda_{\pm} \nabla\Psi_{\pm} \times \nabla\phi. \quad (3.32)$$

A projection of relation (3.32) along the direction of $\nabla\phi$ yields

$$-\Delta^* \Psi_{\pm} = \lambda_{\pm} R \mathcal{A}_{\pm\phi}, \quad (3.33)$$

while a projection of (3.32) along the direction normal to $\nabla\phi$ yields:

$$\mathcal{A}_{\pm\phi} = \frac{1}{R} \lambda_{\pm} \Psi_{\pm}. \quad (3.34)$$

By combining relations (3.33) and (3.34), we arrive at the desired Grad-Shafranov equation for the flux functions Ψ_{\pm}

$$\Delta^* \Psi_{\pm} = -\lambda_{\pm}^2 \Psi_{\pm}. \quad (3.35)$$

Equation (3.35) is a second order partial differential equation of the elliptic type, and it is written, in the cylindrical coordinate system that we adopted, as

$$\frac{\partial^2 \Psi_{\pm}}{\partial R^2} - \frac{1}{R} \frac{\partial \Psi_{\pm}}{\partial R} + \frac{\partial^2 \Psi_{\pm}}{\partial Z^2} = -\lambda_{\pm}^2 \Psi_{\pm}. \quad (3.36)$$

¹Note however that the two fields recovered by relations (3.28) and (3.29) stem only from the homogeneous part of the system; one needs to solve the non-homogeneous one as well in order to attain the full expression for the fields.

We can solve eq. (3.36) by means of the well-known *separation of variables* method [78], [79]. Let²

$$\Psi_{\pm}(R, Z) = F_{\pm}(R)G(Z). \quad (3.37)$$

Then, our Differential Equation reads

$$\frac{1}{F_{\pm}(R)} \frac{d^2 F_{\pm}}{dR^2} - \frac{1}{RF_{\pm}(R)} \frac{dF_{\pm}}{dR} + \lambda_{\pm}^2 = -\frac{1}{G(Z)} \frac{d^2 G}{dZ^2}. \quad (3.38)$$

Setting the separation constant equal to k^2 , where $k \in \mathbb{R}$, we deduce two equations

$$\frac{d^2 F_{\pm}}{dR^2} - \frac{1}{R} \frac{dF_{\pm}}{dR} + (\lambda_{\pm}^2 - k^2)F_{\pm}(R) = 0, \quad (3.39)$$

and

$$\frac{d^2 G}{dZ^2} + k^2 G(Z) = 0. \quad (3.40)$$

In order to find solutions for (3.39), we ought to further investigate the sign of the term $\lambda_{\pm}^2 - k^2$. On the one hand, if $\lambda_{\pm}^2 - k^2 > 0 \Rightarrow \lambda_{\pm}^2 > k^2$, the solutions are Bessel functions³ of the first and second kind and of first order, $J_1(x)$ and $Y_1(x)$ respectively. Hence,

$$F_k^{\pm}(R) = R \left[c_1^{\pm} J_1 \left(R \sqrt{\lambda_{\pm}^2 - k^2} \right) + c_2^{\pm} Y_1 \left(R \sqrt{\lambda_{\pm}^2 - k^2} \right) \right]. \quad (3.41)$$

On the other hand, if $\lambda_{\pm}^2 - k^2 < 0 \Rightarrow \lambda_{\pm}^2 < k^2$, the respective radicand in (3.41) is negative, which means that the argument of the Bessel functions is a complex number. This fact prompts us to seek as solutions *modified* Bessel functions [78] of the first and second kind and of first order, $I_1(x)$ and $K_1(x)$ respectively:

$$\tilde{F}_k^{\pm}(R) = R \left[\tilde{c}_1^{\pm} I_1 \left(R \sqrt{\lambda_{\pm}^2 - k^2} \right) + \tilde{c}_2^{\pm} K_1 \left(R \sqrt{\lambda_{\pm}^2 - k^2} \right) \right]. \quad (3.42)$$

In contrast to the oscillatory behaviour of the ordinary Bessel functions, the modified Bessel functions exhibit an *exponential* behaviour [78]. As concerns eq. (3.40), its solutions are of the well-known plane-wave type

$$G_k(Z) = d_1 \cos(kZ) + d_2 \sin(kZ), \quad (3.43)$$

where $c_1^{\pm}, c_2^{\pm}, \tilde{c}_1^{\pm}, \tilde{c}_2^{\pm}, d_1, d_2$ are constants.

However, there exists another family of solutions to (3.35) which is obtained directly if we perform analytic continuation on k , that is $k \rightarrow ik$. By performing this trick, we assume that our separation constant is a pure imaginary number⁴. From another point of view, the fact that the separation constant has an imaginary part is ultimately equivalent to selecting $-k^2$ instead of k^2 when solving (3.39). Both selections are equally correct since the foresaid constant is arbitrary a priori. The assumption of the complex nature of the separation constant covers both cases - and has valid mathematical grounds! With that being said, the two ODEs that stem from the imaginary part of the separation constant are

$$\frac{d^2 F'_{\pm}}{dR^2} - \frac{1}{R} \frac{dF'_{\pm}}{dR} + (\lambda_{\pm}^2 + k^2)F'_{\pm}(R) = 0, \quad (3.44)$$

²The reason the subscript \pm appears only in the radial part is to be understood soon.

³In fact, when one studies Beltrami fields, they will eventually encounter **Bessel functions**; which are usually recovered as solutions to such fields. Bessel functions are well studied, and most Mathematical Physics textbooks cover them, e.g. see [78] and [80]. Their behaviour resembles that of sines and cosines, divided by powers of the independent variable.

⁴However, one must exercise caution to realise that still $k \in \mathbb{R}$! We just replaced $k \rightarrow \tilde{k} = ik$, with $\tilde{k} \in \mathbb{C}$.

where the prime denotes a different function and not differentiation with respect to some variable, and

$$\frac{d^2 G'}{dZ^2} - k^2 G'(Z) = 0. \quad (3.45)$$

In regard to eq. (3.44), the sum of λ_{\pm}^2 and k^2 is always positive, therefore the solutions will be the ordinary Bessel functions

$$F_k^{\pm}(R) = R \left[c_1^{\pm} J_1 \left(R \sqrt{\lambda_{\pm}^2 + k^2} \right) + c_2^{\pm} Y_1 \left(R \sqrt{\lambda_{\pm}^2 + k^2} \right) \right], \quad (3.46)$$

while for eq. (3.45) we have as solutions increasing and decreasing exponentials

$$G_k'(Z) = d_1' e^{kZ} + d_2' e^{-kZ}, \quad (3.47)$$

where $c_1^{\pm}, c_2^{\pm}, d_1', d_2'$ are some other constants.

Finally, we must emphasize that there exists another kind of solution for the special case of $\lambda_{\pm} = +k$ or $\lambda_{\pm} = -k$, which reads

$$\rho(R) = A_1 R^2 + A_2, \quad (3.48)$$

where A_1, A_2 are constants.

Summing up, the most general solution one can assume for the two Beltrami flux functions is a linear combination of the aforementioned solutions, assuming $k \in \mathbb{N}$:

$$\Psi_{\pm}(R, Z) = \sum_{\substack{k \neq \lambda_{\pm} \\ k \neq -\lambda_{\pm}}}^N \left\{ \left[F_k^{\pm}(R) + \tilde{F}_k^{\pm}(R) + F_k^{\pm}(R) \right] \cdot \left[G_k(Z) + G_k'(Z) \right] \right\} + [A_1 R^2 + A_2] \cdot [A_3 \cos(\lambda_{\pm} Z) + A_4 \sin(\lambda_{\pm} Z)]. \quad (3.49)$$

Now we can proceed to find the desired quantities, viz. the solutions Ψ_h, \mathcal{X}_h to the homogeneous counterpart of (3.22), (3.23). The axisymmetric magnetic field is given by relation (3.29), therefore its toroidal component will be

$$B_{\phi} = c_+ \left(\frac{1}{f_1 d_i} - d_i \lambda_+ \right) \mathcal{A}_{+\phi} + c_- \left(\frac{1}{f_1 d_i} - d_i \lambda_- \right) \mathcal{A}_{-\phi}. \quad (3.50)$$

Due to eq. (3.34), relation (3.50) becomes

$$B_{\phi} = \frac{1}{R} \left[c_+ \left(\frac{1}{f_1 d_i} - d_i \lambda_+ \right) \lambda_+ \Psi_+ + c_- \left(\frac{1}{f_1 d_i} - d_i \lambda_- \right) \lambda_- \Psi_- \right], \quad (3.51)$$

from which we straightforwardly read the axisymmetric flux function

$$\Psi_h = c_+ \left(\frac{1}{f_1 d_i} - d_i \lambda_+ \right) \Psi_+ + c_- \left(\frac{1}{f_1 d_i} - d_i \lambda_- \right) \Psi_-. \quad (3.52)$$

Concerning the axisymmetric velocity field, we can utilise the poloidal representation (2.26). Equivalently, due to (3.28), we have

$$\mathbf{v} = c_+ \mathcal{A}_+ + c_- \mathcal{A}_- = \left(c_+ R \mathcal{A}_{+\phi} + c_- R \mathcal{A}_{-\phi} \right) \nabla \phi + \nabla (c_+ \Psi_+ + c_- \Psi_-) \times \nabla \phi \quad (3.53)$$

Therefore, the toroidal component of the velocity field is $v_\phi = c_+ \mathcal{A}_{+\phi} + c_- \mathcal{A}_{-\phi}$, or:

$$v_\phi = \frac{1}{R} (c_+ \lambda_+ \Psi_+ + c_- \lambda_- \Psi_-), \quad (3.54)$$

from which we straightforwardly read the axisymmetric flux function for the velocity field:

$$\mathcal{X}_h = c_+ \Psi_+ + c_- \Psi_-. \quad (3.55)$$

3.1.3.2 Non-homogeneous system

We shall now figure out a particular solution to the non-homogeneous double Beltrami system (3.24), (3.25). In this regard, let

$$A_1 = -\left(g_0 g_1 - \frac{f_0}{d_i^2 f_1}\right), \quad A_2 = \left(f_1 g_0 + \frac{f_0}{d_i^2 f_1}\right), \quad B_1 = -n_1, \quad \text{and} \quad B_2 = \frac{m_1}{d_i f_1}. \quad (3.56)$$

Using also the coefficients (A.2) defined in Appendix A, the system assumes the form

$$\Delta^* \begin{pmatrix} \Psi \\ \mathcal{X} \end{pmatrix} = \begin{pmatrix} \mathcal{W}_1 & \mathcal{W}_2 \\ \mathcal{W}_3 & \mathcal{W}_4 \end{pmatrix} \begin{pmatrix} \Psi \\ \mathcal{X} \end{pmatrix} + \begin{pmatrix} A_1 \\ A_2 \end{pmatrix} + \begin{pmatrix} B_1 \\ B_2 \end{pmatrix} R^2. \quad (3.57)$$

We impose that the particular solutions have the following form

$$\Psi_p = \Psi_p(R) = \alpha R^2 + \beta, \quad \mathcal{X}_p = \mathcal{X}_p(R) = \gamma R^2 + \delta, \quad (3.58)$$

where $\alpha, \beta, \gamma, \delta$ are coefficients that we want to specify. The main concept is the requirement that the solutions (3.58) satisfy the system (3.57). As a matter of fact, one can observe an interesting consequence of this selection for the particular solutions, viz. that

$$\Delta^* \Psi_p = \frac{d^2 \Psi_p}{dR^2} - \frac{1}{R} \frac{d\Psi_p}{dR} = 0, \quad (3.59)$$

and similarly for $\Delta^* \mathcal{X}_p$. Consequently, we can set the LHS of (3.57) equal to zero and recover the following system of algebraic equations

$$\mathcal{W}_1 \alpha R^2 + \mathcal{W}_1 \beta + \mathcal{W}_2 \gamma R^2 + \mathcal{W}_2 \delta + A_1 + B_1 R^2 = 0, \quad (3.60)$$

$$\mathcal{W}_3 \alpha R^2 + \mathcal{W}_3 \beta + \mathcal{W}_4 \gamma R^2 + \mathcal{W}_4 \delta + A_2 + B_2 R^2 = 0. \quad (3.61)$$

Solving the system (3.60), (3.61) with respect to the unknown coefficients, we find

$$\begin{aligned} \alpha &= \frac{B_1 \mathcal{W}_4 - B_2 \mathcal{W}_2}{\mathcal{W}_2 \mathcal{W}_3 - \mathcal{W}_1 \mathcal{W}_4}, & \beta &= \frac{A_1 \mathcal{W}_4 - A_2 \mathcal{W}_2}{\mathcal{W}_2 \mathcal{W}_3 - \mathcal{W}_1 \mathcal{W}_4}, \\ \gamma &= \frac{B_1 \mathcal{W}_3 - B_2 \mathcal{W}_1}{\mathcal{W}_1 \mathcal{W}_4 - \mathcal{W}_2 \mathcal{W}_3}, & \delta &= \frac{A_2 \mathcal{W}_1 - A_1 \mathcal{W}_3}{\mathcal{W}_2 \mathcal{W}_3 - \mathcal{W}_1 \mathcal{W}_4}. \end{aligned} \quad (3.62)$$

The final solution to the full system of eqs. (3.24), (3.25) will be the sum of the general solution of the homogeneous system and the particular solution of the non-homogeneous system, as

$$\begin{aligned}\Psi(R, Z) &= \Psi_h + \Psi_p = c_+ \left(\frac{1}{f_1 d_i} - d_i \lambda_+ \right) \Psi_+ + c_- \left(\frac{1}{f_1 d_i} - d_i \lambda_- \right) \Psi_- + \alpha R^2 + \beta, \\ \mathcal{X}(R, Z) &= \mathcal{X}_h + \mathcal{X}_p = c_+ \Psi_+ + c_- \Psi_- + \gamma R^2 + \delta,\end{aligned}\tag{3.63}$$

where the flux functions Ψ_{\pm} are given by eq. (3.49), and the coefficients $\alpha, \beta, \gamma, \delta$ are given by eq. (3.62). We also stress again that c_{\pm} are two arbitrary constants, and can be chosen as seen fit.

3.2 Equilibria in terms of the Whittaker functions

We proceed by examining the case where $m_1 \neq 0, n_1 \neq 0, m_2 \neq 0, n_2 \neq 0$ and $g_1 = -1/(d_i^2 f_1)$. This specific selection for g_1 decouples the system of the two differential equations (2.45), (2.47) as

$$\Delta^* \Psi + \left(\frac{1}{d_i^4 f_1^2} - \frac{1}{d_i^2} \right) \Psi + n_2 \Psi R^2 + n_1 R^2 - \frac{f_0 + g_0}{d_i^2 f_1} = 0,\tag{3.64}$$

$$\Delta^* \Phi + \left(\frac{1}{d_i^4 f_1^2} - \frac{1}{d_i^2} \right) \Phi - \frac{m_2}{d_i^2 f_1^2} \Phi R^2 - \frac{m_1}{d_i^2 f_1^2} R^2 - \frac{f_0 + g_0}{d_i^2 f_1} = 0.\tag{3.65}$$

In order to solve it, we will follow the same procedure as in Section 3.1; we first seek a general solution to the homogeneous system, and then we will seek a particular solution to the non-homogeneous one in order to take the superposition of the two as the full solution.

3.2.1 Homogeneous system

The homogeneous counterpart of eqs. (3.64) and (3.65) is

$$\Delta^* \Psi + \gamma \Psi + \delta \Psi R^2 = 0,\tag{3.66}$$

$$\Delta^* \Phi + \gamma \Phi + \delta' \Phi R^2 = 0,\tag{3.67}$$

where ⁵

$$\gamma = \frac{1}{d_i^4 f_1^2} - \frac{1}{d_i^2}, \quad \delta = n_2, \quad \text{and} \quad \delta' = -\frac{m_2}{d_i^2 f_1^2}.\tag{3.68}$$

Both equations have the same form, so we proceed by solving eq. (3.66). Separating variables as

$$\Psi(R, Z) = K(R)T(Z),\tag{3.69}$$

our PDE reduces to

$$-\frac{1}{K(R)} \frac{d^2 K}{dR^2} + \frac{1}{RK(R)} \frac{dK}{dR} - \gamma - \delta R^2 = \frac{1}{T(Z)} \frac{d^2 T}{dZ^2} = -\eta^2,\tag{3.70}$$

where $-\eta^2$ is the separation constant. We deduce two ODEs:

$$\frac{d^2 T}{dZ^2} + \eta^2 T(Z) = 0,\tag{3.71}$$

⁵Those coefficients are not to be confused with the ones of Section 3.1.3.2.

with solutions

$$T(Z) = A_1 \cos(\eta Z) + A_2 \sin(\eta Z), \quad (3.72)$$

and

$$\frac{d^2 K}{dR^2} - \frac{1}{R} \frac{dK}{dR} + (\gamma - \eta^2)K(R) + \delta R^2 K(R) = 0. \quad (3.73)$$

In order to solve this ODE, we perform the transformation: $\rho = i\sqrt{\delta}R^2$, where $i^2 = -1$. Then, since $\frac{d}{dR} = 2i\sqrt{\delta}R \frac{\partial}{\partial \rho}$ and $\frac{\partial^2}{\partial R^2} = 2i\sqrt{\delta} \frac{\partial}{\partial \rho} + 4i\sqrt{\delta}R \frac{\partial^2}{\partial \rho^2}$, eq. (3.73) becomes

$$\frac{d^2 K}{d\rho^2} + \left[\frac{\nu}{\rho} - \frac{1}{4} \right] K(\rho) = 0, \quad (3.74)$$

where we set $\nu = i\frac{\eta^2 - \gamma}{4\sqrt{\delta}}$. Eq. (3.74) is a special type of the *Whittaker differential equation* [81]:

$$y''(x) + \left[\frac{\nu}{x} - \frac{1}{4} + \frac{\frac{1}{4} - \mu^2}{x^2} \right] y(x) = 0, \quad (3.75)$$

for the choice $\mu = 1/2$. Hence, the solution for the radial part reads

$$K(R) = B_1 \mathcal{M}_{\nu, \frac{1}{2}}(i\sqrt{\delta}R^2) + B_2 \mathcal{W}_{\nu, \frac{1}{2}}(i\sqrt{\delta}R^2), \quad (3.76)$$

where $\mathcal{M}_{k,m}(x)$ and $\mathcal{W}_{k,m}(x)$ are the so-called *Whittaker functions*, whose basic properties and behaviour are examined in Appendix C. If we further restrict the separation constant to positive integers, i.e. $\eta \rightarrow k \in \mathbb{N}$, then the solution to eq. (3.66) is written as

$$\begin{aligned} \Psi_h(R, Z) = \sum_{k=1}^{\infty} & \left[a_k \mathcal{M}_{\nu_k, \frac{1}{2}}(i\sqrt{\delta}R^2) \cos(kZ) + b_k \mathcal{M}_{\nu_k, \frac{1}{2}}(i\sqrt{\delta}R^2) \sin(kZ) + \right. \\ & \left. + c_k \mathcal{W}_{\nu_k, \frac{1}{2}}(i\sqrt{\delta}R^2) \cos(kZ) + d_k \mathcal{W}_{\nu_k, \frac{1}{2}}(i\sqrt{\delta}R^2) \sin(kZ) \right], \end{aligned} \quad (3.77)$$

where a_k, b_k, c_k and d_k are constants. Working similarly for eq. (3.67), we obtain:

$$\begin{aligned} \Phi_h(R, Z) = \sum_{k=1}^{\infty} & \left[\tilde{a}_k \mathcal{M}_{\tilde{\nu}_k, \frac{1}{2}}(i\sqrt{\delta'}R^2) \cos(kZ) + \tilde{b}_k \mathcal{M}_{\tilde{\nu}_k, \frac{1}{2}}(i\sqrt{\delta'}R^2) \sin(kZ) + \right. \\ & \left. + \tilde{c}_k \mathcal{W}_{\tilde{\nu}_k, \frac{1}{2}}(i\sqrt{\delta'}R^2) \cos(kZ) + \tilde{d}_k \mathcal{W}_{\tilde{\nu}_k, \frac{1}{2}}(i\sqrt{\delta'}R^2) \sin(kZ) \right], \end{aligned} \quad (3.78)$$

where $\tilde{\nu}_k = i\frac{k^2 - \gamma}{4\sqrt{\delta'}}$, and $\tilde{a}_k, \tilde{b}_k, \tilde{c}_k, \tilde{d}_k$ are some other constants.

3.2.2 Non-homogeneous system

We can write the non-homogeneous Grad-Shafranov equations (3.64) and (3.65) in the form

$$\Delta^* \Psi + \gamma \Psi + \delta \Psi R^2 + \varepsilon R^2 + \zeta = 0, \quad (3.79)$$

$$\Delta^* \Phi + \gamma \Phi + \delta' \Phi R^2 + \varepsilon' R^2 + \zeta = 0, \quad (3.80)$$

where the coefficients γ, δ , and δ' are given by eq. (3.68), and

$$\varepsilon = n_1, \quad \varepsilon' = -\frac{m_1}{d_i^2 f_1^2}, \quad \text{and} \quad \zeta = -\frac{f_0 + g_0}{d_i^2 f_1}. \quad (3.81)$$

The solution to eqs. (3.79) and (3.80) can be found by the *similarity reduction procedure*, which is portrayed in [67]. For (3.79), we will select

$$\Psi_p(R, Z) = \sin\left(\frac{\sqrt{\delta}}{2}R^2 + \sqrt{\gamma}Z\right) + \cos\left(\frac{\sqrt{\delta}}{2}R^2 + \sqrt{\gamma}Z\right) - \frac{\epsilon}{\delta} \quad (3.82)$$

or, equivalently

$$\begin{aligned} \Psi_p(R, Z) = & \sin\left(\frac{\sqrt{n_2}}{2}R^2 + \sqrt{\frac{1}{d_i^4 f_1^2} - \frac{1}{d_i^2}}Z\right) + \\ & \cos\left(\frac{\sqrt{n_2}}{2}R^2 + \sqrt{\frac{1}{d_i^4 f_1^2} - \frac{1}{d_i^2}}Z\right) - \frac{n_1}{n_2}. \end{aligned} \quad (3.83)$$

The only constraint that should hold, in order that (3.83) satisfies eq. (3.79), is that

$$\zeta = \gamma \frac{\epsilon}{\delta}, \quad \text{or, equivalently} \quad \frac{f_0 + g_0}{d_i^2 f_1} = -\left(\frac{1}{d_i^4 f_1^2} - \frac{1}{d_i^2}\right) \frac{n_1}{n_2}. \quad (3.84)$$

Working in a similar manner for the flux function Φ , we end up at

$$\begin{aligned} \Phi_p(R, Z) = & \sin\left(\frac{1}{2}\sqrt{-\frac{m_2}{d_i^2 f_1^2}}R^2 + \sqrt{\frac{1}{d_i^4 f_1^2} - \frac{1}{d_i^2}}Z\right) + \\ & \cos\left(\frac{1}{2}\sqrt{-\frac{m_2}{d_i^2 f_1^2}}R^2 + \sqrt{\frac{1}{d_i^4 f_1^2} - \frac{1}{d_i^2}}Z\right) - \frac{m_1}{m_2}, \end{aligned} \quad (3.85)$$

under the constraint

$$\frac{f_0 + g_0}{d_i^2 f_1} = -\left(\frac{1}{d_i^4 f_1^2} - \frac{1}{d_i^2}\right) \frac{m_1}{m_2}. \quad (3.86)$$

Finally, the full solution will read

$$\Psi = \Psi_h + \Psi_p \quad (3.87)$$

$$\Phi = \Phi_h + \Phi_p. \quad (3.88)$$

Before we close this section, we stress that if we select $m_1 = n_1 = 0$ in eqs. (3.64), (3.65), then albeit both the homogeneous and the non-homogeneous systems can be solved in the same manner as before, the restrictions for the particular solutions (3.84), (3.86) reduce to the constraint: $f_0 + g_0 = 0$, since now $m_1 = n_1 = 0$. This means that the vacuum toroidal magnetic field is non-existent, and that these equilibria correspond to Spheromak-like configurations.

3.3 Solovév equilibria

If one assumes $m_1 \neq 0$, $n_1 \neq 0$, $m_2 = n_2 = 0$, and $f_1 = -g_1 = 1/d_i$ for the general ansatz given by (2.49)-(2.52), then the GS-Bernoulli system (2.45), (2.47), (2.48) reduces to a form that is well known in the theoretical study of magnetic confinement. In particular, Solovév in 1968 [68] proposed a polynomial solution (which is now named after him) for the static MHD Grad-Shafranov equation in the case where the two MHD free functions are constants. The GS equation then becomes linear and can be easily solved. In this section we first present

the Solovév solution to the MHD GS equation for the sake of better understanding. We then proceed to show that, for the above specific selection of the free parameters, the GS-Bernoulli system reduces to two equations of the Solovév type.

3.3.1 Static MHD Solovév solution

The equilibrium of an axisymmetric, static MHD plasma is described by the GS equation [20], which in dimensionless form reads

$$\Delta^* \Psi + FF' + R^2 P' = 0, \quad (3.89)$$

where Ψ is the flux function describing the poloidal magnetic field ⁶, $F = F(\Psi)$ is the poloidal current flux function, Δ^* is the Shafranov operator and $P = P(\Psi)$ is the plasma pressure. Both F and P are not prescribed by the MHD model, and thus serve as *free functions*. With that being said, the choice that we make for them will greatly affect the solution for the GS equation (3.89). By far the simplest selection is to assume that both of them are constants. This ansatz is written as

$$P'(\Psi) = -|P'| = \text{const.} \quad \text{and} \quad FF' = \frac{1}{2}(F^2)' = \epsilon \frac{|P'|}{(1 + \delta^2)}, \quad (3.90)$$

where ϵ and δ are constant geometrical parameters. The first parameter is related to the vacuum toroidal magnetic field, while the latter is connected with the elongation of the formation [82]. The first relation of the above can be integrated to

$$P = P_a - |P'|\Psi, \quad (3.91)$$

where $\Psi \geq 0$ and we select $\Psi_a = 0$ and $P_b = 0$. The subscripts a and b indicate values on the magnetic axis and the plasma boundary, respectively. We further assume that the poloidal flux takes its maximum value Ψ_{max} on the boundary. The so-called Solovév solution to (3.89) is written down as

$$\Psi(\xi, \zeta) = \left[\zeta^2(\xi^2 - \epsilon) + \frac{\delta^2}{4}(\xi^2 - 1)^2 \right] \frac{\xi_a^4 |P'|}{2(1 + \delta^2)}, \quad (3.92)$$

where $\xi = R/R_a$ and $\zeta = Z/R_a$ are the normalised coordinates with respect to the radius of the magnetic axis R_a , and thus $\xi_a = 1$. ⁷

It is intriguing to find the stationary points of the Solovév flux function, by demanding that $B_p = 0$, or equivalently $\nabla \Psi / R = 0$. This leads to two equations, viz.

$$\frac{1}{\xi} \frac{\partial \Psi}{\partial \zeta} \approx \frac{1}{\xi} \zeta (\xi^2 - \epsilon) = 0, \quad (3.93)$$

and

$$\frac{1}{\xi} \frac{\partial \Psi}{\partial \xi} \approx \frac{\partial \Psi}{\partial \xi^2} \approx \zeta^2 + \frac{\delta^2}{2}(\xi^2 - 1) = 0. \quad (3.94)$$

Our aim is to solve eqs. (3.93) and (3.94) simultaneously. The first solution is the magnetic axis's coordinates, namely $\zeta = 0$, and $\xi = 1$, which as a matter of fact, are independent of ϵ . On the magnetic axis, we find that $\Psi = \Psi_a = 0$ and we further choose $P = P_a$. For the second solution, we have $\xi = \sqrt{\epsilon}$, and $\zeta = \pm \frac{\delta}{\sqrt{2}} \sqrt{1 - \epsilon}$. These two points are of major importance, as they are in essence the two X-points that this solution spontaneously possesses. Because the ζ coordinate appears squared in the Solovév solution (3.92), the two X-points will be symmetric

⁶Which we have already studied in the context of Hall MHD.

⁷At this point one may justifiably wonder how can this non-separable, polynomial solution to the Grad-Shafranov equation be related to the ones we found at the previous sections, e.g. the Bessel functions. The answer is that there is a relation; the interested reader is referred to [83] for a relevant discussion.

with respect to the $\zeta = 0$ plane, i.e. they will be *up-down symmetric*. They are located on the last closed flux surface (called **separatrix**), which is the curve that separates magnetic surfaces with different topological properties (i.e. closed and open ones). Outside the separatrix, the flux surfaces are open. This is illustrated in Fig. 3.1.

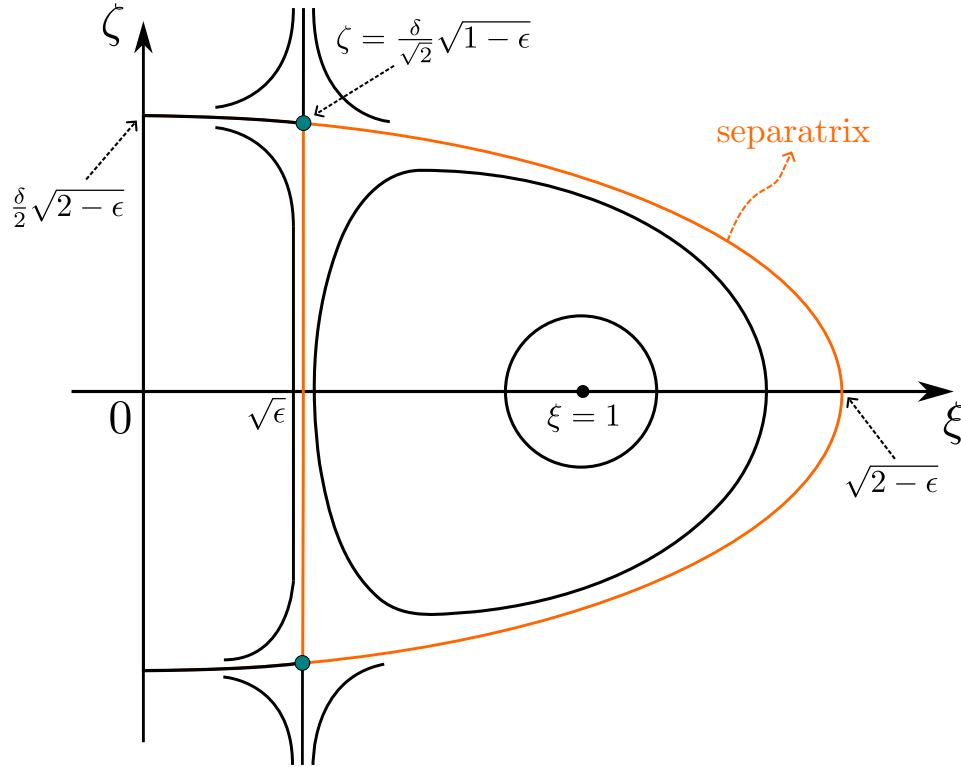


Figure 3.1: Solovév equilibrium configuration.

One may substitute the coordinates of one of the two X-points in the solution (3.92), to find the magnetic flux on the separatrix

$$\Psi_s = \frac{\zeta_a^4 |P'|}{2(1+\delta^2)} \frac{\delta^2}{4} (1-\epsilon)^2 \quad (3.95)$$

If we now equate Ψ with its value on the separatrix, we can determine the separatrix curve. More specifically, $\Psi = \Psi_s$ leads to

$$\zeta^2(\zeta^2 - \epsilon) + \frac{\delta^2}{4}(\zeta^2 - 1)^2 = \frac{\delta^2}{4}(1 - \epsilon)^2. \quad (3.96)$$

If we set

$$\zeta^2 - \epsilon \equiv g, \quad (3.97)$$

then eq. (3.96) translates to

$$g \left[\zeta^2 + \frac{\delta^2}{4}g - \frac{\delta^2}{2}(1 - \epsilon) \right] = 0. \quad (3.98)$$

This equation has two solutions. The first one reads $g = 0 \forall \zeta \Rightarrow \zeta^2 = \epsilon$. This comprises the "inside part" of the separatrix (see Fig. 3.1). The other solution is retrieved by setting the quantity within the square brackets equal to zero in equation (3.98). In other words,

$$\zeta^2 + \frac{\delta^2}{4}g = \frac{\delta^2}{2}(1 - \epsilon) \Rightarrow \zeta^2 + \frac{\delta^2}{4}\zeta^2 = \frac{\delta^2}{4}(2 - \epsilon). \quad (3.99)$$

The latter relation in (3.99) is an ellipse equation in the $\xi\zeta$ plane and is basically the “outer part” of the separatrix (Fig. 3.1).

Before we close this subsection we note that for the Solovév solution, the magnetic surfaces in the vicinity of the magnetic axis and the outer part of the separatrix have elliptical cross-sections. Moreover, if $\epsilon = 0$, then the inner part of the separatrix is located on the axis of symmetry and in this case the configuration becomes compact [82]. This is very important for the current study, which will be evident in the next subsection.

3.3.2 Hall MHD Solovév solution

Let us now return to the GS-Bernoulli system of equations (2.45), (2.47), (2.48) of our originally adopted Hall MHD model. For $m_2 = n_2 = 0$ and $f_1 = -g_1 = 1/d_i$, the two GS equations reduce to

$$\Delta^* \Psi + n_1 \zeta^2 - \frac{f_0 + g_0}{d_i} = 0, \quad (3.100)$$

$$\Delta^* \Phi - m_1 \zeta^2 - \frac{f_0 + g_0}{d_i} = 0, \quad (3.101)$$

which are normalised with respect to the magnetic axis coordinates, without loss of generality⁸. Those equations are of the static Solovév form (3.89). Because we have two fields of interest, viz. \mathbf{B} and \mathbf{v} , it is generally desired to have *one* separatrix, or in other words we would like the magnetic separatrix to coincide with the ion velocity one. Therefore, the parameters δ and ϵ should be common for both configurations. We readily observe that the FF' term in (3.89) corresponds to the constant term $-(f_0 + g_0)/d_i$, which is common in (3.100) and (3.101). Consequently, the ansatz (3.90) implies that the terms n_1 and $-m_1$ (which correspond to $|P'|$), should be identical: $m_1 = -n_1 > 0$ and then the two PDEs (3.100) and (3.101) become identical too. With that being said, it is now evident that such equilibria reduce to MHD-like equilibria with flow, and it holds that $\Psi \equiv \Phi$. Nevertheless, the definition of the toroidal velocity component (2.41) implies that v_ϕ becomes indefinite for $d_i = 0$. Considering a compact toroid we may set $v_\phi = 0$ because the toroidal velocity should vanish on the symmetry axis, i.e. the torus axis. Hence, the flow of the ion fluid ought to be purely poloidal. However, based on a previous study [84], an MHD equilibrium state with purely poloidal flows is possible only if the magnetic field is purely poloidal too. Thus, it should hold that $f_0 + g_0 = 0$ and as a consequence $\epsilon = 0$. This in turn witnesses that such equilibria concern **field-reversed configurations** (see Section 1.3.2.3) **with sheared poloidal flows**. The common solution to eqs. (3.100), (3.101) will read

$$\Psi(\xi, \zeta) \equiv \Phi(\xi, \zeta) = \left[\zeta^2 \xi^2 + \frac{\delta^2}{4} (\xi^2 - 1)^2 \right] \frac{\xi_a^4 m_1}{2(1 + \delta^2)}, \quad (3.102)$$

where $m_1 > 0$ and $\xi_a = 1$ is the radius of the magnetic axis (which is identical to the velocity axis). The coordinates of the separatrix points will be $(0, \pm\delta/\sqrt{2})$, and $(\sqrt{2}, 0)$. We finally note that the value of Ψ on the separatrix (see eq. (3.95)) will be

$$\Psi_s = \frac{\xi_a^4 m_1 \delta^2}{8(1 + \delta^2)}. \quad (3.103)$$

The rest of the analysis remains the same as in the previous subsection, with $\epsilon = 0$. We further mention that in general, the pressure does not vanish on the separatrix due to the presence of flows.

⁸For historical reasons, we will prefer this normalisation scheme for the needs only of the Solovév equilibrium. The rest of the physical quantities are normalised in the standard Alfvén manner, per (1.54). The only difference is that now $L \equiv R_a$

3.4 Generic equilibria

The last type of equilibria that will be studied concerns no restrictions whatsoever for the ansatz parameters; we will just assume that each single parameter is other than zero at the ansatz (2.49)-(2.52). With that being said, the two Grad-Shafranov equations (2.45) and (2.47) read

$$\Delta^* \Psi + g_1(f_0 + g_0) + g_1^2 \Psi + g_1 f_1 \Phi + n_1 R^2 + n_2 \Psi R^2 + \frac{\Phi - \Psi}{d_i^2} = 0, \quad (3.104)$$

$$d_i^2 f_1^2 \Delta^* \Phi - f_1(f_0 + g_0) - f_1^2 \Phi - f_1 g_1 \Psi - m_1 R^2 - m_2 \Phi R^2 + \frac{\Phi - \Psi}{d_i^2} = 0. \quad (3.105)$$

In this section we shall content ourselves with solving the homogeneous counterpart of eqs. (3.104), (3.105), since it suffices in order to delineate the basic properties one might expect from such an equilibrium. In this regard, let

$$\Phi = \Phi(\xi_1), \quad \xi_1 = a_1 R^2 \pm b_1 Z, \quad (3.106)$$

$$\Psi = \Psi(\xi_2), \quad \xi_2 = a_2 R^2 \pm b_2 Z, \quad (3.107)$$

where a_1, b_1, a_2, b_2 are constants. After a brief calculation of the Shafranov operator for this case and a grouping of terms, our differential equations transform to

$$4a_2^2 R^2 \Psi'' + b_2^2 \Psi'' + \left(g_1^2 - \frac{1}{d_i^2}\right) \Psi + \left(f_1 g_1 + \frac{1}{d_i}\right) \Phi + n_2 \Psi R^2 = 0, \quad (3.108)$$

and similarly

$$d_i^2 f_1^2 (4a_1^2 R^2 \Phi'' + b_1^2 \Phi'') + \left(\frac{1}{d_i^2} - f_1^2\right) \Phi - \left(f_1 g_1 + \frac{1}{d_i}\right) \Psi - m_2 R^2 \Phi = 0, \quad (3.109)$$

where the prime denotes differentiation with respect to either ξ_1 or ξ_2 , depending on the flux function. Considering the LHS of eqs (3.108) and (3.109) as polynomials with respect to R we demand that the respective coefficients of R^2 and the R^0 terms are equal to zero. In other words,

$$4a_1^2 d_i^2 f_1^2 \Phi'' - m_2 \Phi = 0, \quad (3.110)$$

$$d_i^2 f_1^2 b_1^2 \Phi'' + \left(\frac{1}{d_i^2} - f_1^2\right) \Phi - \left(f_1 g_1 + \frac{1}{d_i}\right) \Psi = 0, \quad (3.111)$$

$$4a_2^2 \Psi'' + n_2 \Psi = 0, \quad (3.112)$$

$$b_2^2 \Psi'' + \left(g_1^2 - \frac{1}{d_i^2}\right) \Psi + \left(f_1 g_1 + \frac{1}{d_i}\right) \Phi = 0. \quad (3.113)$$

This system can be easily decoupled. Truly, upon setting⁹

$$\alpha = d_i^2 f_1^2, \quad \beta = \frac{1}{d_i^2} - f_1^2, \quad \gamma = f_1 g_1 + \frac{1}{d_i}, \quad \delta = g_1^2 - \frac{1}{d_i^2}, \quad (3.114)$$

the system of equations (3.110)-(3.113) reduces to the following decoupled system

⁹Again, these coefficients should not be confused with the ones of the previous sections.

$$\frac{\alpha}{\gamma} b_1^2 b_2^2 \Phi'''' + \left(\frac{\beta}{\gamma} b_2^2 + \frac{\alpha \delta}{\gamma} b_1^2 \right) \Phi'' + \left(\frac{\beta \delta}{\gamma} + \gamma \right) \Phi = 0, \quad (3.115)$$

$$4a_1^2 \alpha \Phi'' - m_2 \Phi = 0, \quad (3.116)$$

$$\frac{\alpha}{\gamma} b_1^2 b_2^2 \Psi'''' + \left(\frac{\alpha \delta}{\gamma} b_1^2 + \frac{\beta}{\gamma} b_2^2 \right) \Psi'' + \left(\frac{\beta \delta}{\gamma} + \gamma \right) \Psi = 0, \quad (3.117)$$

$$4a_2^2 \Psi'' + n_2 \Psi = 0. \quad (3.118)$$

We can observe that $\Phi = \cos \zeta_1$ is a solution, provided that

$$\frac{\alpha}{\gamma} b_1^2 b_2^2 - \left(\frac{\beta}{\gamma} b_2^2 + \frac{\alpha \delta}{\gamma} b_1^2 \right) + \left(\frac{\beta \delta}{\gamma} + \gamma \right) = 0, \quad (3.119)$$

$$a_1 = \pm \sqrt{-\frac{m_2}{4\alpha}}. \quad (3.120)$$

Similarly, $\Psi = \cos \zeta_2$ is a solution, provided that

$$\frac{\alpha}{\gamma} b_1^2 b_2^2 - \left(\frac{\alpha \delta}{\gamma} b_1^2 + \frac{\beta}{\gamma} b_2^2 \right) + \left(\frac{\beta \delta}{\gamma} + \gamma \right) = 0, \quad (3.121)$$

$$a_2 = \pm \sqrt{\frac{n_2}{4}}. \quad (3.122)$$

Hence, there exist the following analytic solutions

$$\Phi_{\pm}(R, Z) = \cos(a_1 R^2 \pm b_1 Z), \quad (3.123)$$

$$\Psi_{\pm}(R, Z) = \cos(a_2 R^2 \pm b_2 Z), \quad (3.124)$$

under the constraints (3.119)-(3.122).

We now proceed to demonstrate the behaviour that the above solutions (3.123)-(3.124) exhibit. Unfortunately, Φ_{\pm} and Ψ_{\pm} per se present no closed contours, which are necessary for the successful magnetic confinement of plasma (see Section 1.3.2.1). This is depicted in the plots of Figure 3.2.

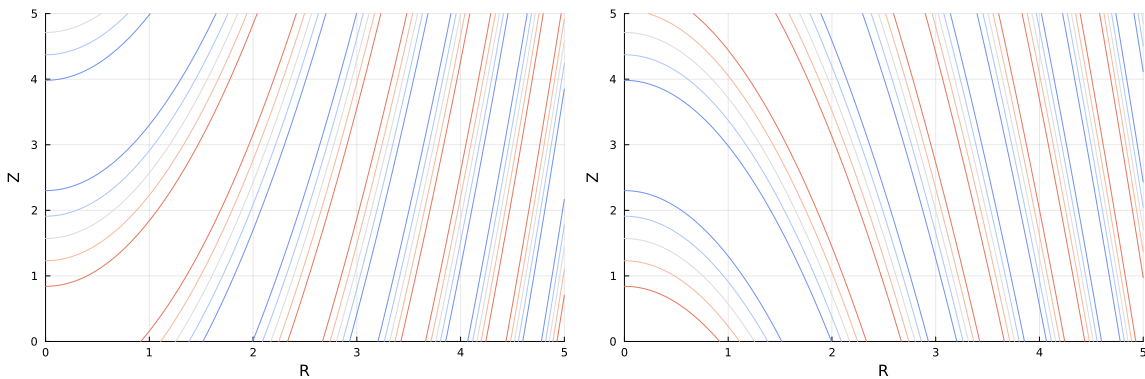


Figure 3.2: Graphical representation of two solutions, Φ_- and Φ_+ respectively, for $a_1 = b_1 = 1$. Contour shading is in arbitrary units.

However if we select as a solution their linear combination

$$\Phi(R, Z) = c_+ \Phi_+ + c_- \Phi_-, \quad (3.125)$$

$$\Psi(R, Z) = d_+ \Psi_+ + d_- \Psi_-, \quad (3.126)$$

where c_{\pm}, d_{\pm} are arbitrary constants, then it is possible to obtain configurations with closed magnetic/ion velocity surfaces, which is illustrated in Figure 3.3.

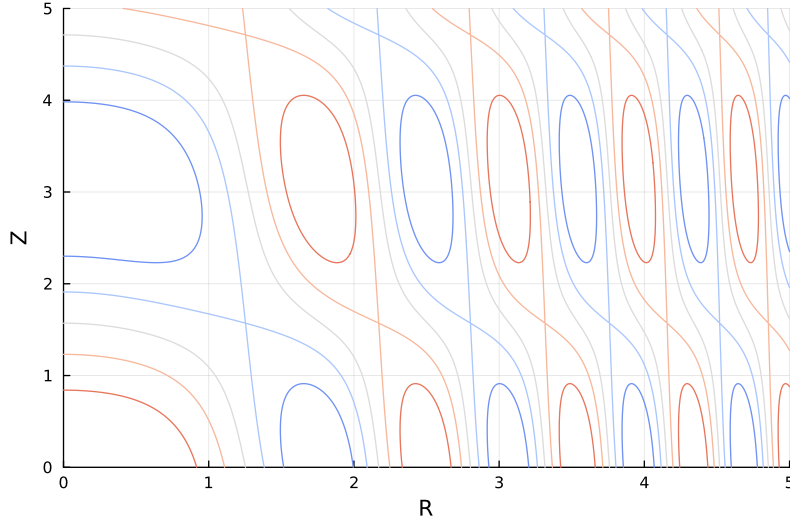


Figure 3.3: Graphical representation of a superposition of solutions like (3.125), for $a_1 = b_1 = 1$ and $c_+ = 1, c_- = 2$. Contour shading is in arbitrary units.

Truly, we notice that closed ion velocity surfaces have emerged; nevertheless Figure 3.3 indicates a *multi-toroidal* configuration. Such configurations have been employed for the study of solar eruptive prominences, coronal loops, etc. [85], [86]. We also observe several X-points in the configuration; more specifically, one may see that their number varies as we alter the values of c_{\pm} .

4

Applications of the solutions to axisymmetric fusion devices

It is now clear to all that our original beliefs, that the doors into the desired region of ultra-high temperatures would open smoothly at the first powerful pressure exerted by the creative energy of physicists, have proved as unfounded as the sinner's hope of entering Paradise without passing through Purgatory. And yet there can be scarcely any doubt that the problem of controlled fusion will eventually be solved. Only we do not know how long we shall have to remain in Purgatory.

Lev Artsimovich¹

The time has come to apply the solutions that were theoretically established in Chapter 3 to more realistic scenarios, namely Tokamak and Field-Reversed Configurations in the scope of Controlled Thermonuclear Fusion. For that purpose, we will endeavour to employ proper shaping methods for determining the boundary in each case, and then we will attempt to specify the unknown parameters so that the resulting configuration exhibits closed, nested magnetic *and* ion velocity surfaces. For the Solovév equilibrium, we will follow a slightly different methodological approach, which was examined in Section 3.3. We will also examine the *equilibrium quantities* for each case, that is the profiles of the magnetic field, the ion velocity field, the current density etc. By far the most notable of these will be the **total plasma pressure** inside the fusion device, since its behaviour directly influences the achievement or not of thermonuclear temperatures (which was discussed in the end of Section 2.2).

4.1 Tokamak-relevant equilibria

4.1.1 Geometry of the D-shaped Tokamak boundary

We begin by discussing the geometry of the boundary that will be used for the construction of axisymmetric Tokamak-relevant equilibria. Generally speaking, we are interested in a *closed* boundary that reflects the toroidal geometry of the Tokamak. More specifically, we will use a boundary of D-shape, because in this case the formation is more stable. The reason lies on the reduced curvature of the magnetic field at the inner side near the axis of the torus. We thus avoid the Rayleigh-Taylor instability, which is particularly dangerous for fusion plasmas. Furthermore, the elongation of the cross-section of the Tokamak from a circle to a D-shape increases the value of the beta parameter to the desired levels, per [18]. In order to describe

¹Lev Artsimovich was the father of the Tokamak. The above (prophetic) words were spoken at the first international conference on plasma physics and controlled nuclear fusion held in Salzburg, in September 1961.

the geometry of the boundary in the poloidal cross-section, we choose three reference points: the *inner equatorial point*, the *outer equatorial point* and the *high point*, as defined in Fig. 4.1.

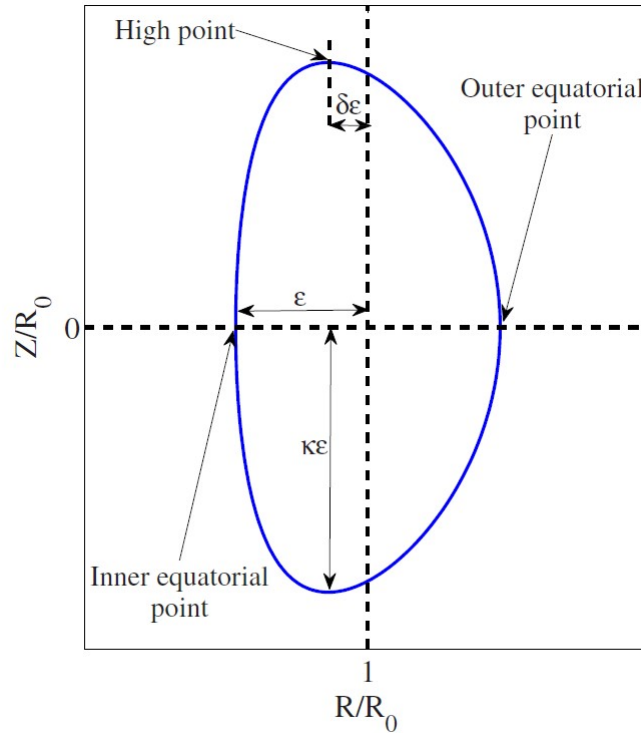


Figure 4.1: The geometry and the three reference points of the D-shaped boundary [87].

The boundary can be defined via the parametric equations introduced in [87], [88], viz.

$$R(\phi) = 1 + \varepsilon \cos(\phi + \alpha \sin \phi), \quad (4.1)$$

$$Z(\phi) = \varepsilon \kappa \sin \phi, \quad (4.2)$$

with $\phi \in [0, 2\pi]$ being the toroidal angle. Three important geometric parameters have also appeared² in the above parametric expressions, namely

$$\varepsilon = \frac{R_{max} - R_{min}}{2R_0} = \frac{a}{R_0} \quad (\text{Inverse aspect ratio}), \quad (4.3)$$

$$\kappa = \frac{Z_{max} - Z_{min}}{R_{max} - R_{min}} = \frac{Z_{max}}{a} \quad (\text{Elongation}), \quad (4.4)$$

$$\delta = \frac{R_0 - R_1}{R_0 - R_{min}} = \frac{R_0 - R_1}{a} \quad (\text{Triangularity}), \quad (4.5)$$

$$\alpha = \arcsin \delta, \quad (4.6)$$

where a and R_0 are the minor and major radii of the torus respectively, R_{min} and R_{max} are the radii of the inner and outer equatorial points, Z_{min} and Z_{max} are the height of the highest and lowest points respectively, and R_1 is the radius corresponding to the highest point [89]. Since the equations we use are dimensionless, it is reasonable to use *dimensionless coordinates* as follows

²Not to be confused with the coefficients of Chapter 3, which bear the same symbols. Also, α should not be confused with a , which is the torus minor radius (see relation (1.19), which is the inverse of (4.3))

$$1 + \varepsilon = \frac{R_{max}}{R_0} \quad (\text{Outer equatorial point radius}), \quad (4.7)$$

$$1 - \varepsilon = \frac{R_{min}}{R_0} \quad (\text{Inner equatorial point radius}), \quad (4.8)$$

$$1 - \delta\varepsilon = \frac{R_1}{R_0} \quad (\text{High point radius}), \quad (4.9)$$

$$\kappa\varepsilon = \frac{Z_{max}}{R_0} \quad (\text{Height of the high point}). \quad (4.10)$$

These coordinates can be easily understood from Figure 4.1, where both R and Z have been normalised, in agreement with the normalisation scheme of Section 1.4.3.2. Relations (4.7)-(4.10) are easily deduced from (4.3)-(4.6), by performing the operations.

4.1.2 Boundary conditions

For the purposes of this thesis, we will use the simplest boundary condition that requires the plasma to be surrounded by a stationary, perfectly conducting wall $\partial\mathcal{S}$, where as we mentioned in a previous chapter, \mathcal{S} is our computational domain - i.e. a torus cross-section. In this case, the electromagnetic boundary conditions (see [26]) require the tangential component of the electric field and the vertical component of the magnetic field to be zero in $\partial\mathcal{S}$,

$$\hat{n} \times E|_{\partial\mathcal{S}} = \mathbf{0}, \quad (4.11)$$

$$\hat{n} \cdot B|_{\partial\mathcal{S}} = 0, \quad (4.12)$$

where \hat{n} is the normal vector to the boundary which points outwards. Since the perfectly conductive wall $\partial\mathcal{S}$ is nothing else but a magnetic surface, relation (4.12) can be written in the light of (2.25) as

$$\hat{n} \cdot B|_{\partial\mathcal{S}} = \frac{1}{R} \nabla\Psi \cdot (\hat{n} \times e_\phi)|_{\partial\mathcal{S}} = 0 \Rightarrow \Psi|_{\partial\mathcal{S}} = \text{const.}, \quad (4.13)$$

which means that $\nabla\Psi$ is normal to the boundary $\partial\mathcal{S}$. Without loss of generality we can choose the constant equal to zero, so we arrive at the following boundary condition

$$\Psi|_{\partial\mathcal{S}} = 0. \quad (4.14)$$

We demand that the flux function for the ion velocity field vanishes on the boundary as well

$$\Phi|_{\partial\mathcal{S}} = 0. \quad (4.15)$$

because otherwise there would be a flow of ions across the boundary.

In order to specify the boundary even better, however, in addition to (4.14) and (4.15), we will impose some more boundary conditions presented in [87]. In particular, the complete set of boundary conditions we will use is the following

$$\Psi(1 + \varepsilon, 0) = 0 \quad (\text{Inner equatorial point}), \quad (4.16)$$

$$\Psi(1 - \varepsilon, 0) = 0 \quad (\text{Outer equatorial point}), \quad (4.17)$$

$$\Psi(1 - \delta\varepsilon, \kappa\varepsilon) = 0 \quad (\text{High point}), \quad (4.18)$$

$$\Psi_R(1 - \delta\varepsilon, \kappa\varepsilon) = 0 \quad (\text{High point maximum}), \quad (4.19)$$

$$\Psi_{ZZ}(1 + \varepsilon, 0) = -N_1\Psi_R(1 + \varepsilon, 0) \quad (\text{Outer equatorial point curvature}), \quad (4.20)$$

$$\Psi_{ZZ}(1 - \varepsilon, 0) = -N_2\Psi_R(1 - \varepsilon, 0) \quad (\text{Inner equatorial point curvature}), \quad (4.21)$$

$$\Psi_{RR}(1 - \delta\varepsilon, \kappa\varepsilon) = -N_3\Psi_Z(1 - \delta\varepsilon, \kappa\varepsilon) \quad (\text{High point curvature}), \quad (4.22)$$

and similarly for the other flux function Φ . In eqs. (4.16)-(4.22), indices denote differentiation and we additionally defined the curvatures at the 3 reference points as

$$N_1 = \left[\frac{d^2 R}{dZ^2} \right]_{\phi=0} = -\frac{(1+\alpha)^2}{\varepsilon\kappa^2}, \quad (4.23)$$

$$N_2 = \left[\frac{d^2 R}{dZ^2} \right]_{\phi=\pi} = \frac{(1-\alpha)^2}{\varepsilon\kappa^2}, \quad (4.24)$$

$$N_3 = \left[\frac{d^2 Z}{dR^2} \right]_{\phi=\pi/2} = -\frac{\kappa}{\varepsilon \cos^2(\alpha)}. \quad (4.25)$$

The proof of relations (4.23)-(4.25) is presented in [90]. This completes the basis of the shaping method that will be used for the construction of axisymmetric Tokamak-relevant equilibria, in the subsections to follow.

4.1.3 Double Beltrami equilibrium

4.1.3.1 Equilibrium construction

The first application that will be studied is based on the solutions that were presented in Section 3.1, and concerns an axisymmetric double Beltrami system. Before we begin the treatment of this equilibrium, it is of utmost importance that we acknowledge the significance of the two Lagrange multipliers $\mu_1 \equiv g_1$ and $\mu_2 \equiv f_1$; the choice that we make for them will affect the Beltrami parameters λ_{\pm} (see eqs. (3.27) and (3.13)), and subsequently the form of the two flux functions Ψ_{\pm} as indicated by the PDE (3.35). Since the choice for the Lagrange multipliers yields different formations depending on the geometry, the need for a reference value arises. Based on previous work of the author [91] that concerned ordinary Beltrami equilibria, it has been established that a Beltrami parameter $\lambda \sim 6$ yields a desirable formation with closed magnetic surfaces, for the geometrical configuration in question (Section 4.1.2). With that being said, we select the reference parameter to be $\ell = 5.52$, and then we ask which values of f_1, g_1 satisfy the relations $\lambda_+ = \ell, \lambda_- = 1.2\ell$. In other words we simply select λ_{\pm} to be close to the reference value of ℓ . Another concern is the appropriate value for the ion skin depth d_i . Given that in Tokamaks the ion skin depth is $\mathcal{O}(cm)$ [51], [92], we choose the (dimensionless) ion skin depth to be $d_i = 0.03$. The rest of the ansatz parameters were found by inspection (see Table 4.1), based on which values yield the most desirable results. Among them, m_0 and n_0 were selected in such a manner that the pressure attains an almost vanishing value on the boundary. Finally, as long as the physical parameters are concerned, we chose the values that are listed in Table 4.1. For the scope of constructing the present equilibrium state, we used ITER parameters that are presented in [93], [94], [95]. We must also underline that the major radius of ITER, R_0 , was used as the reference length for the Alfvén normalisation scheme (Section 1.4.3.2), i.e. $L_0 \equiv R_0$. With the values of Table 4.1 in hand, we can easily calculate the reference Alfvén speed^{3 4}: $v_A = B_0 / \sqrt{\mu_0 m_i n_0}$, as well as the Alfvén time: $\tau_A = R_0 / v_A$. All of these values will be useful for the calculations of the physical quantities of the equilibrium later on. The coefficients $\mathcal{W}_i, i = \{1, 2, 3, 4\}$ (see Appendix A), A_1, A_2, B_1, B_2 (see eq. (3.56)) can be calculated without difficulty via the values of Table 4.1.

³Since our model neglects the inertia of electrons, we are free to substitute the total mass m with the ion mass m_i in the definition of the Alfvén speed.

⁴One should not confuse the Ansatz parameter n_0 with the average plasma density, which bears the same symbol. The reader should be aware of the context in which n_0 appears in order to interpret the symbol correctly.

Table 4.1: Numerical values for the double Beltrami equilibrium parameters.

Parameter		Value	Units
Ion skin depth	d_i	0.03	
Ansatz parameters	f_0	0.2	
	g_0	0.2	
	f_1	28.1937	
	g_1	-27.2659	
	m_0	0.0556	
	n_0	0.0556	
	n_1	-2.5	
ITER Toroidal magnetic field	B_0	5.3	T
ITER Minor radius	a	2	m
ITER Major radius	R_0	6.2	m
ITER Average plasma number density	n_0	1.01×10^{20}	m^{-3}
ITER Inverse aspect ratio	ε	0.32	
ITER Elongation	κ	1.8	
ITER Triangularity	δ	0.45	
Vacuum permeability	μ_0	$4\pi \times 10^{-7}$	H/m
Ion mass (for protonic plasma)	m_i	1.67×10^{-27}	kg

We may now proceed to the analytical determination of the equilibrium. Per Section 3.1, we select⁵ the solutions to the homogeneous equation to be

$$\Psi_{\pm}(R, Z) = R \sum_{j=1}^5 \left\{ a_{j\pm} J_1 \left(R \sqrt{\lambda_{\pm}^2 - j^2} \right) \cos(jZ) + b_{j\pm} Y_1 \left(R \sqrt{\lambda_{\pm}^2 - j^2} \right) \cos(jZ) \right\} + c_{1\pm} R^2 \cos(\lambda_{\pm} Z) + c_{2\pm} \cos(\lambda_{\pm} Z) + c_{3\pm} \cos(\lambda_{\pm} \sqrt{R^2 + Z^2}), \quad (4.26)$$

where $a_{j\pm}$, $b_{j\pm}$, $c_{1\pm}$, $c_{2\pm}$, $c_{3\pm}$, are coefficients that we wish to specify by means of the boundary conditions. As one can notice, no sines are present in (4.26); the reason for this is that we require the formation to be *up-down symmetric*, i.e. symmetric with respect to the mid-plane $Z = 0$. At the solution (4.26), we further added the special, non-separable solution $\cos(\lambda_{\pm} \sqrt{R^2 + Z^2})$, which was suggested by Cerfon and O’Neil [88]. The full solution for the flux functions Ψ and \mathcal{X} is given by equations (3.63), with $c_+ = c_- = 1$ and the coefficients α , β , γ , δ given by eqs. (3.62). The next step is to specify the boundary, per Section 4.1.2 with the aim of obtaining a formation with closed, nested magnetic surfaces. It should be stated that the boundary will be imposed *only* on Ψ . In order to avoid the trivial solution $\Psi = 0$, we will set some coefficients of (4.26) equal to the unity, namely $a_{1+} = a_{1-} = c_{3-} = 1$. The solution in question contains 23 coefficients (not including the ones we set equal to 1), which ought to be determined from the boundary conditions. Since the conditions (4.16)-(4.22) are 7 in total, a first estimate is that we will need 16 extra points for closure, at which we will additionally impose the boundary condition (4.14). Practically, however, we defined 18 points on the boundary to get 16 linearly independent algebraic equations. The extra points are found via the parametric equations (4.1), (4.2) and are depicted in Figure 4.2.

⁵Both λ_{\pm}^2 are always greater than j^2 , thus the solutions are ordinary (and not modified) Bessel functions. We also supposed that the separation constant is a real number.

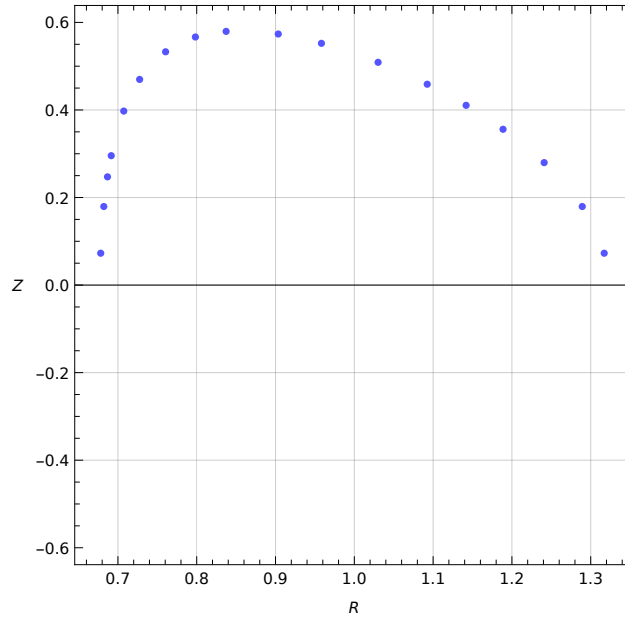


Figure 4.2: The extra points on the boundary for the double Beltrami equilibrium. Due to the up-down symmetry of the formation, only points for $Z > 0$ have been chosen.

The points are of course indicative, and lie at $Z > 0$, due to the previously mentioned up-down symmetry of the formation. Hence, the extra boundary conditions will read

$$\Psi(R = R_{extrai}, Z = Z_{extrai}) = 0, \quad (4.27)$$

where R_{extrai} , $Z = Z_{extrai}$ are the coordinates of the extra points. The problem that we want solved is basically the system of *algebraic* equations (4.16)-(4.22), along with (4.27), with respect to the unknown coefficients. At this point it is appropriate to comment that the system in question is *linear*, since the Beltrami parameters λ_{\pm} are constants. In the opposite case where the λ_{\pm} had spacial dependence, then the system of equations would become *non-linear* and its solution would be significantly complicated. By means of linear solving routines, the above-mentioned system can be successfully solved. A re-scaling of the flux functions was also carried out⁶, in order to obtain better results. Figure 4.3 illustrates the solution, i.e. some magnetic surfaces, along with the respective ion velocity flow surfaces in a poloidal torus cross-section. Of course, since we are addressing an axisymmetric equilibrium, this pattern is going to be the same for every single poloidal cross-section of the confinement system.

The first remarkable finding is witnessed by Figure 4.3; **the departure of the magnetic surfaces with the respect to the ion velocity ones**. This is naturally expected, as the Hall MHD model predicts the separation of the ion fluid from the magnetic surfaces. This separation becomes more evident for greater values of the ion skin depth d_i . For $d_i = 0$, the separation would be non-existent since we would end up at an MHD-like scenario. Despite this, the MHD limit of $d_i \rightarrow 0$ should be interpreted with caution and reluctance, because setting $d_i = 0$ in the Hall MHD Casimir invariants (2.28) does not yield the MHD Casimirs. This occurs because the MHD limit consists a *singular perturbation problem* [28]. In addition, it should be emphasised that, due to the separation of the two fluids, the formation possesses *two* separate axes; a magnetic one *and* a velocity one - though their coordinates differ only slightly. Another finding that can be deduced from Fig. 4.3, is that the equilibrium exhibits a **Shafranov shift** [96]. This phenomenon, proposed by Shafranov at 1963, concerns the outward radial displacement of the magnetic axis with respect to the geometrical center of the boundary, and is caused by

⁶Remember that the two flux functions are defined by the indeterminacy of a multiplicative constant, hence we can choose these constants as seen fit for a proper rescaling.

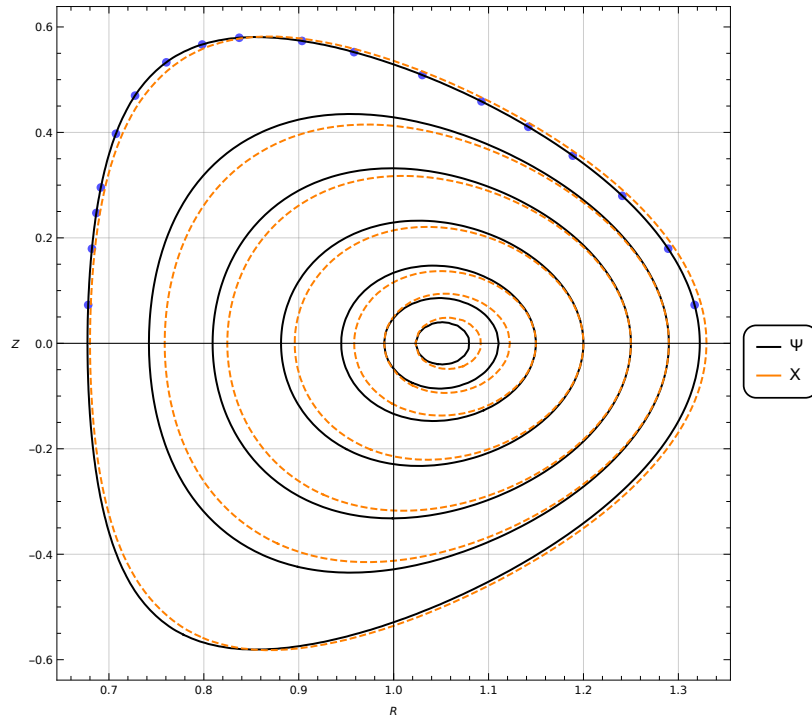


Figure 4.3: The contours of the magnetic and the ion velocity surfaces for the double Beltrami equilibrium. The chosen extra points on the boundary are illustrated as well.

the combined effects of toroidicity, the pressure gradient, and the so-called *hoop force* in the toroidal direction [18].

4.1.3.2 Equilibrium quantities

Our next goal is to demonstrate the behaviour of the physical quantities of interest for the current equilibrium state. The quantities are the following: the two flux functions Ψ and \mathcal{X} , the magnitude of the magnetic field B , the magnitude of the ion velocity field v , the current density J , and the plasma pressure P . Moreover, since the Hall MHD model predicts the separation of the two fluids, it is appropriate to carry out a calculation of the electric field as well, from Ohm's law (1.62). Albeit the plasma is quasineutral, the plasma approximation ($n_i \simeq n_e$ while at the same time $\nabla \cdot E \neq 0$) cannot replace Gauss's law (1.23) in our case.

We begin by examining the profiles of the two flux functions. Those are illustrated in Figures 4.4 and 4.5.

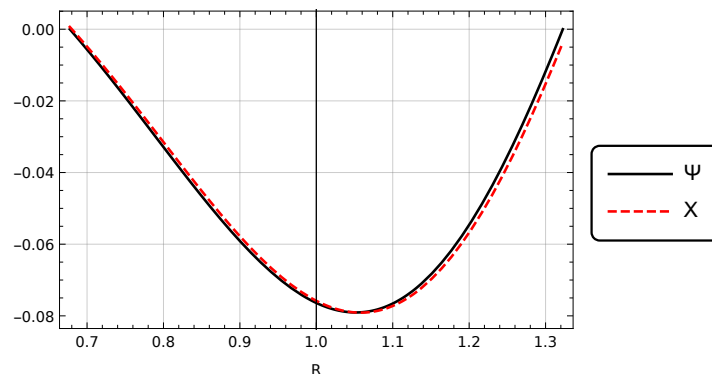


Figure 4.4: The (dimensionless) flux functions' profiles for the double Beltrami equilibrium on the plane $Z = 0$.

We observe that both Ψ and \mathcal{X} present a minimum on the magnetic axis, which is physically acceptable. The Shafranov shift is noticeable here as well, since the minimum is displaced with respect to $R = 1$. The slight deviation of the two flux functions again witnesses their different nature, and subsequently the separation of the ion fluid from the magnetic surfaces. A similar behaviour is seen in the $R = 1$ plane (Fig. 4.5), where we corroborate the up-down symmetry of the formation.

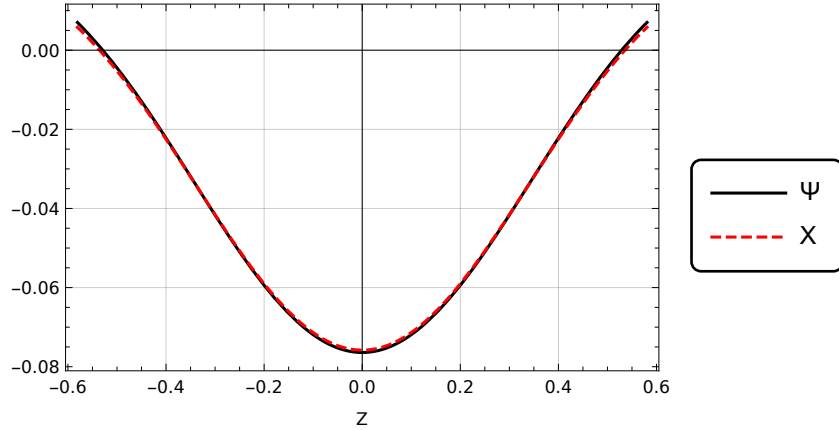


Figure 4.5: The (dimensionless) flux functions' profiles for the double Beltrami equilibrium on the plane $R = 1$.

The next two quantities that will be studied are the magnetic and the velocity fields. Fig. 4.6 depicts two profiles of the former, while Fig. 4.7 two profiles of the latter. For the calculation of the magnetic field we utilised relations (2.40) and (2.25), while for the calculation of the velocity field we employed relations (2.41), (2.42), and (2.26). Both \mathbf{B} and \mathbf{v} have physically acceptable profiles, and their respective values are within acceptable levels [93], [97]; the magnetic field values are $\mathcal{O}(T)$, while the velocity values are $\mathcal{O}(10^6 \text{ m/s})$.

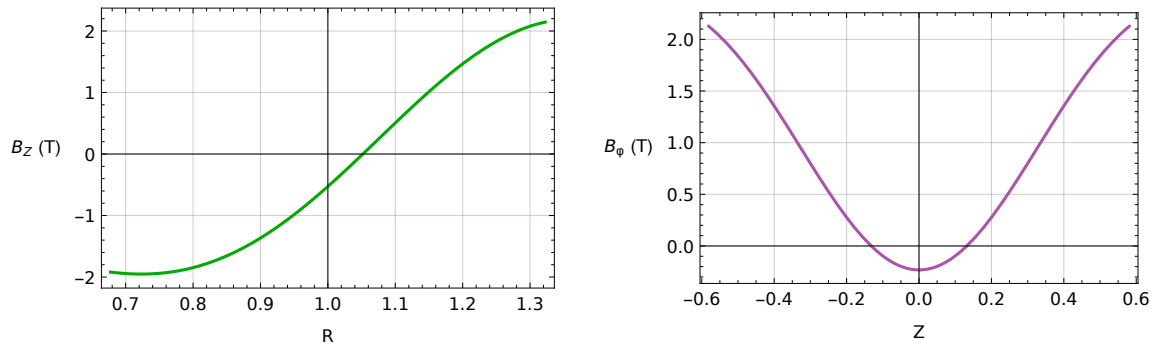


Figure 4.6: Magnetic field profiles for the double Beltrami equilibrium. Left: The Z -component of the magnetic field on the plane $Z = 0$. Right: The toroidal component of the magnetic field on the plane $R = 1$.

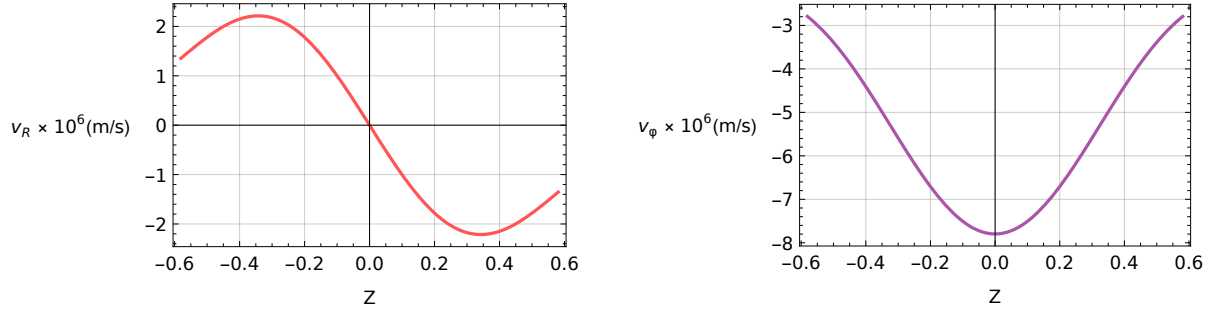


Figure 4.7: Ion velocity field profiles for the double Beltrami equilibrium. Left: The R -component of the velocity field on the plane $R = 1$. Right: The toroidal component of the velocity field on the plane $R = 1$.

Subsequent to this, it is interesting to plot the *poloidal Alfvénic Mach number*, i.e. the poloidal velocity divided by the reference Alfvén speed

$$M_A^p = \frac{v_p v_A}{v_A} \equiv v_p = \sqrt{v_R^2 + v_Z^2}, \quad (4.28)$$

where we multiplied the dimensionless poloidal velocity, v_p , with the Alfvén speed in order to obtain the respective physical quantity. Due to the selected Alfvén normalisation scheme, the poloidal Alfvénic Mach number coincides with the dimensionless poloidal velocity. Its profile is depicted in Figure 4.8. As the plot of Fig. 4.8 suggests, the values of M_A^p are always lower than unity, therefore the poloidal ion velocity is *sub-Alfvénic*, in accordance with experimental evidence [97]. This means that for such ion flows, the development of shock waves and related disturbances is unlikely [5]. On top of that, the behaviour of M_A^p on the velocity axis indicates a discontinuity of the first derivative of the poloidal ion velocity with respect to R thereon.

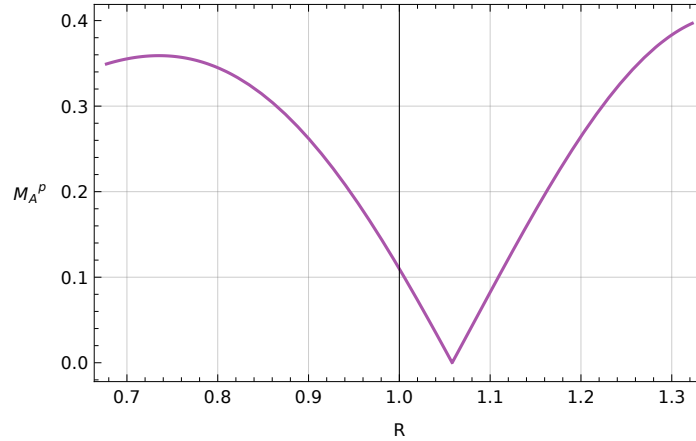


Figure 4.8: The profile of the poloidal Alfvénic Mach number on the plane $Z = 0$ for the double Beltrami equilibrium.

R -profiles of the current density components J_Z and J_ϕ are displayed in Fig. 4.9. As we can see, the profiles are physically acceptable and the current density values are in the MA/m^2 regime, which is typical for most Tokamaks, including ITER [94], [95]. Note that for deducing the current density we used Ampère’s law, (1.37) in dimensionless form.

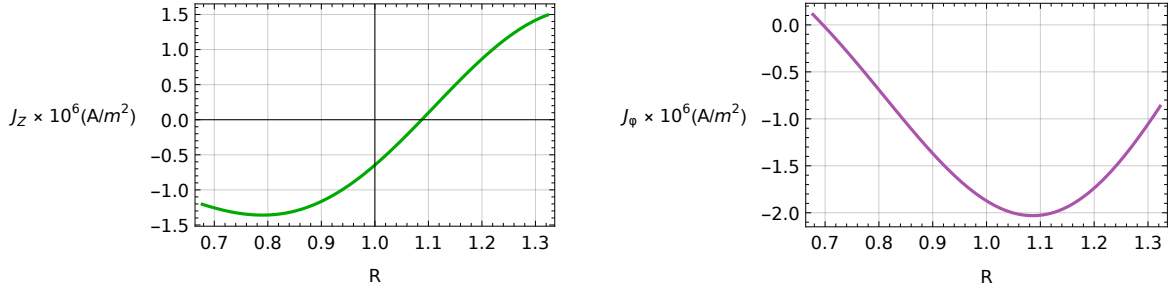


Figure 4.9: Current density profiles for the double Beltrami equilibrium. Left: The R -component of the current density on the plane $R = 1$. Right: The toroidal component of the current density on the plane $Z = 0$.

We proceed by presenting some profiles for the poloidal components of the electric field (Fig. 4.10), calculated in a straightforward manner from Ohm's law (1.62). It is noted here that in the MHD limit the electric field is associated with the component of the velocity non-parallel to the magnetic field. For the current equilibrium the separation of the two fluids generates a purely poloidal electric field, as the toroidal component was found to be equal to zero. This finding is expected, since we have no toroidal loop voltage and the plasma is ideal. The resulting components, namely E_R and E_Z , present a physically expected behaviour and values of the order of MV/m .

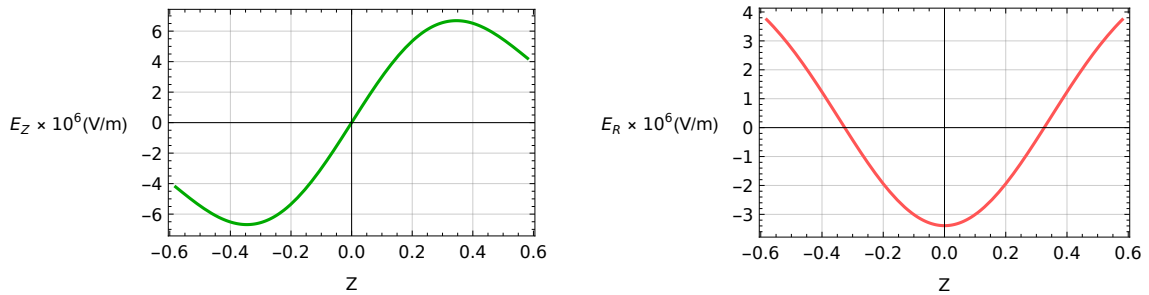


Figure 4.10: Poloidal electric field profiles for the double Beltrami equilibrium. Left: The Z -component of the electric field on the plane $R = 1$. Right: The R -component of the electric field on the plane $R = 1$.

The final equilibrium quantity that is of particular interest for the scope of magnetic confinement is the plasma pressure. Based on the particular ansatz for the double Beltrami equilibrium, we can perform a calculation of P via eq. (2.48). The result is shown in Figure 4.11. The profile is peaked on the magnetic axis (although there is a slight deviation due to the flow), and the pressure values are typical for Tokamaks [94], [98]. Also, we should note that although P attains low values on the boundary it is not exactly zero, which is desirable for more efficient plasma confinement. This is so because, owing to the flow the isobaric surfaces depart from the magnetic surfaces, thus the pressure has the tendency to organise into separate poloidal-cross-section contours, per Fig. 4.12. Before closing this section, it is noteworthy that if the profile of the squared velocity $v^2 = v_R^2 + v_\phi^2 + v_Z^2$ is calculated or chosen in some manner to be hollow (which means that it has a minimum) with respect to the magnetic axis, then the pressure profile would still be peaked on axis. Such a velocity profile is justifiable for

the study of the L-H transition (see Section 1.5), where sheared poloidal flows develop in the pedestal region near the boundary.

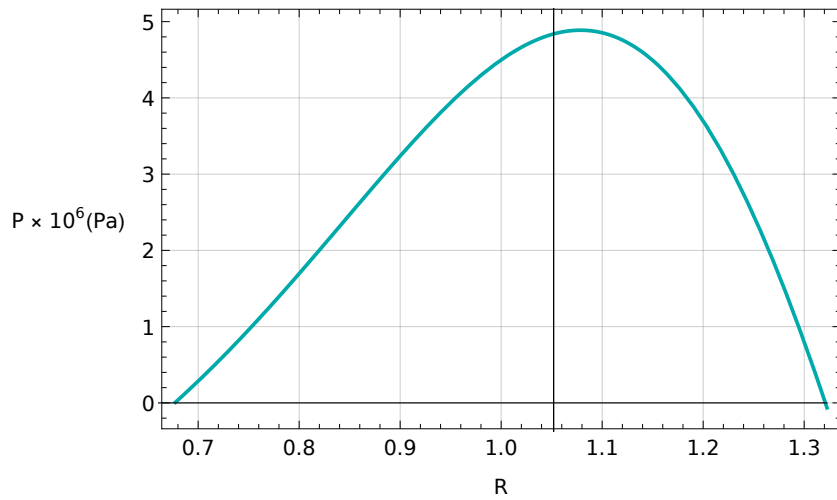


Figure 4.11: The plasma pressure profile on the $Z = 0$ plane for the double Beltrami equilibrium.

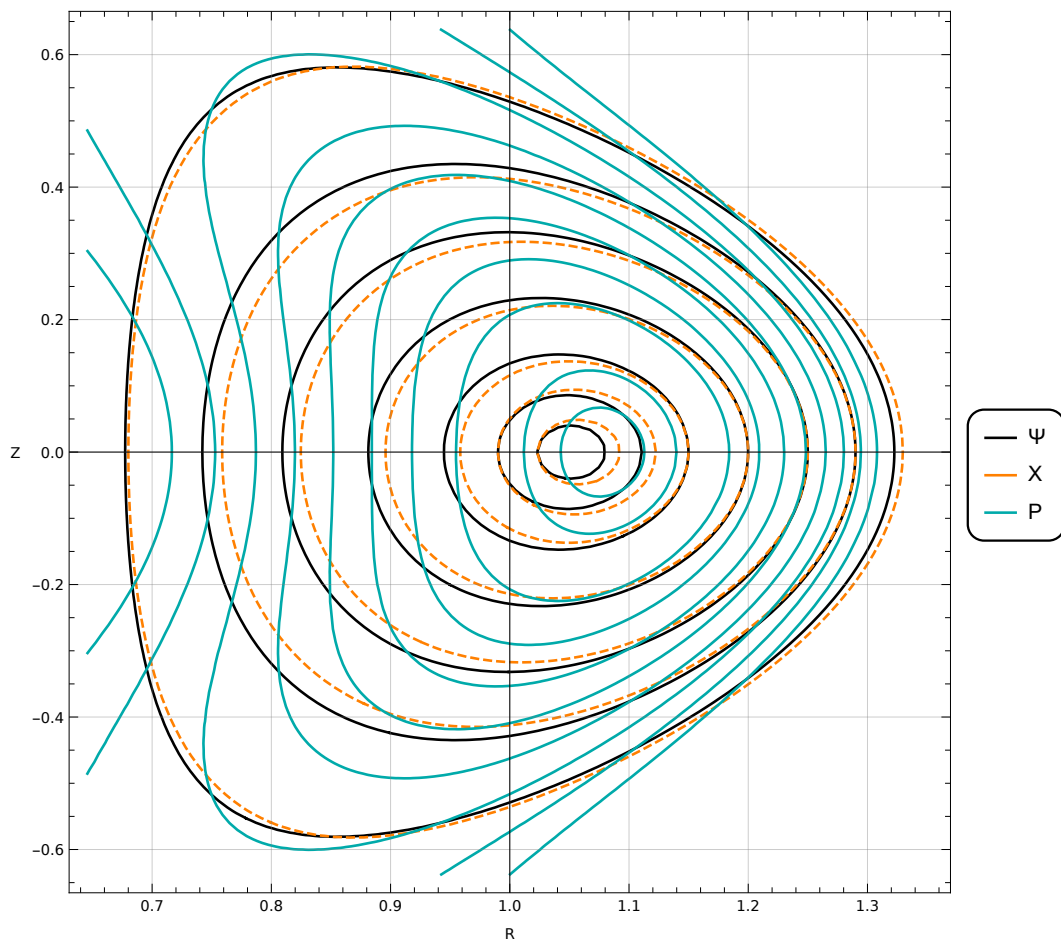


Figure 4.12: The pressure contours in a torus cross section, along with the magnetic and ion surfaces for the double Beltrami equilibrium.

4.1.4 Whittaker equilibrium

4.1.4.1 Equilibrium construction

In this subsection we shall concern ourselves with the construction of an axisymmetric equilibrium state of the Whittaker type, on the basis of the theoretical background that was presented in Section 3.2. From one point of view, this equilibrium state is a more generic counterpart of the one formulated in Section 4.1.3, due to the more general form of the adopted ansatz (2.49)-(2.52). We commence by presenting the fundamental parameters that will be used for the Whittaker equilibrium, per Table 4.2.

Table 4.2: Numerical values for the Whittaker equilibrium parameters.

Parameter		Value	Units
Ion skin depth	d_i	0.02	
Ansatz parameters	f_0	0.5	
	g_0	0.5	
	f_1	50.0156	
	g_1	$-(d_i^2 f_1)^{-1}$	
	m_0	0	
	n_0	0	
	m_1	-1282.25	
	n_1	1282.25	
	m_2	-40	
n_2	40		
ITER Toroidal magnetic field	B_0	5.3	T
ITER Minor radius	a	2	m
ITER Major radius	R_0	6.2	m
ITER Inverse aspect ratio	ε	0.32	
ITER Elongation	κ	1.8	
ITER Triangularity	δ	0.45	
Vacuum permittivity	ϵ_0	8.854×10^{-12}	F/m
Vacuum permeability	μ_0	$4\pi \times 10^{-7}$	H/m
Speed of light in vacuum	c	3×10^8	m/s
Elementary charge	e	1.6×10^{-19}	C
Ion mass (for protonic plasma)	m_i	1.67×10^{-27}	kg
Plasma number density	n_0	3.38×10^{18}	m^{-3}

For the dimensionless ion skin depth, we select again a value of $\mathcal{O}(10^{-2})$, but slightly lower than that of the double Beltrami case. Apart from d_i , the crucial part is once again the choice that we shall make for the ansatz parameters. On the basis of analytical calculations carried out in [99], and having been established that for $n_2 = 40$ and $m_2 = -40$ we end up at a desirable formation, we adopt those values (Table 4.2). In order to refine the calculation more, an empirical rule was discovered, namely that f_1 should be chosen in such a way, that $f_1 d_i \sim 1$. The ansatz parameters m_1, n_1 were found from the constraints (3.84), (3.86) that concern the non-homogeneous solutions to eqs. (3.79), (3.80), while the rest of the ansatz parameters were found by inspection. In regard to the geometrical parameters of the equilibrium, we utilised the same ones from the double Beltrami case, that concern ITER and which are listed in Table 4.1 as well. Another distinct feature from the aforementioned equilibrium is that we did not adopt the ITER average plasma density, (see Table 4.1), but instead we calculated n_0 from the

very definition of the ion skin depth, (1.59), for given $d_i = 0.02$. As for the normalisation of the physical quantities, we once more select the reference length scale to be $L_0 \equiv R_0$.

After calculating the required coefficients γ , δ , δ' , ε , ε' , ζ straightforwardly from relations (3.68) and (3.81), we select as (up-down symmetric) solutions to the homogeneous equations (3.66), (3.67) the following

$$\Psi_h(R, Z) = \sum_{k=1}^{11} \left[a_k \mathcal{M}_{\nu_k, \frac{1}{2}}(i\sqrt{\delta}R^2) \cos(kZ) + b_k \mathcal{W}_{\nu_k, \frac{1}{2}}(i\sqrt{\delta}R^2) \cos(kZ) \right], \quad (4.29)$$

and

$$\Phi_h(R, Z) = \sum_{k=1}^{11} \left[\tilde{a}_k \mathcal{M}_{\tilde{\nu}_k, \frac{1}{2}}(i\sqrt{\delta'}R^2) \cos(kZ) + \tilde{b}_k \mathcal{W}_{\tilde{\nu}_k, \frac{1}{2}}(i\sqrt{\delta'}R^2) \cos(kZ) \right]. \quad (4.30)$$

We also set $a_1 = \tilde{a}_1 = 1$ in order to avoid the trivial solution, and rescale the solutions properly in order to obtain desirable results. For a particular solution to the non-homogeneous equations (3.79), (3.80), we shall select an *up-down symmetric* solution as well in order to preserve the said symmetry of the formation. Since the previously proposed solutions (3.83), (3.85) contain sines, which are up-down *asymmetric*, we shall exploit the freedom that the similarity reduction method [67] bestows us to select another variant of the particular solutions, which is up-down symmetric. Those ones read

$$\Psi_p(R, Z) = \cos\left(\frac{\sqrt{\delta}}{2}R^2 + \sqrt{\gamma}Z\right) + \cos\left(\frac{\sqrt{\delta}}{2}R^2 - \sqrt{\gamma}Z\right) - \frac{\varepsilon}{\delta}, \quad (4.31)$$

and

$$\Phi_p(R, Z) = \cos\left(\frac{\sqrt{\delta'}}{2}R^2 + \sqrt{\gamma}Z\right) + \cos\left(\frac{\sqrt{\delta'}}{2}R^2 - \sqrt{\gamma}Z\right) - \frac{\varepsilon'}{\delta'}. \quad (4.32)$$

Truly, one may corroborate that the above particular solutions (4.31), (4.32) satisfy the non-homogeneous equations (3.79) and (3.80). The full solution will of course be the superposition of (4.29) with (4.31) and (4.30) with (4.32). We should additionally remark that, since the two Whittaker functions are complex in general and given that our PDEs are linear, it is mandatory to retain either the real or the imaginary part of Ψ and Φ , as both of them are solutions. For the current analysis we will select the imaginary part, for both flux functions and their derivatives with respect to R and Z , up to second order.

As concerns the boundary of the formation, we will employ the same shaping method (see Sections 4.1.1, 4.1.2) as with the previous equilibrium. The only difference is that we will impose the boundary on Ψ and Φ *separately* in order to obtain the two kind of surfaces (magnetic and velocity ones). With that being said, although we have 21 coefficients (for each flux function) that we want specified, we need to define 14 extra points on the boundary (Fig. 4.13) via the parametric equations (4.1), (4.2), as well as two extra boundary conditions in addition to (4.16)-(4.22) - namely that $\Psi_Z(1 \pm \varepsilon, 0) = \Phi_Z(1 \pm \varepsilon, 0) = 0$ per [99] - in order to obtain closure.

The determination of the flux surfaces reduces to solving the system of the said algebraic equations (boundary conditions (4.16)-(4.22), along with $\Psi_Z(1 \pm \varepsilon, 0) = \Phi_Z(1 \pm \varepsilon, 0) = 0$ and (4.27)), with respect to the unknown coefficients. This procedure will be carried out twice, since we actually have one system for each flux function. After a successful calculation of the coefficients in question, we proceed to present the contours of both flux functions (Figure 4.14).

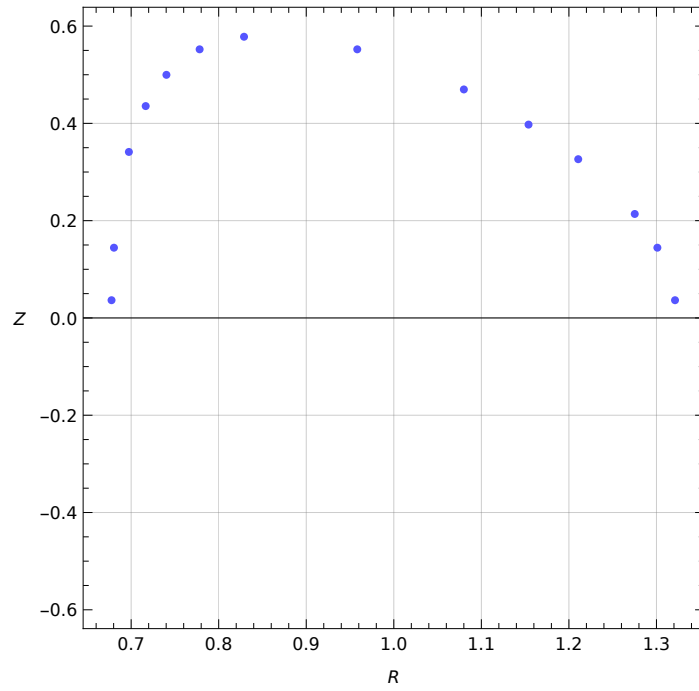


Figure 4.13: The extra points on the boundary for the Whittaker equilibrium.

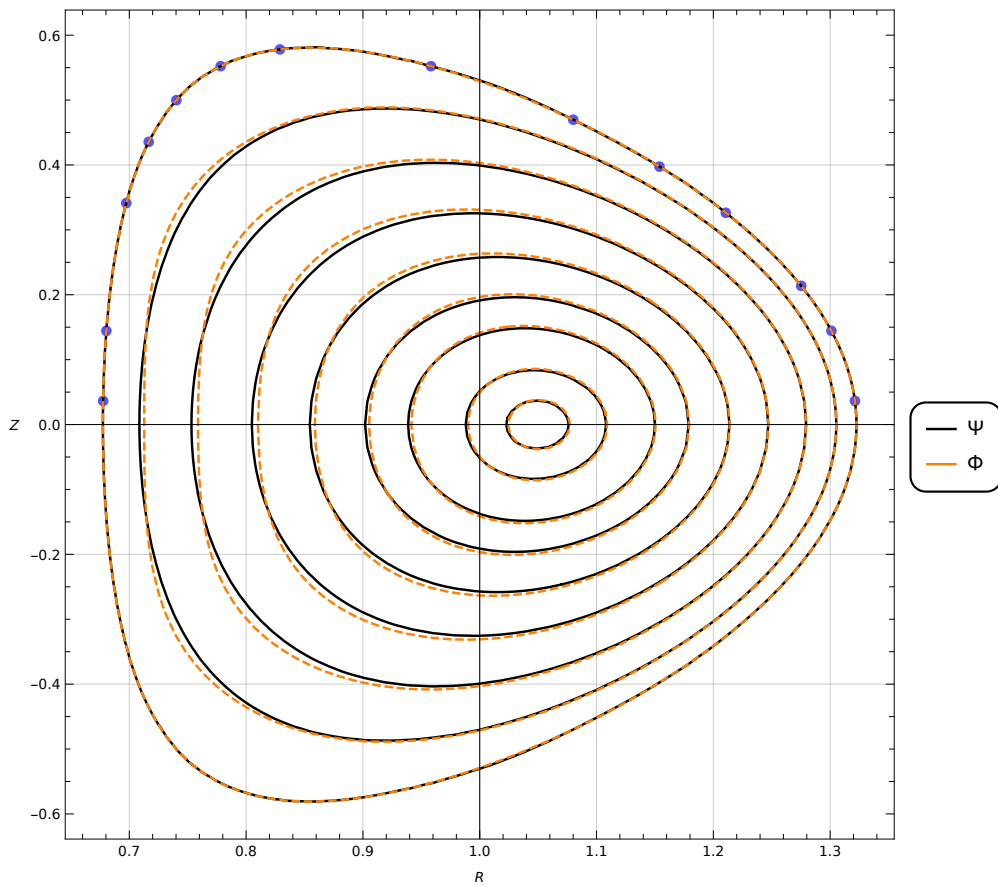


Figure 4.14: The contours of the magnetic and the ion velocity surfaces for the Whittaker equilibrium. The chosen extra points on the boundary are illustrated as well.

As with the double Beltrami equilibrium, the separation of the two flux surfaces is evident.

The velocity surfaces are organised around an axis other than the magnetic one, although once again their deviation is only slight. A Shafranov shift of both surfaces can also be observed, for the same reasons as in the previously-built equilibrium. The difference with the latter is that the two boundaries for Ψ and Φ coincide - which is expected as we imposed the boundary on both of them.

4.1.4.2 Equilibrium quantities

In this subsection we present some equilibrium quantities of interest for the current equilibrium state, by following the footsteps of Section 4.1.3. The first profiles that will be examined are of course those of the two flux functions Ψ and Φ . Figure 4.15 depicts the behaviour of their normalised counterparts with respect to their axial values. This normalisation was carried out because the two quantities would otherwise differ by many orders of magnitude, and thus they could not be displayed in the same plot.

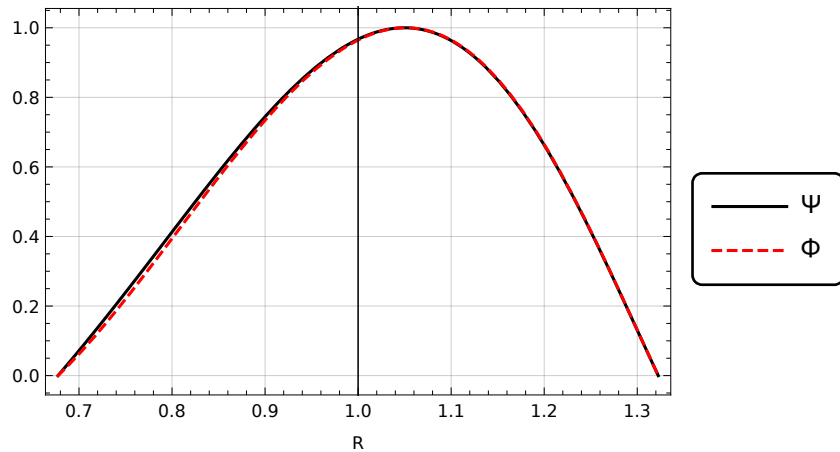


Figure 4.15: The (dimensionless) flux functions' profiles for the Whittaker equilibrium on the plane $Z = 0$.

We notice that both flux functions exhibit a maximum on the respective axes, as expected. The respective profiles on the $R = 1$ plane are not displayed here, since they resemble the ones of Fig. 4.5 and they provide no additional information whatsoever.

As far as the magnetic field is concerned, we present at Fig. 4.16 two profiles for its Z and ϕ (toroidal) component, calculated by relations (2.40) and (2.25) (with the adopted ansatz in mind).

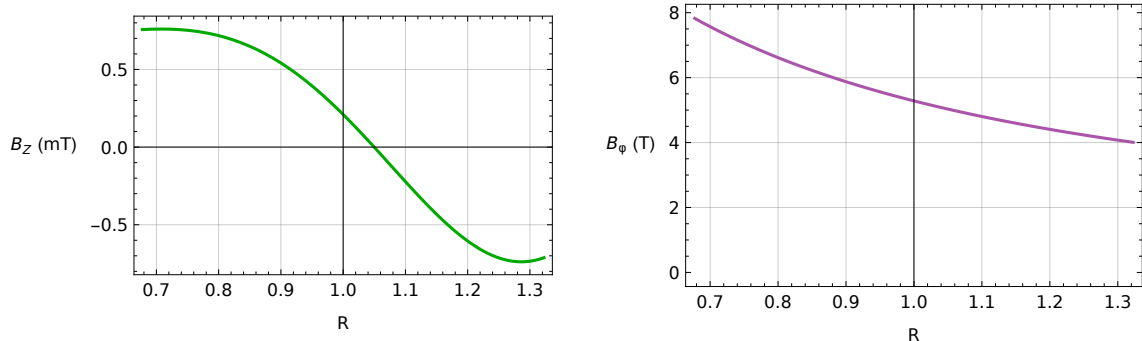


Figure 4.16: Magnetic field profiles for the Whittaker equilibrium. Left: The Z -component of the magnetic field on the plane $Z = 0$. Right: The toroidal component of the magnetic field on the plane $Z = 0$.

The poloidal components of \mathbf{B} attain values of the order of mT , which are two orders of magnitude lower than the respective ones found in Tokamaks [94]. The toroidal component decreases monotonically from the inner to the outer equatorial point of the boundary, as expected because of the R^{-1} dependence of the dominant vacuum magnetic field, and its values are in desirable levels.

Two profiles for the velocity field components are shown in Fig. 4.17. Both the values and the behaviour of the vector field in question are physically acceptable and desirable. The calculation was based in equations (2.41) and (2.26).

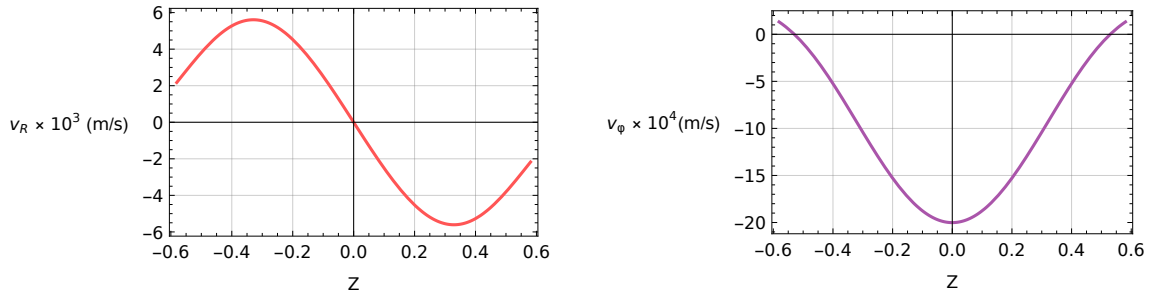


Figure 4.17: Ion velocity field profiles for the Whittaker equilibrium. Left: The R -component of the velocity field on the plane $R = 1$. Right: The toroidal component of the velocity field on the plane $R = 1$.

Additionally, from Fig. 4.18, one can notice that the poloidal Alfvénic Mach number demonstrates a behaviour similar to the one of the double Beltrami equilibrium (Fig. 4.8). Relation (4.28) was used, as in the previous case. The poloidal velocity values are once again sub-Alfvénic, and the first derivative of the poloidal velocity is discontinuous on the velocity axis.

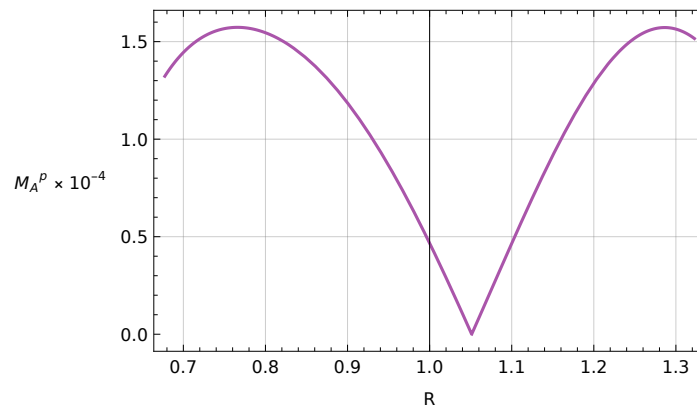


Figure 4.18: The profile of the poloidal Alfvénic Mach number on the plane $Z = 0$ for the Whittaker equilibrium.

The next quantity of interest is the current density, found via Ampere’s law, and two profiles can be seen in Fig. 4.19. We note that both J_Z and J_ϕ have desirable profiles and values that range between $10^2 - 10^4 A/m^2$.

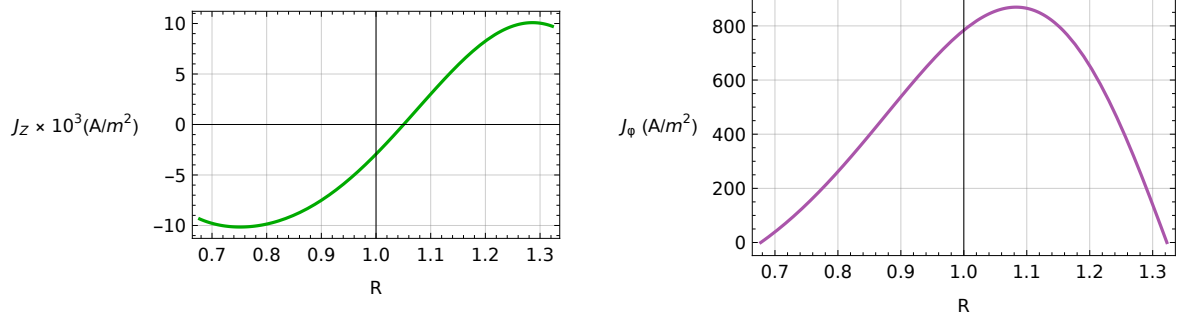


Figure 4.19: Current density profiles for the Whittaker equilibrium. Left: The Z -component of the current density on the plane $Z = 0$. Right: The toroidal component of the current density on the plane $Z = 0$.

The generated electric field (found by Ohm's law (1.62)) ranges from 10^3 to 10^4 V/m (Fig. 4.20). The toroidal component of the electric field is once more equal to zero, for the same reasons as in Section 4.1.3.

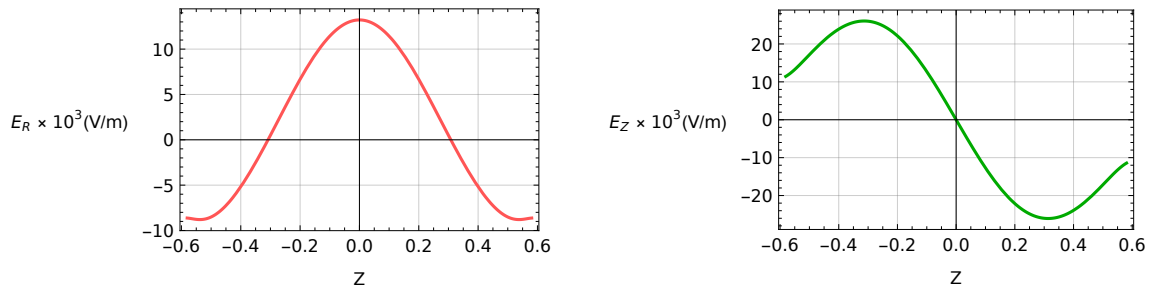


Figure 4.20: Poloidal electric field profiles for the Whittaker equilibrium. Left: The R -component of the electric field on the plane $R = 1$. Right: The Z -component of the electric field on the plane $R = 1$.

Finally, we proceed to a computation of the plasma pressure profile, by means of eq. (2.48) for the current ansatz. The result is shown in Fig. 4.21. This profile is almost optimal for the scope of controlled thermonuclear fusion, for mainly three reasons. In the first place, the plasma pressure values are ideal, for reasons discussed in the double Beltrami equilibrium in the respective section. Secondly, it is a peaked profile, with only a minor deviation from the magnetic axis due to the plasma flow. Thirdly, the pressure attains values very close to zero on the boundary. A final consideration to keep in mind is that the pressure is well stratified, as seen in the contour plot of Fig. 4.22. This organisation is much better than the respective one of the double Beltrami case (Fig 4.12). One should expect a very effective plasma confinement from a stratified pressure profile with the aforementioned characteristics.

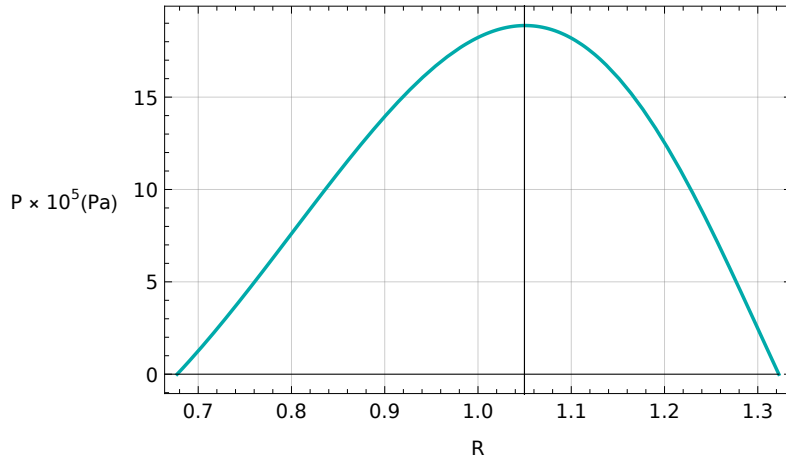


Figure 4.21: The plasma pressure profile on the $Z = 0$ plane for the Whittaker equilibrium.

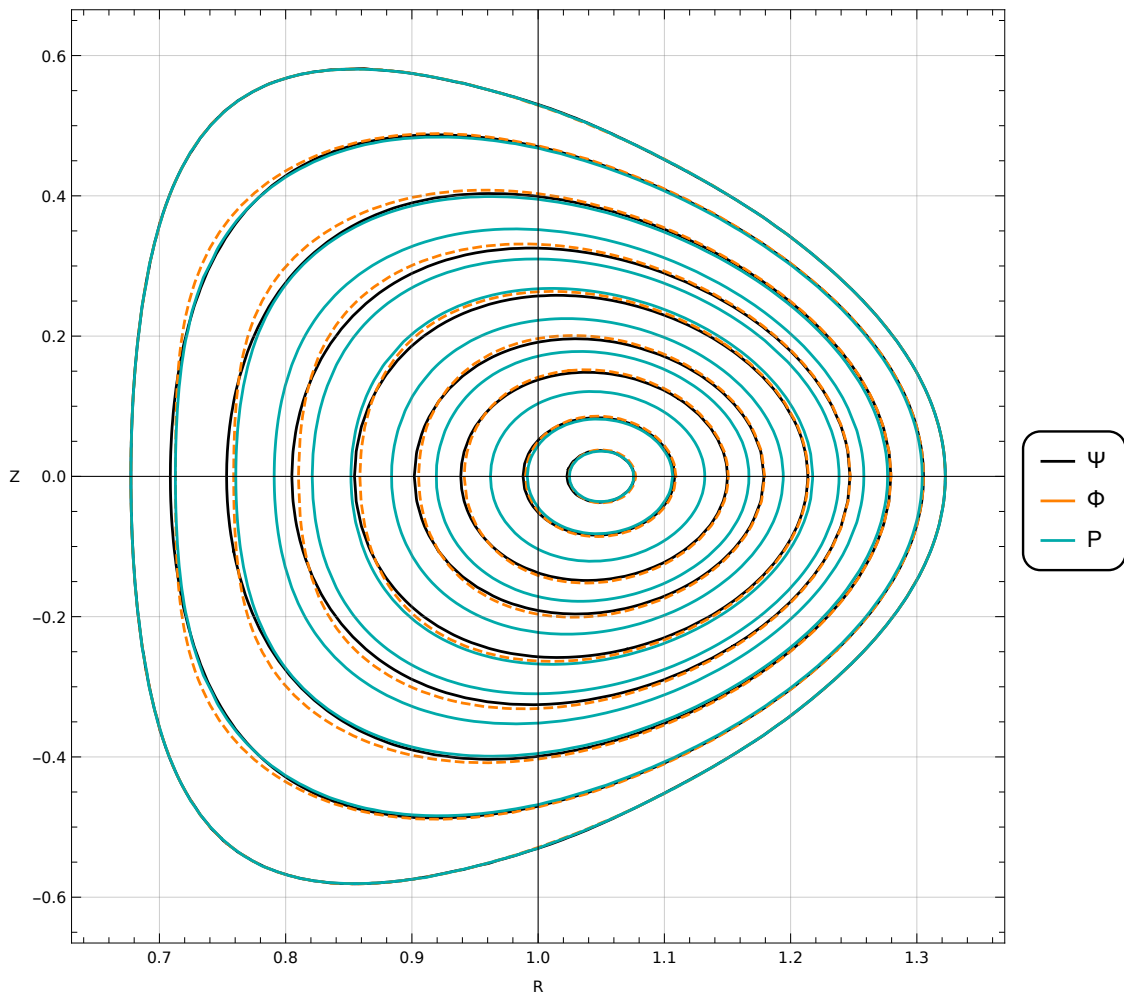


Figure 4.22: The pressure contours in a torus cross section, along with the magnetic and ion surfaces for the Whittaker equilibrium.

4.2 FRC Solovév equilibrium

4.2.1 Equilibrium construction

For the final application we shall utilise the theoretical methodologies and frameworks expounded in Section 3.3 for the construction of another axisymmetric equilibrium state, which concerns field-reversed configurations (FRCs) as we previously argued. We stress again for the sake of clarity that this is an MHD-like equilibrium state with sheared poloidal flows, although it is predicted in the scope of the Hall MHD model for a specific selection of the ansatz for the free parameters. Generally speaking, the analysis is estimated to be much easier from the previous sections, as $\Psi \equiv \Phi$, and we already have a solution at hand, namely (3.102), the behaviour of which is well-studied.

For the needs of this application we will exploit some numerical values of the Princeton FRC (PFRC), presented in [100], which we list in Table 4.3, along with other geometrical and physical parameters.

Table 4.3: Numerical values for the Solovév equilibrium parameters.

Parameter		Value	Units
PFRC Minor axis	a	0.025	m
PFRC Major axis	b	0.075	m
PFRC Major radius	R_0	$b/2$	m
PFRC Axial distance of the magnetic axis	R_a	$2R_0/\sqrt{2}$	m
PFRC Elongation	$\kappa \equiv \delta$	1/3	
PFRC Central plane axial magnetic field	B_a	5.5	T
PFRC Equilibrium electron number density	n_0	5.7×10^{20}	m^{-3}
Vacuum permeability	μ_0	$4\pi \times 10^{-7}$	H/m
Ion mass (for protonic plasma)	m_i	1.67×10^{-27}	kg

It is interesting that only one ansatz parameter appears in the two GS equations - either m_1 or n_1 , since $n_1 = -m_1$. By assumption, $m_2 = n_2 = 0$ and also $f_0 + g_0 = 0$ due to absence of vacuum toroidal magnetic field. As for f_1 and g_1 , they are indefinite and in any case do not concern us since they no longer appear in the GS equations (3.100), (3.101). We shall leave the determination of the only free parameter, m_1 for later when we address the computation of the equilibrium quantities. The parameters m_0 and n_0 will also concern us later, when we will endeavour to optimise the pressure profile so that it vanishes on the separatrix. The reader should also bear in mind that the same normalisation scheme (Section 1.4.3.2) holds, albeit with different coordinates, ξ and ζ which, as we discussed in Section 3.3, are basically the R and Z physical coordinates normalised with respect to the radius of the magnetic axis, R_a .

With that being said, let us work on the part of the solution (3.102) without the constant-term factor, i.e.

$$\Psi(\xi, \zeta) \equiv \Phi(\xi, \zeta) = \left[\zeta^2 \xi^2 + \frac{\delta^2}{4} (\zeta^2 - 1)^2 \right], \quad (4.33)$$

with the aim of presenting the basic characteristics of this flux function on a poloidal cross-section. The constant term will be added later on for the needs of the equilibrium quantities. Figure 4.23 depicts some contours of the flux function in question, with the values of PFRC given.

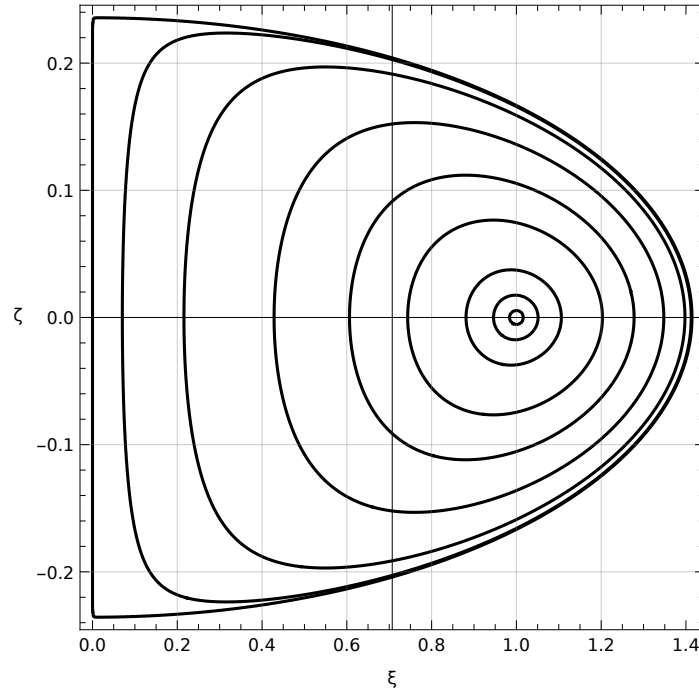


Figure 4.23: The (common) contours of the magnetic and the ion velocity surfaces for the Solovév equilibrium. The outer closed magnetic surface represents the separatrix.

As we can see, the behaviour of the poloidal magnetic flux is the expected for a Solovév equilibrium, with closed, nested magnetic surfaces with elliptical cross sections in the vicinity of the magnetic axis and the outer part of the separatrix. Overall, their form resembles a D-shape, although in this section this topological property is embedded in the solution and was not deemed necessary to be imposed, as in the two previous Tokamak-relevant equilibria. We further observe a Shafranov shift of the magnetic surfaces with respect to the geometrical centre of the formation, the etiology of which we have already discussed in the previous sections.

4.2.2 Equilibrium quantities

In order to calculate the physical quantities of interest for the current equilibrium, we ought to give a numerical value to m_1 , as we stated. In light of the definition of the toroidal current density for an MHD equilibrium, $J_\phi = -\Delta^*\Psi/\zeta = -m_1\zeta$ (due to (3.101)), one may select a reference value of the toroidal current density and specify the value of m_1 in that way. For our scope, we will select as a reference value the following: $J_{\phi_0} = 2 \times 10^5 \text{ A/m}^2$, which stems from experimental evidence [101]. Therefore, the empirical definition of m_1 will read $m_1 = |J_{\phi_0}/J_a|$, where we divided by the reference current density $J_a = B_a/(R_a\mu_0)$. In addition, it was found appropriate to rescale the flux function properly for better results. Nonetheless, since we have a non-homogeneous differential equation, we have to rescale both the flux function Ψ and the non-homogeneous coefficient m_1 in order to be consistent.

After these manipulations, we present a profile of the dimensionless flux function in Figure 4.24. This behaviour is expected, because in Section 3.3 we noted that the magnetic flux vanishes on the magnetic axis (which is located at $\zeta = 1$) for the current equilibrium. On the boundary, the poloidal flux function attains a constant value (see eq. (3.103)).

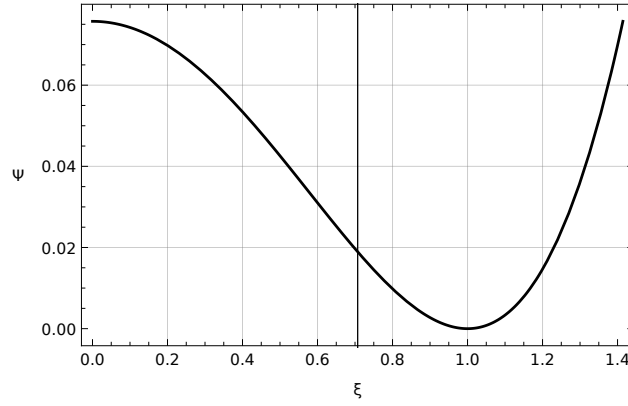


Figure 4.24: The (dimensionless) flux function profile for the Solovév on the plane $\zeta = 0$.

As far as the magnetic field is concerned, we only have to examine its poloidal components since for our application the toroidal magnetic field vanishes (see Section 3.3.2). The components in question are depicted in Fig. 4.25.

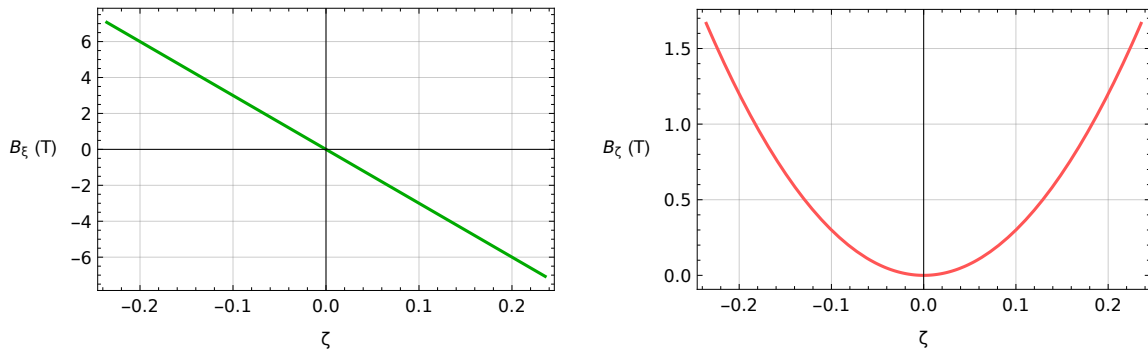


Figure 4.25: Magnetic field profiles for the Solovév equilibrium. Left: The ξ -component of the magnetic field on the plane $\zeta = 1$. Right: The ζ -component of the magnetic field on the plane $\zeta = 1$.

The calculation for B_p was based on the well-known relation $B_p = \zeta^{-1} \nabla \Psi \times \nabla \phi$ (see eq. (2.25)). The plot of Fig. 4.25 indicates an appropriate behaviour of the poloidal magnetic field, with its values within desired levels as well.

Fig. 4.26 demonstrates the well-behaved plasma velocity for the Solovév equilibrium.

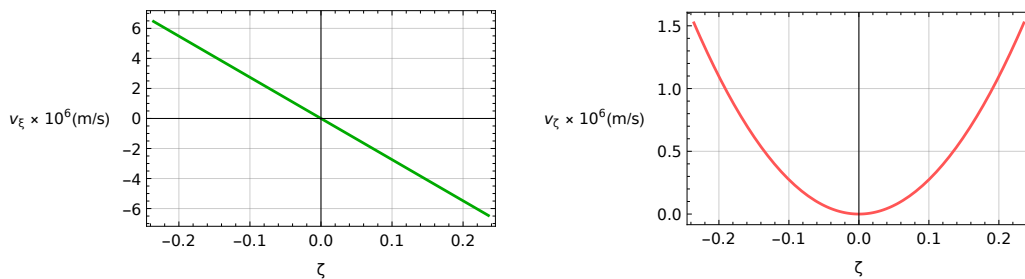


Figure 4.26: Plasma velocity field profiles for the Solovév equilibrium. Left: The ξ -component of the velocity field on the plane $\zeta = 1$. Right: The ζ -component of the velocity field on the plane $\zeta = 1$.

One should note that, since $\Psi \equiv \Phi$, the same relations will hold as those for the magnetic field. Once again, there exists no toroidal velocity field - the flows are purely poloidal. The reader should also bear in mind that **this velocity refers to the whole plasma**⁷ and not the ion fluid, as in this case no separation of fluids has taken place.

The poloidal Alfvénic Mach number (Fig. 4.27) has the same behaviour as in the previous equilibria, indicating sub-Alfvénic plasma velocities.

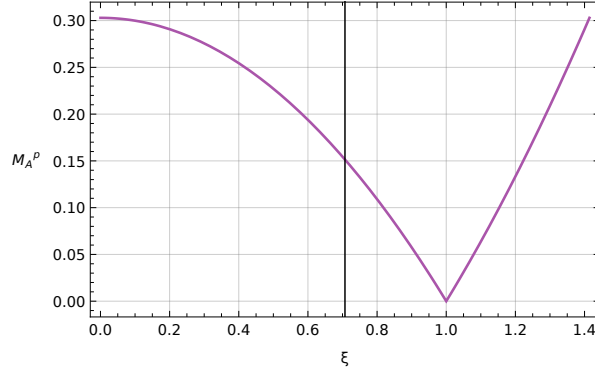


Figure 4.27: The profile of the poloidal Alfvénic Mach number on the plane $\zeta = 0$ for the Solovév equilibrium.

Proceeding to the current density, we deduce that the only non-vanishing component will be the toroidal one, since $B_\phi = 0$. Given by relation: $J_\phi = -m_1 \zeta$, its profile is depicted in Fig. 4.28.

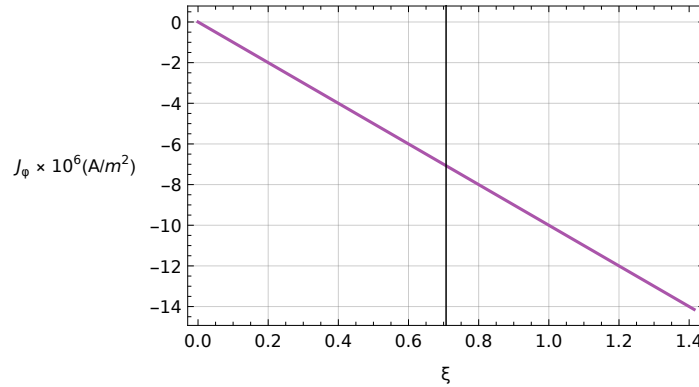


Figure 4.28: Toroidal current density profile for the Solovév equilibrium on the plane $\zeta = 0$.

As expected, it is monotonically decreasing from the inner to the outer part of the separatrix, with values $\mathcal{O}(10^6 \text{ A/m}^2)$ which are physically acceptable. Note that no large-scale electric field develops in the current equilibrium, by virtue of MHD Ohm's law for velocities parallel to the magnetic field.

Last but not least, for the pressure computation we suppose that $m_0 = 0$, and we further select $n_0 = 0.0458814$, a value that renders the pressure zero on the inner part of the separatrix. In view of relation (2.48) under the scope of the current ansatz, we present the pressure profile in Fig. 4.29.

⁷MHD, however, is derived in the limit $\frac{m_e}{m_i} \rightarrow 0$.

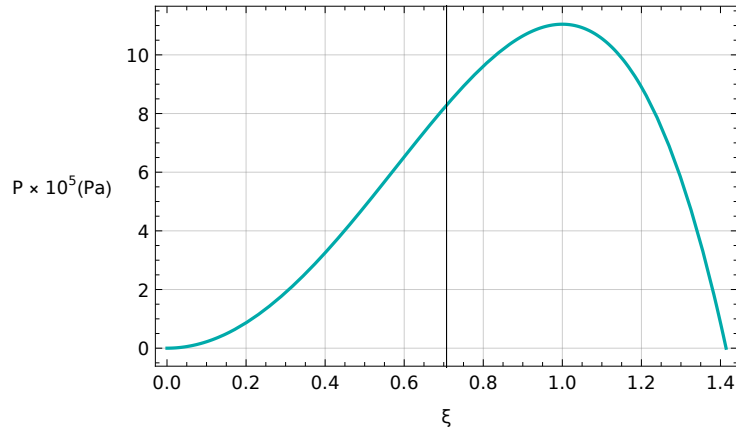


Figure 4.29: The plasma pressure profile on the $\zeta = 0$ plane for the Solovév equilibrium.

This is a fine pressure profile for the needs of magnetic confinement for the same reasons as in the Whittaker equilibrium. Its values are optimal, it is peaked on axis and it is sufficiently stratified (see Fig. 4.30), attaining a vanishing value in the inner part of the separatrix and a value very close to zero in the outer part of it. However, one can notice that this particular pressure function possesses two X-points inside the domain of the configuration, which may be proven to be problematic for the confinement of plasma⁸. It is conjectured that the appearance of these X-points is attributed to the topological properties of the Solovév solution (3.92), which also demonstrates a similar behaviour on the two inner separatrix points: $(0, \pm \frac{\delta}{2} \sqrt{2 - \epsilon})$, as seen in Fig. 3.1.

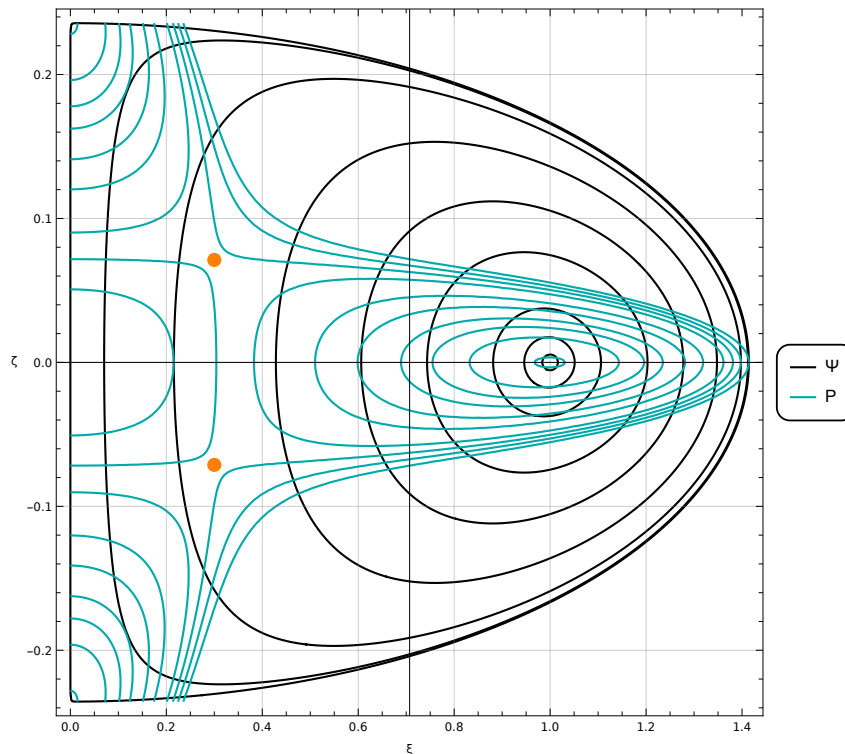


Figure 4.30: The pressure contours in a torus cross section, along with the magnetic surfaces for the Solovév equilibrium. The two X-points that the pressure possesses are also illustrated in orange color.

⁸This interesting result should be a flow effect because in the static MHD Solovév case $P \propto \Psi$. That is, the flow results to displacement of the static pressure X-points in the plasma.

5

Conclusions and future prospects

Entia non sunt multiplicanda praeter necessitatem
(Entities must not be multiplied beyond necessity).

Occam's razor¹

5.1 Summary and main conclusions

In the current thesis a family of analytic solutions to the Hall MHD GS-Bernoulli system was derived, and then applied to axisymmetric configurations in the scope of magnetic confinement fusion.

In the first introductory chapter, we presented the basic principles that govern the bizarre behaviour of plasma, along with the fundamental concepts of controlled thermonuclear fusion. After a brief presentation of the toroidal confinement systems, we presented some notable theorems that dictate the plasma magnetic confinement. We then discussed how one should describe plasma, starting with the widely employed MHD model and its implications, among which is Spitzer's law and the so-called Alfvén's theorem. On this basis we conducted a generalisation of ideal MHD for a two-fluid plasma, introducing the Extended Magneto-hydrodynamics (XMHD) model and the Alfvén normalisation scheme that was used for the needs of the current thesis. The Hall MHD model was then recovered as a special case of the XMHD one in the limit of vanishing electron inertia ($d_e \rightarrow 0$).

In the second chapter we formulated the Hamiltonian description of the ideal fluid, starting with the ordinary, canonical Hamiltonian description and then moving on to the non-canonical Hamiltonian description in the Eulerian frame of description for plasmas. After perceiving the degeneracy of the Poisson operator, we identified the kinematic constants of such a system, the Casimir invariants, and on this basis we postulated the Energy-Casimir variational principle. Owing to the Hamiltonian structure that Hall MHD possesses, this variational principle was then employed for the case of axisymmetric plasmas with incompressible ion flows. After writing down the Hamiltonian functional and the axisymmetric Hall MHD Casimirs, we deduced a system of two Grad-Shafranov equations and a Bernoulli one that concerns the plasma pressure. We then realised that the arbitrariness of the free functions may give rise to different types of equilibria, depending on the ansatz that we select for them. Three notable cases were identified, along with a more general one. All four of them may be potentially suitable for the needs of magnetic confinement fusion.

In the third chapter we proceeded to seek solutions for each of the four types of equilibria that stem from the adopted ansatz. Thereafter, we manipulated the first case properly in order

¹This philosophical principle advocates that when provided with conflicting hypotheses concerning the same prediction, one should usually choose the one that involves the fewest assumptions.

to prove that its solutions are superpositions of Beltrami fields, and then we expressed these solutions in terms of the Bessel functions. Afterwards, the non-homogeneous equation was solved by inspection. The next species was treated in a similar manner, following a strong analytic approach, and we ended up at solutions in terms of the Whittaker functions for the homogeneous equation. For the purpose of solving the non-homogeneous equation, we exploited the similarity reduction procedure owing to which we successfully obtained a solution. The third kind of solutions to the GS-Bernoulli system was found to be the well-known Solovév equilibrium. Thereon we presented the static Solovév solution and on this basis we extended it in the case of Hall MHD, where we ended in an MHD-like equilibrium with sheared poloidal flows. Finally, we examined the most general case which features no restrictions for the ansatz parameters, and demonstrated that even in that case, configurations with closed magnetic and ion velocity surfaces can possibly be retrieved.

In the fourth and foremost chapter, we took a step further to apply the previously derived solutions to axisymmetric fusion devices, viz. Tokamaks and FRCs. However, before proceeding to discuss their general characteristics and the extent to which they may be applicable in fusion or astrophysical plasmas, it is worth realising that the whole subject of this master thesis emerged unexpectedly, originating initially from the double Beltrami states. The impetus for the study of the double Beltrami equilibrium states was given by the author's desire to generalise the well-known force-free states (which are essentially the Beltrami states, see the beginning of Section 3.1.1) to a more general context. This generalisation was further motivated by the problematic aspects that the Beltrami states possess in controlled thermonuclear fusion. To name only a few of them, those problematic aspects include the constant pressure inside the fusion device and the fact that the relaxation towards Taylor states occurs under very specific conditions [75], as mentioned in Chapter 3. So it came to pass that the author engaged in a generalisation of force-free states to other models, namely Hall MHD which is maybe the simplest two-fluid model that predicts superpositions of single Beltrami states as solutions to its equations, when the free functions obtain a specific form. Those solutions are the double Beltrami states, as discussed extensively in Chapter 3. A proper construction of such an equilibrium was successfully carried out in Chapter 4 on the basis of the model's analytic equations presented in Chapter 3. For this purpose, we employed ITER parameters for the physical and geometrical quantities, and for the determination of the flux surfaces we imposed a D-shaped boundary based on the shaping method of [87], [88]. As we saw, this equilibrium possesses desirable characteristics for a fusion application, namely well organised magnetic surfaces and physically appealing values and profiles for the equilibrium quantities of interest. Nevertheless, we observed that the pressure does not vanish on the boundary. As if that were not enough, following a thorough examination of the existing literature on the double Beltrami states, there is considerable evidence [102] to postulate that **double Beltrami states are essentially metastable equilibrium states**, because, as Gondal et al. suggest, they tend to eventually relax to single Beltrami states. This loss of equilibrium may take place under a plethora of circumstances, namely when certain scale parameters become degenerate or even when the product of the magnetic helicity (3.2) with the ion helicity (3.3) becomes positive [102], [103]. The aforementioned termination of equilibrium may also give rise to a conversion of magnetic energy to flow kinetic energy [102]. A connection of the termination of equilibrium with the roots of the Beltrami operator eigenvalues has also been established, viz. the equilibrium comes to an end when one of the two roots disappears or even when they become equal [102]. It therefore becomes evident that the termination of equilibrium for the double Beltrami states is not a rarely encountered phenomenon, and of course it is not something one may wish to encounter in a magnetic confinement scenario. Nonetheless, this very metastability they present may render them proper candidates for the study of other phenomena, mainly in astrophysical environments [103], [104]. Another circumstance where loss of equilibrium takes place was observed during the desire of the author to generalise the double Beltrami states to three dimensional plasmas, following the footsteps of a previous study [91]. This generalisation was going to be executed by perturbing an axisymmetric equilib-

rium state with a similar, translationally symmetric one. Unfortunately, we conjecture that during this perturbation, the resulting three-dimensional state ceases to be in equilibrium due to the presence of the vacuum toroidal magnetic field - which of course does not exist in the Beltrami states. With all of these aspects in mind, the need of resorting to other equilibrium states emerged during the present study. Thus it transpired to extend the initial study of the double Beltrami states to similar equilibria, predicted also from the non-canonical Hamiltonian structure of Hall MHD.

Successive to the double Beltrami states, we studied a more general counterpart of them, namely equilibria in terms of the Whittaker functions for ITER-like scenarios. For the determination of the boundary, the same shaping method was used as with the case of the double Beltrami equilibrium. The Whittaker equilibrium proved to be interesting by many aspects, mainly because the pressure profile presented excellent stratification and optimal values $\mathcal{O}(10^5 - 10^6 \text{ Pa})$. The rest of the quantities demonstrated acceptable profiles, with only exception the poloidal magnetic field - the values of which were slightly low for a Tokamak. More research is needed to assess the applicability of these solutions to realistic scenarios in space and laboratory plasmas.

The last kind of equilibrium was based on the well known Solovév solution to the Grad-Shafranov equation [68]. Here, we generalised this solution in the framework of the Hall MHD model, where we ended back in an MHD-like equilibrium with sheared poloidal flows. This equilibrium was built based on PFRC numerical values, and possessed sufficient characteristics for the scope of controlled thermonuclear fusion, among which was the interesting pressure profile with the 2 spontaneous X-points. The other physical quantities were excellently behaved, both regarding their form and values in a poloidal cross section. This solution has been extensively studied for the needs of magnetic confinement fusion and has even been extended for the presence of MHD flows [105], [106], [107]. For our case, the presence of sheared poloidal flows may signify that this equilibrium may be quite suitable for the study of the L-H transition and ELMs in the pedestal region of the plasma domain. To further strengthen this argument, one should recall that the gradient length scales of the physical quantities may become comparable to the ion skin depth inside the pedestal region, which in turn means that Hall MHD provides an adequate framework for choosing this Solovév solution as a good candidate for transitions towards high confinement modes. We should note, however, that in this case the numerical values of the free parameters should be chosen accordingly so that the resulting profiles resemble typical ones encountered in H-mode Tokamaks. Finally, whether this solution can be extended to astrophysical plasmas is a matter that requires further investigation.

Overall, the calculations of the three equilibrium states from the respective analytic solutions demonstrate that the plasma is organised into well-defined flux surfaces, which are nested with respect to the magnetic axis. The pressure is peaked on axis, and is organised into separate contours. What is truly intriguing though is that the Hall MHD model predicts an evident departure of the ion fluid from the magnetic surfaces. The computations showed that the ion fluid attains sub-Alfvénic velocities, while the separation of the two fluids produces a large scale poloidal electric field which may be significant depending on the application. Albeit the departure of the ion fluid from the magnetic surfaces occurs on scales of the order of the ion depth, the Hall MHD model introduces corrections to the ordinary MHD one that cannot be neglected, especially when one studies phenomena that concern microscales, like transport, turbulence etc.

5.2 Future prospects

Given that the Hall MHD model enriches the - already complicated - underlying physical processes behind plasma and opens the doors for a completely novel way of description, one may wonder what other processes may emerge if one incorporates *dissipation mechanisms* in

the current study. As an example, we present the work done in [108], where it is found that the small-scale part (of the order of the ion skin depth) of a double Beltrami field can give rise to resistive and viscous dissipations, although this part vanishes as the system approaches its relaxed state. The authors also pointed a relation between the small-scale and the macroscale structures of a double Beltrami system, for example that small-scale varying magnetic fields may result in large-scale chaos-induced dissipations. Thus, it is apparent that many physical phenomena are concealed from us when we limit our description to ideal Hall MHD systems, the handling of which however may be very strenuous and complicated.

A further generalisation of this work to Extended Magnetohydrodynamics (XMHD) is also viable, but one may wonder whether this model is excessive for the needs of magnetic confinement fusion, since the introduced length scales, related to electron inertia, are even smaller than the ones of the Hall MHD model. Such a description is followed in [28].

As far as the geometry of the constructed configurations is concerned, a quite interesting prospect this study holds pertains the generalisation of the said equilibria in the case of *helical symmetry*, which is a more general symmetry (see Appendix B) encountered in Stellarators. This kind of symmetry includes axial and translational symmetries as special cases, and may be proper for the description of other confinement systems that feature a more complicated topology of the magnetic surfaces. A study in this framework was carried out in [22].

In addition, the solutions of Chapter 3 could be applied for up-down *asymmetric* configurations, including the one of ITER that features an X-point in the divertor region. This topology is auxiliary for the confinement of plasma, since the particles are guided in a specific region that it designed to withstand the tremendous thermal loads created during thermonuclear reactions, without affecting the rest of the reactor's walls.

As both of the double Beltrami and the Whittaker equilibria feature a vacuum toroidal magnetic field, if we perturb such states with similar translationally symmetric ones with the aim of constructing three-dimensional equilibria (see [91]), it is conjectured that the resulting configuration will be off-equilibrium. Nevertheless, it is interesting to examine such cases to see how the formation changes. Due to the so-called KAM theorem [109], [110], we expect the invariant tori (which in our case are the magnetic surfaces) to collapse, and therefore a subsequent formation of *magnetic islands* should take place, as happened in previous work of the author [91]. However, further analysis and simulations of such scenarios are required to corroborate this conjecture.

Another prospect of the present study is the extension of the GS-Bernoulli system for non-constant plasma density. The reader should recall that all of the current analysis was carried out for $\rho = 1$, which leads to incompressible ion velocity flows. A further extension may concern the addition of pressure anisotropy, for which an extensive analysis can be found in [22]. Unfortunately, in this case no analytic solutions exist, and one should resort in complicated numerical schemes to solve the resulting Generalised Grad-Shafranov-Bernoulli (GGSB) system.

In the scope of astrophysics and particularly solar physics, we reckon that the proposed analytic solutions may be appropriate for the study of many systems, especially the ones that include small-scale processes (e.g. magnetic reconnection). Some examples have already been given in the previous section regarding the double Beltrami states and their metastable behaviour. The reader should bear in mind that although the underlying physics remain the same as in laboratory environments, the boundary conditions differ. As always, what matters the most is to make hypotheses that reflect the physics of the system in hand in the greatest extent possible.

Finally, it should be noted that there is potential for further study in large-scale numerical frameworks such as HELENA, EFIT and VMEC, whereon the methods that we presented have yet to be implemented.

It is our earnest hope that the equilibria constructed in this thesis will contribute - even if only slightly - towards understanding the physical processes that occur in two-fluid laboratory or even astrophysical plasmas.

A

An alternative way to solve the Double Beltrami system

The homogeneous counterpart of the system of equations (3.24) and (3.25) can be put in matrix form as

$$\Delta^* \begin{pmatrix} \Psi \\ \mathcal{X} \end{pmatrix} = \begin{pmatrix} \mathcal{W}_1 & \mathcal{W}_2 \\ \mathcal{W}_3 & \mathcal{W}_4 \end{pmatrix} \begin{pmatrix} \Psi \\ \mathcal{X} \end{pmatrix}, \quad (\text{A.1})$$

where the coefficients \mathcal{W}_i , $i = \{1, 2, 3, 4\}$ are

$$\begin{aligned} \mathcal{W}_1 &= -\left(g_1^2 - \frac{1}{d_i^2}\right), \quad \mathcal{W}_2 = -\left(\frac{g_1}{d_i} + \frac{1}{f_1 d_i^3}\right), \quad \mathcal{W}_3 = \left(\frac{g_1}{d_i} + \frac{1}{f_1 d_i^3}\right), \\ \text{and } \mathcal{W}_4 &= \left(\frac{1}{d_i^2} - \frac{1}{f_1^2 d_i^4}\right). \end{aligned} \quad (\text{A.2})$$

We observe that the system (A.1) is in fact an eigenvalue problem for the the Shafranov operator Δ^* . Hence, it is reasonable to write down both flux functions in (A.1) as a linear combination of eigenfunctions ζ_i of the Shafranov operator

$$\Psi = \sum_i C_i^\Psi \zeta_i, \quad \text{and} \quad \mathcal{X} = \sum_i C_i^\mathcal{X} \zeta_i, \quad (\text{A.3})$$

where $C_i^{\Psi, \mathcal{X}}$ are some coefficients that we seek. Since ζ_i are the eigenfunctions of the Shafranov operator, it is evident that

$$\Delta^* \begin{pmatrix} \Psi \\ \mathcal{X} \end{pmatrix} = \sum_i \begin{pmatrix} \lambda_i C_i^\Psi \zeta_i \\ \lambda_i C_i^\mathcal{X} \zeta_i \end{pmatrix}, \quad (\text{A.4})$$

where λ_i are the eigenvalues of the Shafranov operator - not to be confused with the eigenvalues of the curl operator (3.27). Therefore, the system (A.1) assumes the form

$$\sum_i \begin{pmatrix} \lambda_i C_i^\Psi \zeta_i \\ \lambda_i C_i^\mathcal{X} \zeta_i \end{pmatrix} = \sum_i \begin{pmatrix} \mathcal{W}_1 & \mathcal{W}_2 \\ \mathcal{W}_3 & \mathcal{W}_4 \end{pmatrix} \begin{pmatrix} C_i^\Psi \zeta_i \\ C_i^\mathcal{X} \zeta_i \end{pmatrix}, \quad (\text{A.5})$$

or, equivalently

$$\sum_i \lambda_i \zeta_i \begin{pmatrix} C_i^\Psi \\ C_i^\mathcal{X} \end{pmatrix} = \sum_i \zeta_i \begin{pmatrix} \mathcal{W}_1 & \mathcal{W}_2 \\ \mathcal{W}_3 & \mathcal{W}_4 \end{pmatrix} \begin{pmatrix} C_i^\Psi \\ C_i^\mathcal{X} \end{pmatrix}. \quad (\text{A.6})$$

The above equation must hold for every single term, due to the fact that the eigenfunctions ξ_i are linearly independent from their very definition. Hence, we omit the index i and we get

$$\lambda \xi \begin{pmatrix} C_\Psi \\ C_\chi \end{pmatrix} = \xi \begin{pmatrix} \mathcal{W}_1 & \mathcal{W}_2 \\ \mathcal{W}_3 & \mathcal{W}_4 \end{pmatrix} \begin{pmatrix} C_\Psi \\ C_\chi \end{pmatrix}. \quad (\text{A.7})$$

It is evident that our problem reduces to the eigenvalue problem

$$\begin{pmatrix} \mathcal{W}_1 & \mathcal{W}_2 \\ \mathcal{W}_3 & \mathcal{W}_4 \end{pmatrix} \begin{pmatrix} C_\Psi \\ C_\chi \end{pmatrix} = \lambda \begin{pmatrix} C_\Psi \\ C_\chi \end{pmatrix}, \quad (\text{A.8})$$

for which the characteristic equation reads

$$\det(\mathcal{W} - \lambda_{\pm} \mathbb{1}_{2 \times 2}) = 0, \quad (\text{A.9})$$

where \mathcal{W} is the \mathcal{W}_i -coefficient matrix, λ_{\pm} are the two eigenvalues we seek and $\mathbb{1}_{2 \times 2}$ is the 2×2 identity matrix. A straightforward calculation results in

$$\lambda_{\pm} = \pm \frac{1}{2d_i^4 f_1^2} \left\{ \mp 1 \pm 2d_i^2 f_1^2 \mp d_i^4 f_1^2 g_1^2 + (1 + d_i^2 f_1 g_1) \sqrt{1 + d_i^2 f_1 [-4f_1 + g_1(-2 + d_i^2 f_1 g_1)]} \right\}. \quad (\text{A.10})$$

The next step is to find the eigenvectors of the \mathcal{W} -matrix. By substituting $\lambda = \lambda_+$ to the system (A.8), we find

$$\begin{pmatrix} \mathcal{W}_1 - \lambda_+ & \mathcal{W}_2 \\ \mathcal{W}_3 & \mathcal{W}_4 - \lambda_+ \end{pmatrix} \begin{pmatrix} C_\Psi^+ \\ C_\chi^+ \end{pmatrix} = 0. \quad (\text{A.11})$$

As concerns the system (A.11), the 2 equations are linearly dependent, since we imposed that the determinant of the coefficient matrix is zero. An apparent consequence of the above statement is that the system is underdetermined, and one of the two coefficients ought to be considered as a free parameter. Hence, we have the freedom to set $C_\Psi^+ = 1$ and then the system becomes

$$(\mathcal{W}_1 - \lambda_+) + \mathcal{W}_2 C_\chi^+ = 0, \quad (\text{A.12})$$

$$\mathcal{W}_3 + \mathcal{W}_4 - \lambda_+ C_\chi^+ = 0, \quad (\text{A.13})$$

from which we conclude that

$$\boxed{C_\chi^+ = \frac{\lambda_+ - \mathcal{W}_1}{\mathcal{W}_2}}, \quad \text{and similarly for } \lambda = \lambda_- : \quad \boxed{C_\chi^- = \frac{\lambda_- - \mathcal{W}_1}{\mathcal{W}_2}}. \quad (\text{A.14})$$

What remains is to find the eigenstates ξ_{\pm} of the Shafranov operator, via the equation

$$\Delta^* \xi_{\pm} = \lambda_{\pm} \xi_{\pm}, \quad (\text{A.15})$$

for which the solutions are recovered if one follows exactly the same procedure as the one presented in Section 3.1.3.1. Finally, the two flux functions now read

$$\boxed{\Psi_h = \xi_+ + \xi_-}, \quad (\text{A.16})$$

$$\boxed{\tilde{\chi}_h = C_\chi^+ \xi_+ + C_\chi^- \xi_-}. \quad (\text{A.17})$$

B

Generalisation of the Double Beltrami Grad-Shafranov equation for helical symmetry

In this section of the Appendix we provide a generalisation of the Double Beltrami Grad-Shafranov equation (3.35) in *helical coordinates*. This coordinate system, along with the assumption of *helical symmetry*, are core concepts for the study of magnetic confinement in devices of three-dimensional geometry, like Stellarators. Here, we carry out a brief discussion concerning the basics aspects of the coordinate system in question; the interested reader is referred to [22], [111] and [112] for a more thorough approach.

The helical coordinate system (r, u, ζ) is related to the ordinary cylindrical coordinate system for toroidal systems, (R, ϕ, Z) , as

$$r = R, \quad (\text{B.1})$$

$$u = \ell\phi + nZ, \quad (\text{B.2})$$

$$\zeta = Z, \quad (\text{B.3})$$

where ℓ and n are real constants, and u can be interpreted as a "helical angle". We may define a helical vector tangent to any helicoid, i.e. a surface with $u = \text{const.}$ as

$$\mathbf{h} = \frac{\ell\hat{\mathbf{e}}_Z - nr\hat{\mathbf{e}}_\phi}{\ell^2 + n^2r^2}, \quad \text{with: } \mathbf{h} \cdot \mathbf{h} \equiv k^2 = \frac{1}{\ell^2 + n^2r^2} \quad (\text{scaling factor}). \quad (\text{B.4})$$

The helical vector \mathbf{h} is tangent to the helix ($r = \text{const.}; u = \text{const.}$) and points along the direction resulting from a rotation around the Z axis and a parallel translation along the same axis. We must stress the fact that \mathbf{h} is a divergence-free, Beltrami vector

$$\nabla \cdot \mathbf{h} = 0, \quad \nabla \times \mathbf{h} = -2n\ell k^2 \mathbf{h}. \quad (\text{B.5})$$

Helical symmetry translates to $\mathbf{h} \cdot \nabla f = 0 \quad \forall f = f(r, u)$, which means that any scalar function f does not change along the helical direction \mathbf{h} , or equivalently that there is no explicit dependence from the ζ coordinate. With that being said, the poloidal representations (3.30) for the Beltrami fields \mathcal{A}_\pm are generalised to

$$\mathcal{A}_\pm = k^{-1} \mathcal{A}_{\pm h}(r, u) \mathbf{h} + \nabla \Psi_\pm(r, u) \times \mathbf{h}, \quad (\text{B.6})$$

This representation decomposes each one of the two Beltrami fields in two components; one along the helical direction \mathbf{h} and one lying on the "poloidal" plane, that is the plane perpendicular to the helical vector \mathbf{h} . Owing to (B.6) and (B.5), the curl of the Beltrami fields reads

$$\nabla \times \mathcal{A}_\pm = (k^{-2} \mathcal{L} \Psi_\pm - 2n\ell k \mathcal{A}_{\pm h}) \mathbf{h} + \nabla(k^{-1} \mathcal{A}_{\pm h}) \times \mathbf{h}, \quad (\text{B.7})$$

Appendix B – Generalisation of the Double Beltrami Grad-Shafranov equation for helical symmetry

where $\mathcal{L} = -\nabla \cdot (k^2 \nabla)$ is a Shafranov-like, linear self-adjoint differential operator. Employing (B.5) and (B.7) the equation respective to (3.1) takes the form

$$(k^{-2} \mathcal{L} \Psi_{\pm} - 2n\ell k \mathcal{A}_{\pm h}) \mathbf{h} + \nabla(k^{-1} \mathcal{A}_{\pm h}) \times \mathbf{h} = \lambda_{\pm} k^{-1} \mathcal{A}_{\pm h} \mathbf{h} + \lambda_{\pm} \nabla \Psi_{\pm} \times \mathbf{h} \quad (\text{B.8})$$

A projection of relation (B.8) along the direction of the helical vector yields

$$k^{-2} \mathcal{L} \Psi_{\pm} - 2n\ell k \mathcal{A}_{\pm h} = \lambda_{\pm} k^{-1} \mathcal{A}_{\pm h}, \quad (\text{B.9})$$

while a projection normal to \mathbf{h} yields

$$\mathcal{A}_{\pm h} = k \lambda_{\pm} \Psi_{\pm} \quad (\text{B.10})$$

By combining relations (B.9) and (B.10), we readily retrieve the generalised helically symmetric Grad-Shafranov equation for the Double Beltrami states

$$\boxed{k^{-2} \mathcal{L} \Psi_{\pm} - 2n\ell k^2 \lambda_{\pm} \Psi_{\pm} = \lambda_{\pm}^2 \Psi_{\pm}.} \quad (\text{B.11})$$



Digression on the Whittaker functions

In 1903, Whittaker proposed a limiting case of the so-called *hypergeometric function*, in order to show that many important special functions - that even arise in physics - can be derived by specialising and transforming a single new function [113]. Whittaker addressed the problem of solving the following second order ODE

$$\frac{d^2u}{dz^2} + \left(-\frac{1}{4} + \frac{k}{z} + \frac{\frac{1}{4} - m^2}{z^2} \right) u(z) = 0, \quad (\text{C.1})$$

where $k, m, z \in \mathbb{C}$ and $u(z)$ is a complex function of z . Eq. (C.1) has a regular singularity at 0 and an irregular singularity at ∞ . In the case where $2m \notin \mathbb{Z}$, the linearly independent solutions to this equation are

$$\begin{aligned} \mathcal{M}_{k,m}(z) &= z^{m+1/2} e^{-z/2} \sum_{n=0}^{\infty} \frac{(m-k+\frac{1}{2})_n}{n!(2m+1)_n} z^n \\ &= z^{1/2+m} e^{-z/2} \left[1 + \frac{\frac{1}{2} + m - k}{1!(2m+1)} z + \frac{(\frac{1}{2} + m - k)(\frac{3}{2} + m - k)}{2!(2m+1)(2m+2)} z^2 + \dots \right], \end{aligned} \quad (\text{C.2})$$

and $\mathcal{M}_{k,-m}(z)$ [81]. In equation (C.2), the notation $(a)_n$ has been used that indicates a *Pochhammer symbol* [78], i.e. a rising factorial

$$(a)_n = \begin{cases} 1, & n = 0, \\ a(a+1)(a+2) \dots (a+n-1), & n \neq 0. \end{cases} \quad (\text{C.3})$$

The solutions $\mathcal{M}_{k,\pm m}$ are regular at $z = 0$ and valid for every finite z [81]. However, owing to the fact that the aforementioned solutions cease to be valid for integer values of $2m$, Whittaker and Watson [81] proposed another solution to eq. (C.1), that has the following integral representation

$$\mathcal{W}_{k,m}(z) = \frac{e^{-z/2} z^k}{\Gamma(\frac{1}{2} - k + m)} \int_0^{\infty} t^{-k-1/2+m} \left(1 + \frac{t}{z} \right)^{k-1/2+m} e^{-t} dt, \quad (\text{C.4})$$

which is valid whenever $\text{Re}(k - 1/2 - m) \leq 0$ and $k - 1/2 - m \notin \mathbb{Z}$. In (C.4), $\Gamma(z)$ is the so-called *Gamma function* [78]. The solutions (C.2) and (C.4) to the ODE (C.1) comprise a set of special functions that are known in the literature as the **Whittaker functions**. There also exist relations that connect the latter with the known *confluent hypergeometric functions*, as

$$\mathcal{M}_{k,m}(z) = e^{-z/2} z^{m+1/2} M \left(\frac{1}{2} + m - k, 1 + 2m; z \right), \quad (\text{C.5})$$

$$\mathcal{W}_{k,m}(z) = e^{-z/2} z^{m+1/2} U \left(\frac{1}{2} + m - k, 1 + 2m; z \right), \quad (\text{C.6})$$

where $M(a, b; z)$ and $U(a, b; z)$ are the confluent hypergeometric functions of the first and second kind respectively, for which there exist the following convenient integral representations [78]

$$M(a, b; z) = \frac{\Gamma(b)}{\Gamma(a)\Gamma(b-a)} \int_0^1 e^{zt} t^{a-1} (1-t)^{b-a-1} dt, \quad \text{for } b > a > 0, \quad (\text{C.7})$$

$$U(a, b; z) = \frac{1}{\Gamma(a)} \int_0^\infty e^{-zt} t^{a-1} (1+t)^{b-a-1} dt, \quad \text{for } \text{Re}(z) > 0, \quad b > a > 0. \quad (\text{C.8})$$

On the basis of Whittaker functions, one may deduce many well-known special functions that arise in physics. The interested reader is referred to [113] for some notable examples.

Finally, we illustrate the behaviour of the Whittaker functions for some values of k and m in the plots of Figures C.1 and C.2.

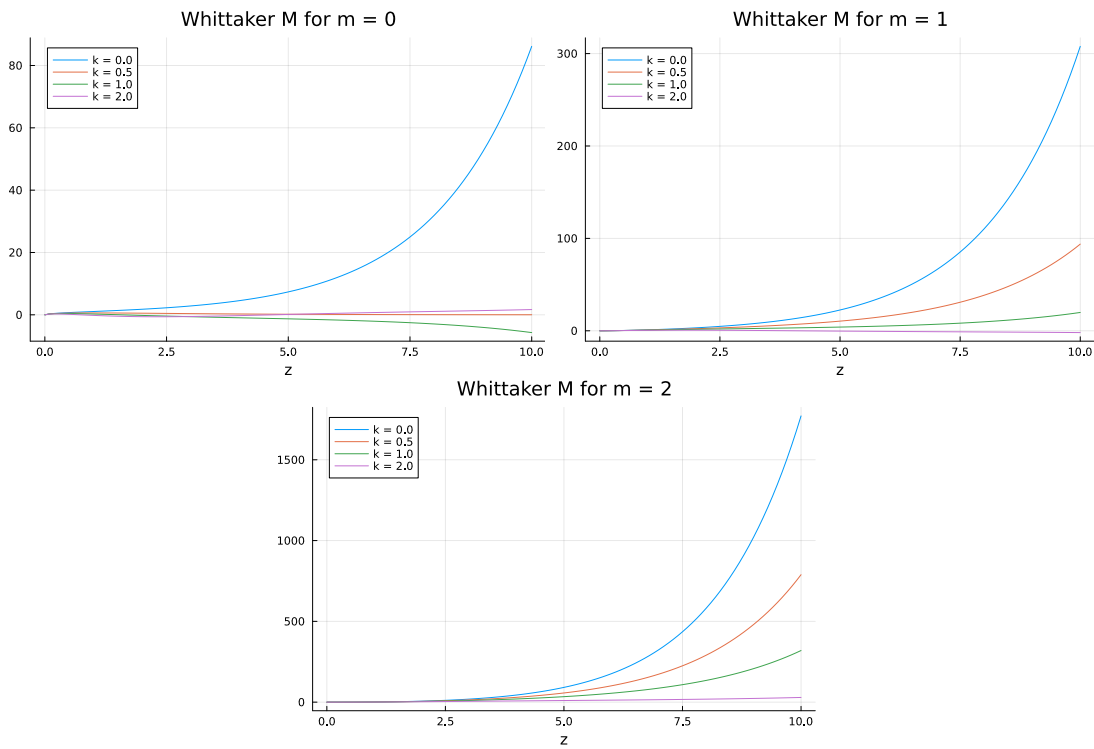


Figure C.1: Plot of the Whittaker $\mathcal{M}_{k,m}(z)$ function for some values of k and m .

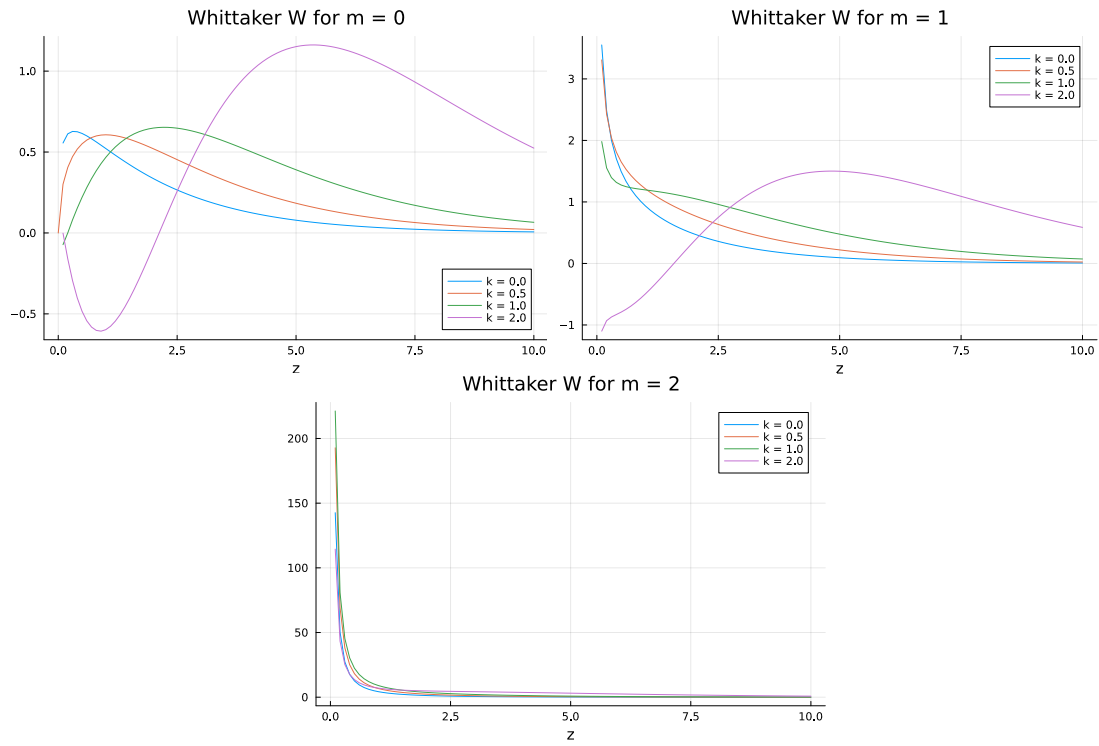


Figure C.2: Plot of the Whittaker $\mathcal{W}_{k,m}(z)$ function for some values of k and m .

Bibliographical references

- [1] I. Langmuir. Oscillations in ionized gases. *Proceedings of the National Academy of Sciences of the United States of America*, 14(8):627–637, 1928. URL <http://www.jstor.org/stable/85270>.
- [2] F. Chen. *Introduction to Plasma Physics and Controlled Fusion*. Springer, Switzerland, third edition, 2016. doi:<https://doi.org/10.1007/978-3-319-22309-4>.
- [3] A. F. Alexandrov, L. S. Bogdankevich, A. A. Rukhadze. *Principles of Plasma Electrodynamics*. Springer Berlin, Heidelberg, 2013. URL <https://link.springer.com/book/9783642692499>.
- [4] M. J. Aschwanden. *Physics of the Solar Corona*. Springer Berlin, Heidelberg, 2006. doi:<https://doi.org/10.1007/3-540-30766-4>.
- [5] E. Priest. *Magnetohydrodynamics of the Sun*. Cambridge University Press, Cambridge, 2014. doi:[10.1017/CBO9781139020732](https://doi.org/10.1017/CBO9781139020732).
- [6] U. S. Inan, M. Gołkowski. *Principles of Plasma Physics for Engineers and Scientists*. Publ. Cambridge University Press, 2010. doi:<https://doi.org/10.1017/CBO9780511761621>.
- [7] J. P. Freidberg. *Plasma Physics and Fusion Energy*. Cambridge University Press, Cambridge, 2007. doi:[10.1017/CBO9780511755705](https://doi.org/10.1017/CBO9780511755705).
- [8] J. P. Hans Goedbloed, S. Poedts. *Principles of Magnetohydrodynamics: With Applications to Laboratory and Astrophysical Plasmas*. Cambridge University Press, Cambridge, 2004. doi:[10.1017/CBO9780511616945](https://doi.org/10.1017/CBO9780511616945).
- [9] L. Jin, K. Duan, X. Tang. What Is the Relationship between Technological Innovation and Energy Consumption? Empirical Analysis Based on Provincial Panel Data from China. *Sustainability*, 10(2):145, 2018. doi:[10.3390/su10010145](https://doi.org/10.3390/su10010145).
- [10] C. Wolfram, O. Shelef, P. Gertler. How will energy demand develop in the developing world? *Journal of Economic Perspectives*, 26(1):119–138, 2012. doi:[10.1257/jep.26.1.119](https://doi.org/10.1257/jep.26.1.119).
- [11] B. J. van Ruijven, E. De Cian, I. Sue Wing. Amplification of future energy demand growth due to climate change. *Nature Communications*, 10(1):2762, 2019. doi:[10.1038/s41467-019-10399-3](https://doi.org/10.1038/s41467-019-10399-3).
- [12] H. Ritchie, Max Roser, and Pablo Rosado. Fossil fuels. *Our World in Data*, 2022. URL <https://ourworldindata.org/fossil-fuels>.
- [13] S. O. Amrouche, D. Rekioua, T. Rekioua, S. Bacha. Overview of energy storage in renewable energy systems. *International Journal of Hydrogen Energy*, 41(45):20914–20927, 2016. doi:<https://doi.org/10.1016/j.ijhydene.2016.06.243>.
- [14] S. A. Zwickler. Nuclear fuel service centers. *Alternative Energy Sources*, 6, 1 1981. URL <https://www.osti.gov/biblio/5208568>.

- [15] D. Kramer. National ignition facility surpasses long-awaited fusion milestone. *Physics Today*, 2022. URL <https://physicstoday.scitation.org/doi/10.1063/PT.6.2.20221213a/full/>.
- [16] S. Glasstone, R. H. Lovberg. *Controlled thermonuclear reactions*. Robert E. Krieger Publishing, New York, 1975.
- [17] J. D. Lawson. Some criteria for a power producing thermonuclear reactor. *Proceedings of the Physical Society. Section B*, 70(1):6, 1957. doi:10.1088/0370-1301/70/1/303.
- [18] J. P. Freidberg. *Ideal MHD*. Cambridge University Press, New York, 2014. doi:<https://doi.org/10.1017/CBO9780511795046>.
- [19] R. D. Hazeltine, J. D. Meiss. *Plasma Confinement*. Dover Publications, 2003.
- [20] J. P. Hans Goedbloed, S. Poedts. *Advanced Magnetohydrodynamics With Applications to Laboratory and Astrophysical Plasmas*. Cambridge University Press, New York, 2010. doi:<https://doi.org/10.1017/CBO9781139195560>.
- [21] J. F. Wang, T. Yamamoto, Y. Ogawa. Conceptual design of pf coil system and operation scenario on inductively-operated day-long pulsed tokamak reactor. 1994. URL <https://www.osti.gov/biblio/196905>.
- [22] A. Evangelias. *Equilibrium and Stability of Helically Symmetric Magnetized Plasmas*. PhD thesis, University of Ioannina, 2020. URL <https://www.didaktorika.gr/eadd/handle/10442/48018?locale=en>.
- [23] A. Gibson, J. B. Taylor. Single particle motion in toroidal stellarator fields. *The Physics of Fluids*, 10(12):2653–2659, 1967. doi:10.1063/1.1762089.
- [24] P. Helander et al. Stellarator and tokamak plasmas: a comparison. *Plasma Physics and Controlled Fusion*, 54(12):124009, 2012. doi:10.1088/0741-3335/54/12/124009.
- [25] V. D. Shafranov. *Reviews of Plasma Physics*, volume II. Consultants Bureau, New York, 1966.
- [26] D. J. Griffiths. *Introduction to Electrodynamics*. Cambridge University Press, Cambridge, fourth edition, 2017. doi:10.1017/9781108333511.
- [27] L. D. Landau, E. M. Lifshitz. *The Classical Theory of Fields*. Pergamon, Amsterdam, fourth edition, 1975. URL <https://www.sciencedirect.com/book/9780080250724/the-classical-theory-of-fields>.
- [28] D. Kaltsas. *Equilibrium and Stability of Magnetically Confined Plasmas in the Framework of Extended Magnetohydrodynamic Models via Hamiltonian Variational Principles*. PhD thesis, University of Ioannina, 2019. URL https://www.researchgate.net/publication/337470723_Equilibrium_and_Stability_of_Magnetically_Confined_Plasmas_in_the_Framework_of_Extended_Magnetohydrodynamic_Models_via_Hamiltonian_Variational_Principles.
- [29] A. Vlasov. On the kinetic theory of an assembly of particles with collective interaction. *Russ. Phys. J.*, 9:25–40, 1945. URL <https://cds.cern.ch/record/426186>.
- [30] A. Vlasov. The vibrational properties of an electron gas. *Soviet Physics Uspekhi*, 10(6):721, 1968. doi:10.1070/PU1968v010n06ABEH003709.
- [31] B. V. Somov. *Plasma Astrophysics, Part I*. Springer, New York, 2010. ISBN 978-1-4419-2244-1. doi:<https://doi.org/10.1007/978-0-387-48427-3>.

- [32] H. Ratcliffe. *Electron Beam Evolution and Radio Emission in the Inhomogeneous Solar Corona*. PhD thesis, University of Glasgow, 2013. URL <https://arxiv.org/abs/1307.1321>.
- [33] E. P. Kontar, H. Ratcliffe, and N. H. Bian. Wave-particle interactions in non-uniform plasma and the interpretation of hard X-ray spectra in solar flares. *Astronomy & Astrophysics*, 539:A43, 2012. doi:10.1051/0004-6361/201118216.
- [34] A. A. Schekochihin et al. Astrophysical gyrokinetics: Kinetic and fluid turbulent cascades in magnetized weakly collisional plasmas. *The Astrophysical Journal Supplement Series*, 182(1):310, 2009. doi:10.1088/0067-0049/182/1/310.
- [35] D. A. St-Onge, M. W. Kunz. Fluctuation dynamo in a collisionless, weakly magnetized plasma. *The Astrophysical Journal Letters*, 863(2):L25, 2018. doi:10.3847/2041-8213/aad638.
- [36] R. S. Cohen, L. Spitzer, P. McR. Routly. The electrical conductivity of an ionized gas. *Phys. Rev.*, 80:230–238, 1950. doi:10.1103/PhysRev.80.230.
- [37] L. Spitzer, R. Härm. Transport phenomena in a completely ionized gas. *Phys. Rev.*, 89:977–981, 1953. doi:10.1103/PhysRev.89.977.
- [38] H. Alfvén. On the existence of electromagnetic-hydrodynamic waves. *Arkiv för matematik, astronomi och fysik*, 29B(2):1–7, 1943.
- [39] P. A. Sweet. The neutral point theory of solar flares. *Symposium - International Astronomical Union*, 6:123–134, 1958. doi:10.1017/S0074180900237704.
- [40] E. N. Parker. Sweet’s mechanism for merging magnetic fields in conducting fluids. *Journal of Geophysical Research (1896-1977)*, 62(4):509–520, 1957. doi:<https://doi.org/10.1029/JZ062i004p00509>.
- [41] H. E. Petschek. Magnetic field Annihilation. In *The Physics of Solar Flares, Proceedings of the AAS-NASA Symposium*, page 425, Goddard Space Flight Center, Greenbelt, MD, 28–30 October 1963.
- [42] P.S. Iroshnikov. Turbulence of a conducting fluid in a strong magnetic field. *Soviet Astronomy - AJ*, 7(4):566–571, 1964. URL <https://adsabs.harvard.edu/full/1964SvA....7..566I>.
- [43] R. H. Kraichnan. Inertial-range spectrum of hydromagnetic turbulence. *The Physics of Fluids*, 8(7):1385–1387, 1965. doi:10.1063/1.1761412.
- [44] C. Shi. Generalized Ohm’s law of a MHD plasma, 2018. URL https://chenshihelio.github.io/notes/generalized_ohms_law.pdf.
- [45] N. Murphy. Beyond Ideal MHD (lecture notes for Plasma Astrophysics), 2014. URL https://lweb.cfa.harvard.edu/~namurphy/Lectures/Ay253_04_BeyondIdealMHD.pdf.
- [46] J. D. Huba. *Hall Magnetohydrodynamics - A Tutorial*, pages 166–192. Springer, Berlin, Heidelberg, 2003. doi:10.1007/3-540-36530-3_9.
- [47] F. Wagner. et. al. Regime of Improved Confinement and High Beta in Neutral-Beam-Heated Divertor Discharges of the ASDEX Tokamak. *Phys. Rev. Lett.*, 49:1408–1412, 1982. doi:10.1103/PhysRevLett.49.1408.
- [48] F. Wagner. A quarter-century of H-mode studies. *Plasma Physics and Controlled Fusion*, 49(12B):B1, 2007. doi:10.1088/0741-3335/49/12B/S01.

- [49] P. H. Diamond, S-I. Itoh, K. Itoh, T. S. Hahm. Zonal flows in plasma—a review. *Plasma Physics and Controlled Fusion*, 47(5):R35, 2005. doi:10.1088/0741-3335/47/5/R01.
- [50] K. G. McClements, M. J. Hole. On steady poloidal and toroidal flows in tokamak plasmas. *Physics of Plasmas*, 17(8):082509, 2010. doi:10.1063/1.3469580.
- [51] W. Zhang, Z. W. Ma, S. Wang. Hall effect on tearing mode instabilities in tokamak. *Physics of Plasmas*, 24(10), 2017. doi:10.1063/1.5004430.
- [52] U. Stroth. *Transport in Toroidal Plasmas*, pages 213–267. Springer Berlin Heidelberg, Berlin, 2005. doi:10.1007/11360360_9.
- [53] M. J. Lighthill. Studies on magneto-hydrodynamic waves and other anisotropic wave motions. *Philosophical Transactions of the Royal Society of London. Mathematical and Physical Sciences*, 252(1014):397–430, 1960. doi:10.1098/rsta.1960.0010.
- [54] P. A. Gourdain. The impact of the Hall term on tokamak plasmas. *arXiv*, 2017. doi:10.48550/ARXIV.1703.00987.
- [55] N. Andrés, P. Dmitruk, D. Gómez. Influence of the Hall effect and electron inertia in collisionless magnetic reconnection. *Physics of Plasmas*, 23(2):022903, 2016. doi:10.1063/1.4942418.
- [56] R. Berkowitz. Satellites glimpse the microphysics of magnetic reconnection. *Physics Today*, 72(2):20–23, 2019. doi:10.1063/PT.3.4129.
- [57] P. D. Mininni, D. O. Gómez, S. M. Mahajan. Dynamo action in magnetohydrodynamics and hall-magnetohydrodynamics. *The Astrophysical Journal*, 587(1):472, 2003. doi:10.1086/368181.
- [58] V. D. Shafranov. Plasma equilibrium in a magnetic field. *Reviews of Plasma Physics*, II: 103. Consultants Bureau, New York, 1966.
- [59] H. Grad, H. Rubin. *Hydromagnetic equilibria and force-free fields*. United Nations (UN), 1958. URL http://www-naweb.iaea.org/napc/physics/2ndngenconf/data/Proceedings%201958/papers%20Vol131/Paper25_Vol131.pdf. INIS-XU-021.
- [60] H. Goldstein, C. Poole, J. Safko. *Classical Mechanics*. Addison-Wesley, New York, third edition, 2000.
- [61] P. J. Morrison. Hamiltonian description of the ideal fluid. *Rev. Mod. Phys.*, 70:467–521, 1998. doi:10.1103/RevModPhys.70.467.
- [62] T. W. B. Kibble, F. H. Berkshire. *Classical Mechanics*. Imperial College Press, London, fifth edition, 2004.
- [63] V. I. Arnold. *Mathematical Methods of Classical Mechanics*. Springer-Verlag, New York, second edition, 1989.
- [64] N. J. Hitchin, G. B. Segal, R. S. Ward. *Integrable Systems: Twistors, Loop Groups, and Riemann Surfaces*. Clarendon Press, Oxford, 1999.
- [65] Z. Yoshida, P. J. Morrison, F. Dobarro. Singular Casimir Elements of the Euler Equation and Equilibrium Points. *Journal of Mathematical Fluid Mechanics*, 16(1):41–57, 2014. doi:10.1007/s00021-013-0143-4.
- [66] D. A. Kaltsas, G. N. Throumoulopoulos, P. J. Morrison. Helically symmetric extended magnetohydrodynamics: Hamiltonian formulation and equilibrium variational principles. *Journal of Plasma Physics*, 84(3), 2018. doi:10.1017/S0022377818000338.

- [67] D. A. Kaltsas, G. N. Throumoulopoulos. Exact solutions of the Grad–Shafranov equation via similarity reduction and applications to magnetically confined plasmas. *Physics Letters A*, 380(41):3373–3377, 2016. doi:<https://doi.org/10.1016/j.physleta.2016.08.011>.
- [68] L. S. Solovév. The theory of hydromagnetic stability of toroidal plasma configurations. *Soviet Physics JETP*, 26(2):400–407, 1968. URL http://jetp.ras.ru/cgi-bin/dn/e_026_02_0400.pdf.
- [69] S. R. Hudson, M. J. Hole, R. L. Dewar. Eigenvalue problems for Beltrami fields arising in a three-dimensional toroidal magnetohydrodynamic equilibrium problem. *Physics of Plasmas*, 14(5):052505, 2007. doi:[10.1063/1.2722721](https://doi.org/10.1063/1.2722721).
- [70] R. V. Buniy, Th. W. Kephart. Generalized helicity and Beltrami fields. *Annals of Physics*, 344:179–193, 2014. doi:<https://doi.org/10.1016/j.aop.2014.02.014>.
- [71] G. E. Marsh. *Force Free Magnetic Fields: Solutions, Topology and Applications*. World Scientific Publishing Company, Singapore, 1996.
- [72] T. Wiegelmann, T. Sakurai. Solar force-free magnetic fields. *Living Reviews in Solar Physics*, 9(1):5, 2012. doi:[10.12942/lrsp-2012-5](https://doi.org/10.12942/lrsp-2012-5).
- [73] L. Woltjer. A theorem on Force-Free magnetic fields. *Proceedings of the National Academy of Sciences*, 44(6):489–491, 1958. doi:[10.1073/pnas.44.6.489](https://doi.org/10.1073/pnas.44.6.489).
- [74] B. J. Taylor. Relaxation of Toroidal Plasma and Generation of Reverse Magnetic Fields. *Phys. Rev. Lett.*, 33:1139–1141, 1974. doi:[10.1103/PhysRevLett.33.1139](https://doi.org/10.1103/PhysRevLett.33.1139).
- [75] Z. Yoshida, S. M. Mahajan. Variational Principles and Self-Organization in Two-Fluid Plasmas. *Phys. Rev. Lett.*, 88:095001, 2002. doi:[10.1103/PhysRevLett.88.095001](https://doi.org/10.1103/PhysRevLett.88.095001).
- [76] S. Ohsaki, Z. Yoshida. Variational principle with singular perturbation of hall magnetohydrodynamics. *Physics of Plasmas*, 12(6):064505, 2005. doi:[10.1063/1.1936585](https://doi.org/10.1063/1.1936585).
- [77] S. M. Mahajan, M. Lingam. Multi-fluid systems—Multi-Beltrami relaxed states and their implications. *Physics of Plasmas*, 22(9):092123, 2015. doi:[10.1063/1.4931069](https://doi.org/10.1063/1.4931069).
- [78] G. B. Arfken, H. J. Weber, F. E. Harris. *Mathematical Methods for Physicists*. Academic Press, Oxford, seventh edition, 2012.
- [79] W. A. Strauss. *Partial Differential Equations*. Wiley, second edition, 2008.
- [80] N. N. Lebedev, R. A. Silverman. *Special Functions and Their Applications*. Dover Books on Mathematics. Dover Publications, 1972. URL <https://books.google.gr/books?id=po-6Yxz851MC>.
- [81] E. T. Whittaker, G. N. Watson. *A Course of Modern Analysis*. Cambridge Mathematical Library. Cambridge University Press, fourth edition, 1996. doi:[10.1017/CBO9780511608759](https://doi.org/10.1017/CBO9780511608759).
- [82] G. N. Throumoulopoulos. *Magnetohydrodynamics*. Lectures from the 10th School of Fusion Physics and Technology, Volos, Greece, p. 41-44, 2011.
- [83] H. L. Berk, J. H. Hammer, H. Weitzner. Analytic field-reversed equilibria. *Physics of Fluids*, 24(9):1758–1759, 1981.
- [84] G. N. Throumoulopoulos, H. Tasso. On Hall magnetohydrodynamics equilibria. *Physics of Plasmas*, 13(10), 2006. doi:[10.1063/1.2358111](https://doi.org/10.1063/1.2358111).

- [85] V. Osherovich. The study of toroidal magnetic configurations in a spherically symmetric gravitational field with applications to coronal loops and transients. *Astrophysics and Space Science*, 86(2):453–469, 1982. doi:[10.1007/BF00683348](https://doi.org/10.1007/BF00683348).
- [86] V. Osherovich, J. Fainberg, A. Webb. Observational Evidence for a Double-Helix Structure in CMEs and Magnetic Clouds. *Solar Physics*, 284(1):261–274, 2013. doi:[10.1007/s11207-013-0278-8](https://doi.org/10.1007/s11207-013-0278-8).
- [87] A. J. Cerfon, J. P. Freidberg. “One size fits all” analytic solutions to the Grad–Shafranov equation. *Physics of Plasmas*, 17(3):032502, 2010. doi:[10.1063/1.3328818](https://doi.org/10.1063/1.3328818).
- [88] A. J. Cerfon, M. O’Neil. Exact axisymmetric Taylor states for shaped plasmas. *Physics of Plasmas*, 21(6):064501, 2014. doi:[10.1063/1.4881466](https://doi.org/10.1063/1.4881466).
- [89] R. H. Weening. Analytic spherical torus plasma equilibrium model. *Physics of Plasmas*, 7(9):3654–3662, 2000. doi:[10.1063/1.1287828](https://doi.org/10.1063/1.1287828).
- [90] G. N. Throumoulopoulos, H. Tasso. International thermonuclear experimental reactor-like extended Solovév equilibria with parallel flow. *Physics of Plasmas*, 19(1):014504, 2012. doi:[10.1063/1.3672509](https://doi.org/10.1063/1.3672509).
- [91] A. Giannis, D. A. Kaltsas, G. N. Throumoulopoulos. Three-dimensional Beltrami states for toroidal, shaped plasmas. Poster presented at 19th European Fusion Theory Conference, Consorzio RFX, Padova, 2021. URL <https://indi.to/KGm33>.
- [92] W. Zhang et al. Improved confinement and edge plasma fluctuations in the STOR-M tokamak. *Physics of Fluids B: Plasma Physics*, 4(10):3277–3284, 1992. doi:[10.1063/1.860383](https://doi.org/10.1063/1.860383).
- [93] L. Guazzotto, J. P. Freidberg. A family of analytic equilibrium solutions for the Grad–Shafranov equation. *Physics of Plasmas*, 14(11), 2007. doi:[10.1063/1.2803759](https://doi.org/10.1063/1.2803759).
- [94] R. Aymar, P. Barabaschi, Y. Shimomura. The ITER design. *Plasma Physics and Controlled Fusion*, 44(5):519, 2002. doi:[10.1088/0741-3335/44/5/304](https://doi.org/10.1088/0741-3335/44/5/304).
- [95] A. C. C. Sips. Advanced scenarios for iter operation. *Plasma Physics and Controlled Fusion*, 47(5A):A19, 2005. doi:[10.1088/0741-3335/47/5A/003](https://doi.org/10.1088/0741-3335/47/5A/003).
- [96] V. D. Shafranov. Equilibrium of a toroidal pinch in a magnetic field. *Soviet Atomic Energy*, 13(6):1149–1158, 1963. doi:[10.1007/BF01312317](https://doi.org/10.1007/BF01312317).
- [97] D. R. Ernst et al. Notched velocity profiles and the radial electric field in high ion temperature plasmas in the Tokamak Fusion Test Reactor. *Physics of Plasmas*, 5(3):665–681, 1998. doi:[10.1063/1.872771](https://doi.org/10.1063/1.872771).
- [98] A. C. C. Sips et al. Progress in preparing scenarios for operation of the International Thermonuclear Experimental Reactor. *Physics of Plasmas*, 22(2), 12 2014. doi:[10.1063/1.4904015](https://doi.org/10.1063/1.4904015).
- [99] A. Evangelias, G. N. Throumoulopoulos. Axisymmetric equilibria with pressure anisotropy and plasma flow. *Plasma Physics and Controlled Fusion*, 58(4):045022, 2016. doi:[10.1088/0741-3335/58/4/045022](https://doi.org/10.1088/0741-3335/58/4/045022).
- [100] C. Galea et al. The Princeton Field-Reversed Configuration for Compact Nuclear Fusion Power Plants. *Journal of Fusion Energy*, 42(1):4, 2023. doi:[10.1007/s10894-023-00342-2](https://doi.org/10.1007/s10894-023-00342-2).
- [101] A. J. Knight, I. R. Jones. A quantitative investigation of rotating magnetic field current drive in a field-reversed configuration. *Plasma physics and controlled fusion*, 32(8):575, 1990.

- [102] S. M. Gondal et al. Double Beltrami states and loss of equilibrium in electron, positron and ion plasmas. *Journal of Plasma Physics*, 85(3):905850306, 2019. doi:[10.1017/S0022377819000436](https://doi.org/10.1017/S0022377819000436).
- [103] S. Ohsaki et al. Energy Transformation Mechanism in the Solar Atmosphere Associated with Magnetofluid Coupling: Explosive and Eruptive Events. *The Astrophysical Journal*, 570(1):395, 2002. doi:[10.1086/339499](https://doi.org/10.1086/339499).
- [104] D. Kagan, S. M. Mahajan. Application of double Beltrami states to solar eruptions. *Monthly Notices of the Royal Astronomical Society*, 406(2):1140–1145, 2010.
- [105] D. A Kaltsas, G. N. Throumoulopoulos. Generalized Solovév equilibrium with sheared flow of arbitrary direction and stability consideration. *Physics of Plasmas*, 21(8), 2014. doi:[10.1063/1.4892380](https://doi.org/10.1063/1.4892380).
- [106] R. Srinivasan, L. L. Lao, M. S. Chu. Analytical description of poloidally diverted tokamak equilibrium with linear stream functions. *Plasma Physics and Controlled Fusion*, 52(3):035007, 2010. doi:[10.1088/0741-3335/52/3/035007](https://doi.org/10.1088/0741-3335/52/3/035007).
- [107] H. Li, P. Zhu. Solving the Grad-Shafranov equation using spectral elements for tokamak equilibrium with toroidal rotation, 2019.
- [108] Z. Yoshida, S. M. Mahajan, S. Ohsaki. Scale hierarchy created in plasma flow. *Physics of Plasmas*, 11(7):3660–3664, 2004. doi:[10.1063/1.1762877](https://doi.org/10.1063/1.1762877).
- [109] V. I. Arnold. Proof of a theorem of A. N. Kolmogorov on the invariance of quasi-periodic motions under small perturbations of the Hamiltonian. *Collected Works: Representations of Functions, Celestial Mechanics and KAM Theory, 1957–1965*, pages 267–294, 2009.
- [110] L. Chierchia. Kolmogorov’s 1954 paper on nearly-integrable Hamiltonian systems. *Regular and Chaotic Dynamics*, 13(2):130, 2008.
- [111] W. D. D’haeseleer, W. N. G. Hitchon, J. D. Callen, J. L. Shoet. *Flux Coordinates and Magnetic Field Structure*. Springer, Berlin, 1990.
- [112] A. Evangelias, A. Kuiroukidis, G. N. Throumoulopoulos. Helically symmetric equilibria with pressure anisotropy and incompressible plasma flow. *Plasma Physics and Controlled Fusion*, 60(2):025005, 2017. doi:[10.1088/1361-6587/aa93a7](https://doi.org/10.1088/1361-6587/aa93a7).
- [113] E. T. Whittaker. An expression of certain known functions as generalized hypergeometric functions. *Bulletin of the American Mathematical Society*, 10(3):125 – 134, 1903.

List of figures

1.1	The various manifestations of plasma in our universe.	2
1.2	Debye shielding in plasma.	3
1.3	Experimentally measured cross sections for the D–T, D– ³ He, and D–D fusion reactions as a function of deuterium energy $K_D = m_D v_D^2 / 2$ [16].	6
1.4	The general geometry of a toroidal magnetic confinement system [19].	8
1.5	Schematic representation of the magnetic confinement in a Tokamak [8].	9
1.6	Schematic representation of the pressure isosurfaces, as well as the current density and magnetic field vectors in a Tokamak device [18].	9
1.7	Schematic representation of the magnetic confinement in the W7-X Stellarator in Greifswald, Germany. From "Stellarators, Confining plasma with carefully shaped magnetic fields" (https://terpconnect.umd.edu/~protect/unhbox/voidb@x\penalty\@M\{}mattland/projects/1_stellarators/)	10
1.8	Schematic representation of a field-reversed configuration: a toroidal electric current (brown arrow) is induced inside a cylindrical plasma (blue region), creating a poloidal magnetic field (orange), reversed with respect to the direction of the externally applied magnetic field (black). From Wikipedia: https://en.wikipedia.org/wiki/Field-reversed_configuration#/media/File:Field-Reversed_Configuration.svg	11
1.9	A comparison between Spheromaks and field reversed configurations. From Wikipedia: https://en.wikipedia.org/wiki/Spheromak#/media/File:A_comparison_of_an_FRC_and_A_Spheromak.png	11
1.10	Necessity for the helicity of the magnetic field for a purely toroidal field.	12
1.11	Point charges in cubic arrangement [26].	13
1.12	Schematic representation of the magnetic reconnection process on a typical scale of $2L_e$. $2L$ is the scale of the diffusion region (shaded), while v_e is the inflow plasma velocity [5].	17
3.1	Solovév equilibrium configuration.	47
3.2	Graphical representation of two solutions, Φ_- and Φ_+ respectively, for $a_1 = b_1 = 1$. Contour shading is in arbitrary units.	50
3.3	Graphical representation of a superposition of solutions like (3.125), for $a_1 = b_1 = 1$ and $c_+ = 1, c_- = 2$. Contour shading is in arbitrary units.	51
4.1	The geometry and the three reference points of the D-shaped boundary [87].	54
4.2	The extra points on the boundary for the double Beltrami equilibrium. Due to the up-down symmetry of the formation, only points for $Z > 0$ have been chosen.	58
4.3	The contours of the magnetic and the ion velocity surfaces for the double Beltrami equilibrium. The chosen extra points on the boundary are illustrated as well.	59
4.4	The (dimensionless) flux functions' profiles for the double Beltrami equilibrium on the plane $Z = 0$	59
4.5	The (dimensionless) flux functions' profiles for the double Beltrami equilibrium on the plane $R = 1$	60

4.6	Magnetic field profiles for the double Beltrami equilibrium. Left: The Z -component of the magnetic field on the plane $Z = 0$. Right: The toroidal component of the magnetic field on the plane $R = 1$	60
4.7	Ion velocity field profiles for the double Beltrami equilibrium. Left: The R -component of the velocity field on the plane $R = 1$. Right: The toroidal component of the velocity field on the plane $R = 1$	61
4.8	The profile of the poloidal Alfvénic Mach number on the plane $Z = 0$ for the double Beltrami equilibrium.	61
4.9	Current density profiles for the double Beltrami equilibrium. Left: The R -component of the current density on the plane $R = 1$. Right: The toroidal component of the current density on the plane $Z = 0$	62
4.10	Poloidal electric field profiles for the double Beltrami equilibrium. Left: The Z -component of the electric field on the plane $R = 1$. Right: The R -component of the electric field on the plane $R = 1$	62
4.11	The plasma pressure profile on the $Z = 0$ plane for the double Beltrami equilibrium.	63
4.12	The pressure contours in a torus cross section, along with the magnetic and ion surfaces for the double Beltrami equilibrium.	63
4.13	The extra points on the boundary for the Whittaker equilibrium.	66
4.14	The contours of the magnetic and the ion velocity surfaces for the Whittaker equilibrium. The chosen extra points on the boundary are illustrated as well.	66
4.15	The (dimensionless) flux functions' profiles for the Whittaker equilibrium on the plane $Z = 0$	67
4.16	Magnetic field profiles for the Whittaker equilibrium. Left: The Z -component of the magnetic field on the plane $Z = 0$. Right: The toroidal component of the magnetic field on the plane $Z = 0$	67
4.17	Ion velocity field profiles for the Whittaker equilibrium. Left: The R -component of the velocity field on the plane $R = 1$. Right: The toroidal component of the velocity field on the plane $R = 1$	68
4.18	The profile of the poloidal Alfvénic Mach number on the plane $Z = 0$ for the Whittaker equilibrium.	68
4.19	Current density profiles for the Whittaker equilibrium. Left: The Z -component of the current density on the plane $Z = 0$. Right: The toroidal component of the current density on the plane $Z = 0$	69
4.20	Poloidal electric field profiles for the Whittaker equilibrium. Left: The R -component of the electric field on the plane $R = 1$. Right: The Z -component of the electric field on the plane $R = 1$	69
4.21	The plasma pressure profile on the $Z = 0$ plane for the Whittaker equilibrium.	70
4.22	The pressure contours in a torus cross section, along with the magnetic and ion surfaces for the Whittaker equilibrium.	70
4.23	The (common) contours of the magnetic and the ion velocity surfaces for the Solovév equilibrium. The outer closed magnetic surface represents the separatrix.	72
4.24	The (dimensionless) flux function profile for the Solovév on the plane $\zeta = 0$	73
4.25	Magnetic field profiles for the Solovév equilibrium. Left: The ζ -component of the magnetic field on the plane $\zeta = 1$. Right: The ζ -component of the magnetic field on the plane $\zeta = 1$	73
4.26	Plasma velocity field profiles for the Solovév equilibrium. Left: The ζ -component of the velocity field on the plane $\zeta = 1$. Right: The ζ -component of the velocity field on the plane $\zeta = 1$	73
4.27	The profile of the poloidal Alfvénic Mach number on the plane $\zeta = 0$ for the Solovév equilibrium.	74
4.28	Toroidal current density profile for the Solovév equilibrium on the plane $\zeta = 0$	74
4.29	The plasma pressure profile on the $\zeta = 0$ plane for the Solovév equilibrium.	75

4.30	The pressure contours in a torus cross section, along with the magnetic surfaces for the Solovév equilibrium. The two X-points that the pressure possesses are also illustrated in orange color.	75
C.1	Plot of the Whittaker $\mathcal{M}_{k,m}(z)$ function for some values of k and m	86
C.2	Plot of the Whittaker $\mathcal{W}_{k,m}(z)$ function for some values of k and m	87